WEAK POWER GRID ANALYSIS FOR RENEWABLE ENERGY SOURCES INTEGRATION

A Dissertation
Submitted to the Graduate Faculty
of the
North Dakota State University
of Agriculture and Applied Science

By

Al-Motasem Ihssan Aldaoudeyeh

In Partial Fulfillment of the Requirements
for the Degree of
DOCTOR OF PHILOSOPHY

Major Department:
Electrical and Computer Engineering

June 2019

Fargo, North Dakota

North Dakota State University

Graduate School

Title

WEAK POWER GRID ANALYSIS FOR RENEWABLE ENERGY SOURCES INTEGRATION

By

Al-Motasem Ihssan Aldaoudeyeh

The Supervisory Committee certifies that this ***disquisition*** complies with North Dakota State University's regulations and meets the accepted standards for the degree of

DOCTOR OF PHILOSOPHY

SUPERVISORY COMMITTEE:

Di Wu, PhD

Chair

Benjamin Braaten, PhD

Jacob Glower, PhD

Ying Huang, PhD

Approved:

Jun-20-2019	Benjamin Braaten, PhD
Date	Department Chair

ABSTRACT

Weakness analysis based on grid strength assessment is useful for identifying potential weak grid issues. However, when taking into account the impact of the interactions among Renewable Energy Sources (RESs), the weakness analysis becomes computationally challenging. Different combinations of Points-of-Interconnections (POIs) of RESs may have different impacts on grid strength at each POI. Due to the combination nature, such weakness analysis may be time-consuming when identifying the weakest combination of POIs from a large number of potential candidate locations in realistic power grids. This dissertation addresses the topic of determination of the weakest RESs combinations. Based on impedance ratios as a criterion, the dissertation shows that the impacts of impedance ratios magnitudes and angles are 'quasi-mutually exclusive'. Such a concept is then used to reduce the computational burden with a fast screening algorithm.

To further understand the impact of network components on grid strength, vector-based interaction analysis is developed based on the concepts of operational transfer impedances and operational interaction operators. In particular, this dissertation shows how mathematical models of interaction of multiple RESs can be simplified by replacing them with equivalent impedances, allowing us to simplify the mathematical expressions that quantify interactions among RESs. The conclusions and concepts established based on simplified models are statistically tested for their applicability to the generalized interaction model. The result would be a more simplified mathematical representation of interaction among RESs.

Finally, a new technique is presented to efficiently update the Bus Impedance Matrix ($\boldsymbol{Z}_{bus}$) following changes in the series impedance of a branch. Conventionally, such update requires redundant re-calculations, which involve matrix inversion operations (i.e., inverting the Bus Admittance Matrix, $\boldsymbol{Y}_{bus}$) and thus cause high computational burden because of potential

matrix ill-conditioning, especially for large-scale power grids. This dissertation overcomes these shortcomings by deriving an analytical expression for changes in $\boldsymbol{Z}_{bus}$ in terms of its old elements and the variation of the impedance of a given branch. Hence, the computation overhead is comparatively small, and no issues arise due to the new $\boldsymbol{Y}_{bus}$ being ill-conditioned. Such contribution helps facilitate real-time applications of methods that rely on $\boldsymbol{Z}_{bus}$.

TABLE OF CONTENTS

LIST OF TABLES

LIST OF FIGURES

LIST OF APPENDIX FIGURES

CHAPTER 1. INTRODUCTION

1.1. Background

1.1.1. Short-Circuit Ratio

Grid strength assessment helps transmission operators and operation engineers identify and understand 'weak' grid issues for reliably planning and operating the power grid. Grid strength characterizes the capability of the grid to resisting perturbations such as changes in load or switching of equipment. It is common to quantify the strength of a power grid at a Point-of-Interconnection (POI) with Short-Circuit Ratio (SCR), which is the ratio of the short-circuit capacity at the POI to the rated capacity of the RES [1]. Mathematically, the SCR of the grid at POI i is

$$SCR_i = \frac{|S_{ac,\,i}|}{P_{r,\,i}} = \frac{|V_i|^2}{|Z_{th,\,ii}|}\frac{1}{P_{r,\,i}} \tag{1.1}$$

Where $S_{ac,\,i}$ is the short-circuit capacity of the grid at POI i, $|V_i|$ is the voltage magnitude at POI i, $Z_{th,\,ii}$ is the magnitude of Thevenin equivalent impedance at POI i, and $P_{r,\,i}$ is the rated power of the Renewable Energy Source (RES) connected to POI i. At the planning stage, analysts usually consider the normal operating conditions. Thus, we set $|V_i|$ to 1 and Eq. (1.1) becomes

$$SCR_i = \frac{|S_{ac,\,i}|}{P_{r,\,i}} = \frac{1}{|Z_{th,\,ii}|\ P_{r,\,i}} \tag{1.2}$$

Eq. (1.2) shows that the strength of POI i mainly depends on the rated power of its RES (i.e., $P_{r,\,i}$) and the electrical distance from bus i to the grid (i.e., $|Z_{th,\,ii}|$). The latter can be represented with the magnitude of Thevenin impedance in the equivalent system (as shown in Fig. 1.1.) reduced from a complex power grid. Eq. (1.2) suggests that, under normal operating conditions,

POI i is strong if bus i is electrically close to the system and if the power injection of the RES at i is relatively small.

According to [2], the strength of the power grid at a POI can be quantified using the following SCR ranges: **a)** the grid is *strong* at a POI if its SCR is larger than 3; **b)** the grid is *weak* at a POI if its SCR is in a range between 2 and 3, and **c)** the grid is *very weak* at a POI if its SCR is smaller than 2.

It is worth mentioning that many manufacturers, such as GE, design their wind turbines for POIs with SCR of 5 or higher. Thus, for an RES connection with a weak POI, we need further analysis [2].

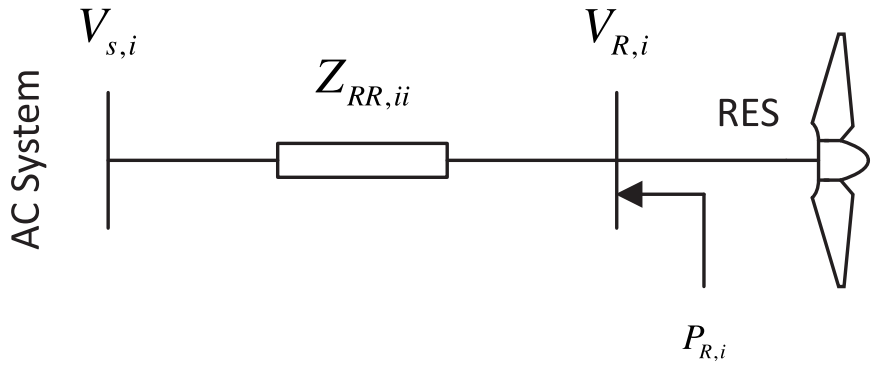

Fig. 1.1. POI Equivalence of an AC Power Grid with a Single RES

1.1.2. Problems Due to Low Short-Circuit Ratio

In this section, we present some of the problems that arise when a power system has a low SCR. These are enumerated as follows: **a) Responsiveness of RES Controllers**. The Voltage Source Controller (VSC) becomes more difficult to control, with poor tracking, and even possibility of instability after drastic changes in set-points [3]. Zhou and Gole [3] justify this by telling us that a sudden increase in active power causes a much bigger difference in the voltage angle difference between the POI and the rest of the system (as represented by Thevenin voltage

source), increasing the chance of loss of stability. Zhou *et al.* [4] study the voltage stability when a Wind Turbine (WT) controller is to track reference active and reactive powers. They show that as the SCR varies from 5.5 to 1.5, the root locus (of the closed-loop transfer function of voltage with respect to active power) crosses the $j\omega$ axis, meaning that a WT can lose stability when connected with weak grids. Zhang *et al.* [2] and Schmall *et al.* [5] report similar conclusion; poor damping of voltage oscillation happens due to low short-circuit level at POIs of wind farms. Lorenzen *et al.* [6] study an LCL filter as a means to reduce harmonics, with the transfer function of injected current with respect to POI voltage being the focus of the study. The authors noted that the closed-loop transfer function becomes unstable due to low SCR. Thus, they reduced the gain of the PI controller, but such counter-measure negatively reshaped the open-loop response of the VSC. Specifically, it shifted the magnitude of the frequency response characteristics to the lower left, thereby decreased the bandwidth of the closed-loop response, which reduced responsiveness; **b) Overvoltage and Overvoltage Cascading**. When the grid is weak, two different mechanisms can cause overvoltage: **1.** Some grid codes and standards require large reactive current injection during disturbances or undervoltages. When the grid is weak, attempting to meet such requirement may cause a temporary overvoltage which triggers overvoltage relays to send trip signals and isolate the WT or wind farm from the grid [4], and **2.** When the system is weak at certain POI, the dV/dQ sensitivity is high (i.e., the voltage can vary substantially due to variation of reactive power injection). When a fault occurs and gets cleared, most wind plants will not restore their output to the original level. Thus, the power flow in lines close to one wind farm may substantially get reduced which causes the charging current in these lightly loaded lines to increase the voltage in nearby buses (because dV/dQ is high when a POI is weak). Next, if more plants exist nearby, these plants will experience further overvoltage, which encourages relays to trip these

plants. When such a process continues to happen by sustaining itself, we say that 'overvoltage cascading' happened [5]; **c) Oversized Converters are Needed**. This emerges as consequence of Item b. Grunau and Fuchs [7] argue that if the grid is weak and we have voltage fluctuations or under/overvoltages, then the converters need to be over-sized to accommodate such situation; **d) Vulnerability to Faults and Maloperation of Protection Relays**. Urdal *et al.* [8] argue that low grid strength can lead to angular stability issues after faults. This was also confirmed (but for voltage rather than the angle) by [9] whose study shows that with weaker grids, Doubly-Fed Induction Generators (DFIG) stabilizes slower after a fault happens and clears. Further, since distance protection is based on calculated fault impedance, the fault impedance of VSC and RES converters will appear to be higher than it really is, which could eventually cause mal-operation [8], and **e) Commutation Failure**. Many power electronic interfaces rely on 'natural commutation' to turn off switches that cannot be turned off by a current impulse into their gate (e.g., thyristors). Wang *et al.* [10] state that if the grid strength is weak, the HVDC system can suffer commutation failure, typically after fault-induced voltage reduction. Further, Wang *et al.* [10] confirm that voltage oscillations in an AC/DC system cause persistent commutation failures

1.2. Literature Review and Proposed Solutions

The earliest interest in AC system strength and the implications of the weakness of buses goes back to the early 90s [11]. The main focus of the efforts was to explore the impact of AC system weakness on High-Voltage DC (HVDC) systems (e.g., the maximum available power to the DC side when the SCR varies). Such interest was motivated by even earlier research on how the equivalent impedance of the system (i.e., Thevenin impedance as seen from the bus connected to HVDC) influences different aspects of interest in the operation of HVDC systems. The following is some examples of conclusions of earlier works as covered in [11]: **a)** in weak systems, harmonic

instability can happen and lead to valve control maloperation (i.e., commutation failure) in the three-phase rectifier in HVDC systems; **b)** DC links in HVDC system could become unstable if SCR dropped below a certain value, and **c)** possible voltage collapse when the DC link in HVDC systems operate at constant power mode.

Despite the emergence of a guide by the IEEE on planning HVDC interfaces connected to weak AC systems or systems with low inertia [11], [12], there are still many troubles encountered when connecting an RES to weak buses, implying that we cannot extend the standards developed for HVDC interfaces to RES integration, or, at least, the concepts available in these standards need re-evaluation from RES integration perspective rather than HVDC one. These troubles are summarized in SubSection 1.1.2. and many of which date to as late as 2014 (within five years of writing this proposal). Further, some troubles seem to still apply even to HVDC systems themselves despite the monumental improvements on power electronics technologies in the last two decades [10].

1.2.1. Review of System Strength Evaluation Literature

A part of the origin of weakness analysis has just been explained. However, the reasons for the growing interest in weakness analysis for RESs integration are as follows: **a)** Unlike synchronous machines, RESs do not contribute to the short-circuit capacity at their buses. This means that they do not contribute to smaller Thevenin impedance to their buses or nearby buses [13]; **b)** Unlike synchronous machines, RESs do not provide inertia that helps maintain rotor angle stability [13]. RESs use Phase-Locked Loop (PLL) to rapidly track changes in the voltage phase angle of the grid and modify the output voltage of their converters in such a way they will stay in synchronism with the grid. However, PLL converters do not vary their output power for a disturbance of the grid's rotor angle [8]. By contrast, synchronous machines naturally provide

such functionality with synchronizing torque that brings the rotor speed back to the synchronous speed and, when damper windings exist in their design, damping torque which prevents oscillations [14]; **c)** Manufacturers design their controllers under the assumption that the grid is very strong, usually $SCR > 5$. Such an assumption is overly optimistic considering that stable and persistent wind gusts exist away from load centers. Thus, RESs are usually connected to unfavorable locations from a structural perspective, making it very likely that the SCR is substantially less than 5. In fact, even if the system is strong at an RES POI, the fact that RES is located in these unfavorable locations could mean a significant drop in SCR when a power line outage occurs. For instance, Zhang *et al.* [2] mention a real-life example of a Wind Power Plant (WPP) connected to ERCOT grid through two $69\,\mathrm{kV}$ transmission lines with $SCR \approx 4$. When one of these lines disconnected, the SCR dropped to less than 2, resulting in poorly damped or un-damped voltage oscillations. Investigations revealed that the aggressive voltage control (e.g., increasing the gain in response to strength decrease at an RES POI) was the reason for such an undesired behavior, and **d)** The parameters of synchronous machines necessary to conduct analysis simulations are either provided by the manufacturers or can be estimated by, usually, non-complex tests. By contrast, the parameters of RES inverter controllers necessary to stability analysis are seldom provided by the manufacturers of RESs. When multiple RESs from different vendors are available in close proximity to each other, it becomes even more difficult to analyze how these RESs will behave using detailed modeling [13].

Here, Items a and b explain why RESs are inherently different from synchronous machines despite the fact they both could be modeled as current injections in load flow analysis, while Item c explains why the usual designs of RESs control interfaces experience problems such as the ones we discussed in SubSection 1.1.2. Finally, Item d explains why doing detailed study

for interactions of too many RES plants is not feasible which necessitates the evaluation of potential risk using faster methods, with possible detailed investigations being done only for the weakest scenarios or weakest RES combinations. Thus, it is now easier for us to understand why an accurate evaluation of system strength is necessary.

One drawback of the conventional SCR (defined in Eq. (1.1)) is the assumption that wind plants are electrically far enough from each other that they will not oscillate together. However, when these RESs are electrically close, they indeed oscillate together or 'interact'. Such behavior is referred to as *interaction*. Hence, SCR does not capture the effect of such interactions and strength of the system, as measured by SCR, is highly optimistic when RESs are electrically close [1], i.e., the predicted system strength at a particular bus is more than it actually is.

Motivated by overcoming the shortcoming of the conventional SCR, General Electric (GE) [15] and Minnesota Department of Commence [13] propose a modified version of it. This index is called Composite Short-Circuit Ratio (CSCR) and is based on the assumption of neglecting all electric distances among RESs and calculating a 'unified' SCR for all of them. They define it verbally as [13].

"*CSCR is calculated as the ratio of the composite short-circuit MVA at the points of interconnection of all wind/solar plants in a given area to the combined MW rating of all those wind and solar generation resources.*"

Thus, using such definition, and by putting that all RESs buses indices in a single set $\boldsymbol{R}$ and setting the symbol of any RES bus to j, we write the CSCR in terms of divisions of summations as follows

$$CSCR = \frac{\sum_{j \in \boldsymbol{R}} |S_{ac,\,j}|}{\sum_{j \in \boldsymbol{R}} P_{r,\,j}} \tag{1.3}$$

Here, $S_{ac,\,j}$ is the short-circuit MVA capacity at bus j, and $P_{r,\,j}$ is the rated power of bus j. Another extension to the conventional SCR is the Weighted Short-Circuit Ratio (WSCR) method developed by ERCOT [2], [16]. WSCR is the same as the CSCR with one major difference: it assigns a 'weight' for each bus short-circuit MVA capacity based on the rating of the wind plant at that bus. Using the same meaning of $\boldsymbol{R}$ and j as that of Eq. (1.3), we write the WSCR as

$$WSCR = \frac{Weighted\ SCMVA}{\sum_{j \in \boldsymbol{R}} P_{r,\,j}} \tag{1.4}$$

Where $SCMVA$ stands for Short-Circuit MVA (capacity) and $Weighted\ SCMVA$ is defined as

$$\begin{matrix} Weighted \\ SCMVA \end{matrix} = \frac{\sum_{j \in \boldsymbol{R}} |S_{ac,\,j}|\ P_{r,\,j}}{\sum_{j \in \boldsymbol{R}} P_{r,\,j}} \tag{1.5}$$

Substituting, Eq. (1.5) in Eq. (1.4)

$$WSCR = \frac{\dfrac{\sum_{j \in \boldsymbol{R}} |S_{ac,\,j}|\ P_{r,\,j}}{\sum_{j \in \boldsymbol{R}} P_{r,\,j}}}{\sum_{j \in \boldsymbol{R}} P_{r,\,j}} \tag{1.6}$$

$$WSCR = \frac{\sum_{j \in \boldsymbol{R}} |S_{ac,\,j}|\ P_{r,\,j}}{\left(\sum_{j \in \boldsymbol{R}} P_{r,\,j}\right)^2} \tag{1.7}$$

The main disadvantage of Eqs. (1.3) and (1.7) as estimators of system strength is *negligence of real electrical distances.* CSCR and WSCR assume full interaction among different RES and they disregard any real electrical distance among the buses of RESs, which is equivalent to assuming that all buses are connected to the same virtual POI [1] (also called 'super' POI by [16]).

However, these electrical distances reduce the level of interaction that actually exists in real life. Thus, unless RESs are very electrically close to each other, the assumption of full interaction among RESs renders the accuracy of CSCR and WSCR questionable.

Another consequence of neglecting real electrical distances and placing all RESs of interest in a super/virtual POI is *'pooling' the strength of various buses in an area*. Some plants can be very electrically close, thus will substantially interact. By contrast, some other plants can have significant electrical distance among them, thus will not interact as much as the ones that are electrically close to each other. Such behavior suggests that unless all plants are extremely electrically close, an accurate measure of system strength should provide a numerical measure for each bus. However, pooling RES plants to the same virtual POI means that their buses must be treated as one aggregated bus. Consequently, CSCR and WSCR assign a single strength measure for all buses of RESs under consideration, which would render pooling the strength of various RES buses questionable.

To explain the implication of neglecting electric distances and pooling RESs in the same virtual POI, we introduce very brief example

1. Let us say that we have two buses, t and u, with similar power ratings and real power injections
2. If t and u have some significant electric distances between them, we expect that they do not share similar driving-point impedances magnitudes, which could mean the short-circuit MVA capacities of buses t and u are not similar (the MVA short-circuit capacity is $|S_{ac,\,i}| = \frac{|V_i|^2}{|Z_{th,\,ii}|}$ as in Eq. (1.1)).
3. Thus, assigning a single index for multiple RES buses may not be an accurate representation of the actual strength of each bus.

We briefly discuss how to address these concerns in Section 1.4.

1.2.2. Review of Control or Compensation Based Techniques to Mitigate Grid Weakness Symptoms

Despite the importance of grid strength and the problems that emerge from grid weakness at RES buses (see SubSection 1.1.2.), there is a little done to improve the situation. Very few efforts exist to address such topic as the main design criterion of wind/photovoltaic plants and their power electronic interfaces with the grid. Here, we cite these efforts.

To minimize the size of reactive power compensation, Zhou *et al.* [4] propose a coordinated control of wind power plants where wind power plants work (ideally) as stiff voltage sources. Authors do this by setting a controller for each WT generator to regulate its terminal voltage with inverse droop characteristics for the reactive power. The high speed of the controller is achieved by increasing its bandwidth, which, especially if the SCR is low, will lead to shunt resonance between the voltage controller and the grid.

One typical solution for grid strength at an RES bus is synchronous condensers, which, in practice, was applied near the interconnection points between England and Scotland, where the interconnection is known to be weak [8]. Synchronous condensers have the advantage of providing higher short-circuit capacity, which helps improve system strength at the POI of RESs. Further, they provide increased inertia for the system [5], which is beneficial for rotor angle stability.

Static Voltage Compensators (SVCs) are an alternative to synchronous condensers because they provide faster responsiveness to voltage support, but without increasing the short-circuit capacity. Further, they could cause undesired oscillations if not appropriately tuned [5].

Lorenzen *et al.* [6] propose simplified design procedure for PI controllers to ensure the stability of RESs VSCs (simplification such neglecting the capacitance in LCL filter). They claim that with their design strategy, varying the SCR does not have much of impact on the stability

(but lowering it will lower the system's bandwidth, meaning reduced responsiveness). Lorenzen *et al.* [6] verify their work using a comparison of step response of their simulation against an experimental testbed.

In the literature, one noticeable trend in authors investigations is their willingness to continue working on their designs/solutions and improve them. For instance, Zhou *et al.* [17] mention that increasing the bandwidth of the voltage controller and decreased strength grid strength could potentially lead to resonance between the controller and the grid. Thus, they express their willingness to investigate such a topic in later work. Urdal *et al.* [8] recommend a mixture of synchronous compensators and advanced controllers that are designed to 'emulate' the synchronous generator performance (e.g., the synchronizing torque or damping torque). Urdal *et al.* [8] recommended revising the accuracy of converter models when applied to systems with high non-synchronous generation levels (including the PLL functionalities and its implications), then make such models more amenable for data exchange in the system.

1.3. Morale

One crucial question that we could ask ourselves is: if other research works focus on control of RES power electronic interfaces, evaluating system strength at RESs POIs, or evaluating the accuracy of RES models in weak grid conditions, then why do we need to investigate system strength from a structural perspective? Is not it enough to merely focus on developing better control methods of RES power electronic interfaces or deployment of compensation apparatus at RES buses?

Multiple reasons motivate us to investigate system strength from a structural perspective: **a)** Developing more advanced/innovative control strategies that mitigate the troubles of RES bus weakness only deals with the symptoms without actually enhancing the strength of the system;

that is to say, more innovative controller structures (or better parameter tuning of controllers) only help us to cope with Item a in SubSection 1.1.2. For instance, The controllers will not contribute the synchronizing torque that helps maintain angle stability; **b)** Using FACTS devices to provide reactive power may sound to some engineers as a viable solution. However, one reason that an RES bus is weak is injecting too much complex power into that bus. To explain this further, we can look at Eqs. (1.11) and (1.12) which show that POI i strength is inversely proportional with the complex power injected at it. Thus, injecting more reactive power into a bus that already has too much power input compared to its short-circuit MVA capacity (i.e., low strength) could make the POI i even weaker. One exception, however, is if FACTS devices (for a particular system and operating conditions) can improve voltage significantly that they could offset their increased contribution to the apparent power as seen from bus i. Such exception is especially true since if bus i voltage is much less than 1 but significantly increased after FACTS deployment. In such a case, the strength of POI i increases significantly because it is proportional to the *square* of voltage. Another reason that FACTS may not be suitable is that they are power electronic interfaces, suggesting that if the system is already weak, they may further exacerbate or result in harmonics or voltage oscillations as discussed in SubSection 1.1.2., and Section 1.2., and **c)** Improvement of controllers or FACTS deployment are attempts to mitigate the symptoms of system weakness without actually understanding or determining what caused such weakness and what combination of RES POIs are the weakest. In this dissertation, we will develop different theoretical concepts to help us develop a mathematical understanding of RES interaction using a vector-based approach. Thus, apart from advancing the theoretical understanding of RESs interaction, it will help us explain why specific lines are responsible for the strength or weakness of certain buses. As such, we obtain multiple benefits: **1. transmission system expansion planning benefits**.

when we know what line influences the strength of an RES bus of interest, it becomes easier to identify potential system upgrades that could help improve the strength of a weak RES POI (e.g., building a line in parallel with another or implementing series or shunt compensation); **2. operational benefits**. when a line is identified as being 'critical' to maintain the strength of a certain RES, the system operator can then plan ahead for contingencies related to that line (e.g., by procuring more ancillary services that help support the voltage of the weak RES buses); **3. controllers design benefits**. As we mentioned in SubSection 1.2.2., one approach to deal with the problems of RES POIs weakness is to develop specific control schemes or better controller parameter tuning with system weakness issues being a criterion for the design. However, in real life, the design of RES controller must satisfy multiple criteria and is aimed to achieve multiple objectives. When the strength of an RES POI is improved by transmission expansion (say from very weak to weak), the constraints on controller design can be 'relaxed', allowing the designer to either achieve better results with other objectives (e.g., efficiency or measurement noise) or reduce the complexity or cost of the design; **4. loadability and utilization benefit**. According to [18], [19], curtailment of RES generation happens for different reasons, including operational constraints or mitigation strategy for a POI weakness. The strength of a POI is directly correlated with its loadability (because the strength is a measure of how close we are to the voltage instability which occurs when the system is heavily loaded; see SubSection 1.4.2.), that is, the strength of a POI is an index that quantifies how far we are from the maximum power that can be injected into it. Thus, improving the strength means that a POI can accommodate more power injection from RESs. Grant [13] investigate the improvement of RESs integration in Minnesota and report that upgrading existing transmission could help minimize curtailment of RES generation. Achilles *et al.* [18] also report that transmission reinforcement can help accommodate new generation

resources in weak POIs, and **5. electricity market competition benefits**. From Item d, we can say that when the power injection from RESs is more feasible with fewer occasions of RES curtailment, then this helps greatly in encouraging competition since wind curtailment usually happens when the system is congested (or near its operational limits), a time at which electricity prices usually increase or even spike.

1.4. The Need for Site-Dependent Short-Circuit Ratio

1.4.1. Drawbacks of the Conventional SCR

One drawback of the conventional SCR is the assumption that wind plants are electrically far enough from each other that they will not oscillate together. However, when these RESs are electrically close, they indeed oscillate together or 'interact'. Such behavior is referred to as *interaction*. Hence, SCR does not capture the effect of such interactions and strength of the system, as measured by SCR, is highly optimistic when RESs are electrically close [1], i.e., the predicted system strength at a particular bus is more than it actually is. To take into account the effect of RESs interactions on the grid strength, several new methods were developed, such as the Weighted Short-Circuit Ratio (WSCR) method developed by ERCOT [2] and [16] and the Composite Short-Circuit Ratio (CSCR) method developed by General Electric (GE) [15] and Minnesota Department of Commence [13]. However, these two new indices still have the following disadvantages:: **a) Negligence of real electrical distances.** CSCR and WSCR assume full interaction among different RESs (which results in what is called a 'super POI' as mentioned in [5] and they disregard any real electrical distance among the buses of RESs. However, these electrical distances reduce the level of interaction that actually happens in real life. Thus, unless RESs are very electrically close to each other, the assumption of full interaction among RESs renders the accuracy of CSCR and WSCR questionable, and **b) 'Pooling' the strength various buses**

in an area. Another consequence of neglecting real electrical distances is that some plants can be very electrically close, thus will substantially interact. By contrast, some other plants can have significant electrical distance among them. Thus, they will not substantially interact. Such behavior suggests that unless all plants are extremely electrically close, an accurate measure of system strength should provide a numerical strength measure for each bus. However, one important outcome of neglecting the electrical connections between RES plants is that different buses must be treated as one aggregated bus. Consequently, CSCR and WSCR assign a single strength measure for all buses of RESs under consideration, which would render pooling the strength of various RES buses questionable.

To overcome these two shortcomings, Wu *et al.* [20] devise the Site-Dependent Short-Circuit Ratio (SDSCR) index, which is derived by analyzing the relationship between grid strength and voltage stability. In particular, they use voltage-current relationship analysis and set the singularity of the Jacobian to obtain the boundary condition of stability (i.e., the point at which we reach the point-of-collapse on the PV curve of a bus).

1.4.2. Site-Dependent Short-Circuit Ratio

For the reasons mentioned after Eqs. (1.3) and (1.7) and in SubSection 1.4.1., Wu *et al.* [20] propose a new index of POIs strength called the Site-Dependent Short-Circuit Ratio (SDSCR). It is derived by assuming that we have a system with multiple conventional sources and multiple RESs (as in Fig. 1.2.) with the voltage-current relationships being given (in terms of vectors of conventional generation and RES voltages and current injections) as follows

$$\left[\begin{array}{c} \boldsymbol{V}_G \\ \hline \boldsymbol{V}_R \end{array}\right] = \left[\begin{array}{c|c} \boldsymbol{Z}_{GG} & \boldsymbol{Z}_{GR} \\ \hline \boldsymbol{Z}_{RG} & \boldsymbol{Z}_{RR} \end{array}\right] \left[\begin{array}{c} \boldsymbol{I}_G \\ \hline \boldsymbol{I}_R \end{array}\right] \tag{1.8}$$

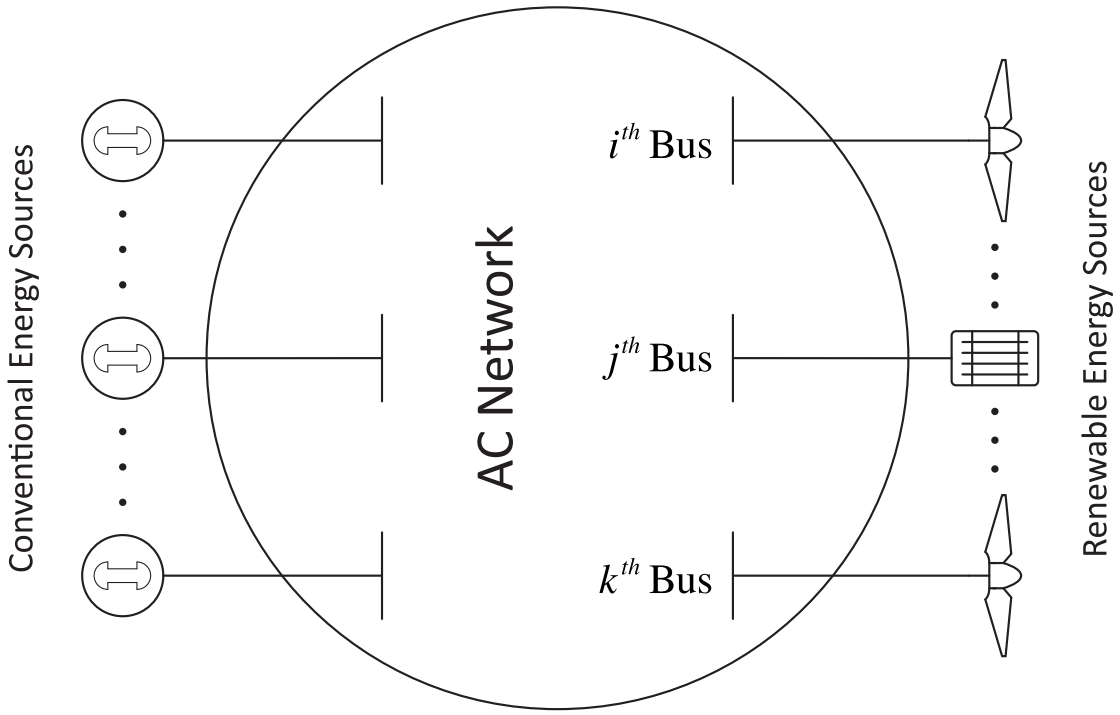

Fig. 1.2. An AC System with Multiple RESs

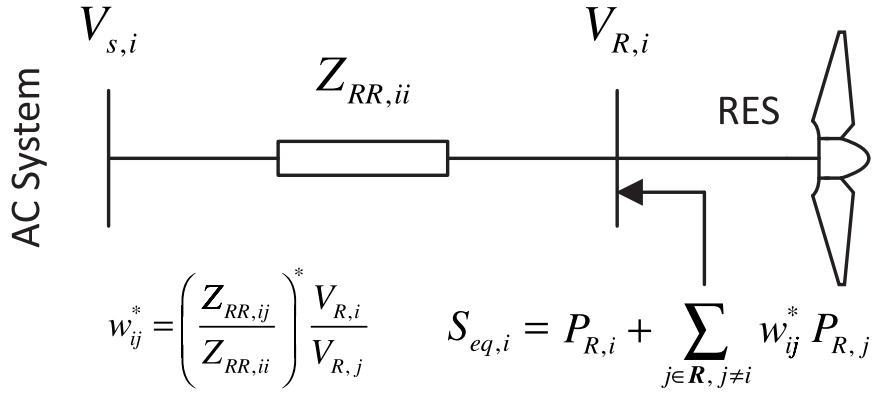

Fig. 1.3. POI Equivalence of an AC Power Grid with Multiple RESs

With the singularity of the Jacobian matrix being set as a criterion (the Jacobian is made singular by calculating the boundary condition for voltage stability at bus i), Wu *et al.* [20] show that

$$\bar{r}_i = \frac{|S_{ac,i}|}{\left|S_{eq,i}^{*}\right|} = \frac{|V_{R,i}|^2}{\left|S_{eq,i}^{*}\right| |Z_{RR,ii}|} = \frac{|V_{R,i}|^2}{\left|S_{R,i}^{*} + \sum_{j \in \boldsymbol{R},\, j \neq i} S_{R,j}^{*} w_{ij}\right| |Z_{RR,ii}|} = 1 \tag{1.9}$$

Where

$$w_{ij} = \frac{Z_{RR,\,ij}}{Z_{RR,\,ii}} \left(\frac{V_{R,\,i}}{V_{R,\,j}} \right)^{*} \tag{1.10}$$

Which is given as

$$SDSCR_i = \frac{|V_{R,\,i}|^2}{\left| S^{*}_{eq,\,i} \right| |Z_{RR,\,ii}|} \tag{1.11}$$

Where

$$S_{eq,\,i} = S_{R,\,i} + \sum_{j \in \boldsymbol{R},\, j \neq i} S_{R,\,j}\, w^{*}_{ij} \tag{1.12}$$

$$SDSCR_i = \frac{|V_{R,\,i}|^2}{\left| S^{*}_{R,\,i} + \sum_{j \in \boldsymbol{R},\, j \neq i} S^{*}_{R,\,j}\, w_{ij} \right| |Z_{RR,\,ii}|} \tag{1.13}$$

If RESs operate at unity power factor, Eqs. (1.11) and (1.12) become

$$SDSCR_i = \frac{|V_{R,\,i}|^2}{\left| P_{R,\,i} + \sum_{j \in \boldsymbol{R},\, j \neq i} P_{R,\,j}\, w_{ij} \right| |Z_{RR,\,ii}|} \tag{1.14}$$

$$S_{eq,\,i} = P_{R,\,i} + \sum_{j \in \boldsymbol{R},\, j \neq i} P_{R,\,j}\, w^{*}_{ij} \tag{1.15}$$

Where

$$w_{ij} = \frac{Z_{RR,\,ij}}{Z_{RR,\,ii}} \left(\frac{V_{R,\,i}}{V_{R,\,j}} \right)^{*} \tag{1.16}$$

Eq. (1.14) is the same as Eq. (1.1) except for the additional term $\sum_{j \in \boldsymbol{R},\, j \neq i} P_{R,\,j}\, w_{ij}$ (which accounts for interactions between each j^{th} RES and the RES at bus i) that is added to $P_{R,\,i}$. Hence, devising an equivalent circuit similar to the one in Fig. 1.1. is possible. The equivalent circuit in

Fig. 1.3. is therefore a more generalized form of that in Fig. 1.1. in the sense that interactions among RESs are accounted for.

Eqs. (1.14) to (1.16) show that system strength at a POI depends on some elements of the Bus Impedance Matrix related to that POI and other RESs POIs in the system. The purpose of the next section is to provide a brief description of the Bus Impedance Matrix and the method used to calculate it (Brown's method).

1.5. The Bus Impedance Matrix

1.5.1. Definition of The Bus Impedance Matrix

The Bus Impedance Matrix ($\boldsymbol{Z}_{bus}$) is a matrix that characterizes the relationship between current injections and voltages in a system. More specifically, the voltage level at any bus, say bus i, in a power system is the sum of current injection at every bus multiplied by the transfer impedance with respect to bus i. Mathematically

$$V_i = \sum_j Z_{ij} I_j \tag{1.17}$$

If we define $\boldsymbol{V}$ and $\boldsymbol{I}$ as vectors of N voltages and current injections, then

$$\boldsymbol{V} = \boldsymbol{Z}_{bus} \boldsymbol{I} \tag{1.18}$$

$\boldsymbol{Z}_{bus}$ matrix contains diagonal elements which are called *driving point impedances* or *self impedances*. These are the equivalent impedances between each bus and the reference bus [21], and they are the same as the Thevenin impedances of each bus. Thus, the diagonal elements reflect important characteristics of the entire system as seen from each corresponding bus [22]. The off-diagonal elements are called *transfer impedances*, and they are less intuitive to understand. They are parameters for every possible combination of two buses of the system (excluding

any combination that has the reference bus in it) which are defined as the ratio of the voltage at certain bus over the current injection at another bus (say bus m) when all current injections, except the one at m, are set to zero [21]. Mathematically, both of them are defined as

$$Z_{lm} = \left.\frac{V_l}{I_m}\right|_{I_i=0,\ \substack{i=1,2,\cdots,N \\ i\neq m}} \tag{1.19}$$

In Eq. (1.19), Z_{lm} is a driving point impedance if $l = m$ and is a transfer impedance if $l \neq m$.

1.5.2. Brown Method to Calculate The Bus Impedance Matrix

A conceptually simple method to find $\boldsymbol{Z}_{bus}$ is by inverting the Bus Admittance Matrix ($\boldsymbol{Y}_{bus}$). Such a method has two major drawbacks: **a)** matrix inversion is computationally intensive and requires a lot of memory, and **b)** ill-conditioning and round-off errors. Thus, for large systems, it is almost always better to build $\boldsymbol{Z}_{bus}$ by analyzing the relationship between currents and voltages. Even though it is utterly impossible to build $\boldsymbol{Z}_{bus}$ directly for a pre-existing system, it is still possible to build it by: **a)** starting from one bus connected to the reference node (usually the ground) via a shunt admittance; **b)** expanding $\boldsymbol{Z}_{bus}$ by adding one series impedance or shunt admittance at a time, and **c)** each time we add a new element, we augment or modify the preceding matrix to an updated one. Such procedure is used in Brown's method, which finds $\boldsymbol{Z}_{bus}$ by direct construction and is described in detail in [21]–[25]. Brown's method depends on a careful examination of the current-voltage relationship changes for possible modifications in the system. There are four basic cases that are defined in Brown's method that include adding a branch whose impedance is Z_b as follows 1. From a new bus k to the reference node 2. From an existing bus k to a new bus p 3. From an existing bus k to the reference node 4. From an existing bus k to an existing bus p In some cases (e.g., series compensation of transmission lines), the reactance of the

line changes. In Brown modeling technique, the network sees this as a change of the impedance of a branch between two existing buses. However, none of the previously mentioned cases in Brown's method provides means to modify a pre-existing $\boldsymbol{Z}_{bus}$ to account for the change of the series impedance of a branch. Such a topic is one of the contributions of this dissertation and will be discussed in details in Chapter 3.

1.6. Background About Round-Off Errors During the Inversion of Ill-Conditioned Matrices

This section presents some theoretical background about ill-conditioned matrices, and why they are vulnerable to rounding errors. The *condition number* of a matrix is

$$\kappa(\boldsymbol{A}) = \left\|\boldsymbol{A}\right\| \left\|\boldsymbol{A}^{-1}\right\|, \quad \kappa(\boldsymbol{A}) \geq 1 \tag{1.20}$$

Where $\|\Diamond\|$ is the norm. A matrix with small $\kappa(\boldsymbol{A})$ is said to be *well-conditioned*. When $\kappa(\boldsymbol{A}) = \infty$, then $\boldsymbol{A}$ is singular, whereas a value much larger than 1 indicates near-singular (i.e., ill-conditioned) matrix. A matrix is said to be *ill-conditioned* if a small changes in it causes a large change in its inverse.

The condition number $\kappa(\boldsymbol{A})$ in Eq. (1.20) characterizes the sensitivity of the inverse of $\boldsymbol{A}$ with respect to small perturbations in $\boldsymbol{A}$. Specifically, for small enough ϵ and $\|\Delta\boldsymbol{A}\| = \epsilon \|\boldsymbol{A}\|$, the following inequality is true [26]

$$\frac{\left\|(\boldsymbol{A} + \Delta\boldsymbol{A})^{-1} - \boldsymbol{A}^{-1}\right\|}{\epsilon \|\boldsymbol{A}^{-1}\|} \leq \kappa(\boldsymbol{A}) \tag{1.21}$$

Such sensitivity to perturbations pertains well to rounding errors in numerical softwares. For instance, the IEEE double-format precision does not use a 'continuous' spectrum of numbers, that is, numbers in IEEE double-format precision are an approximation of the continuous

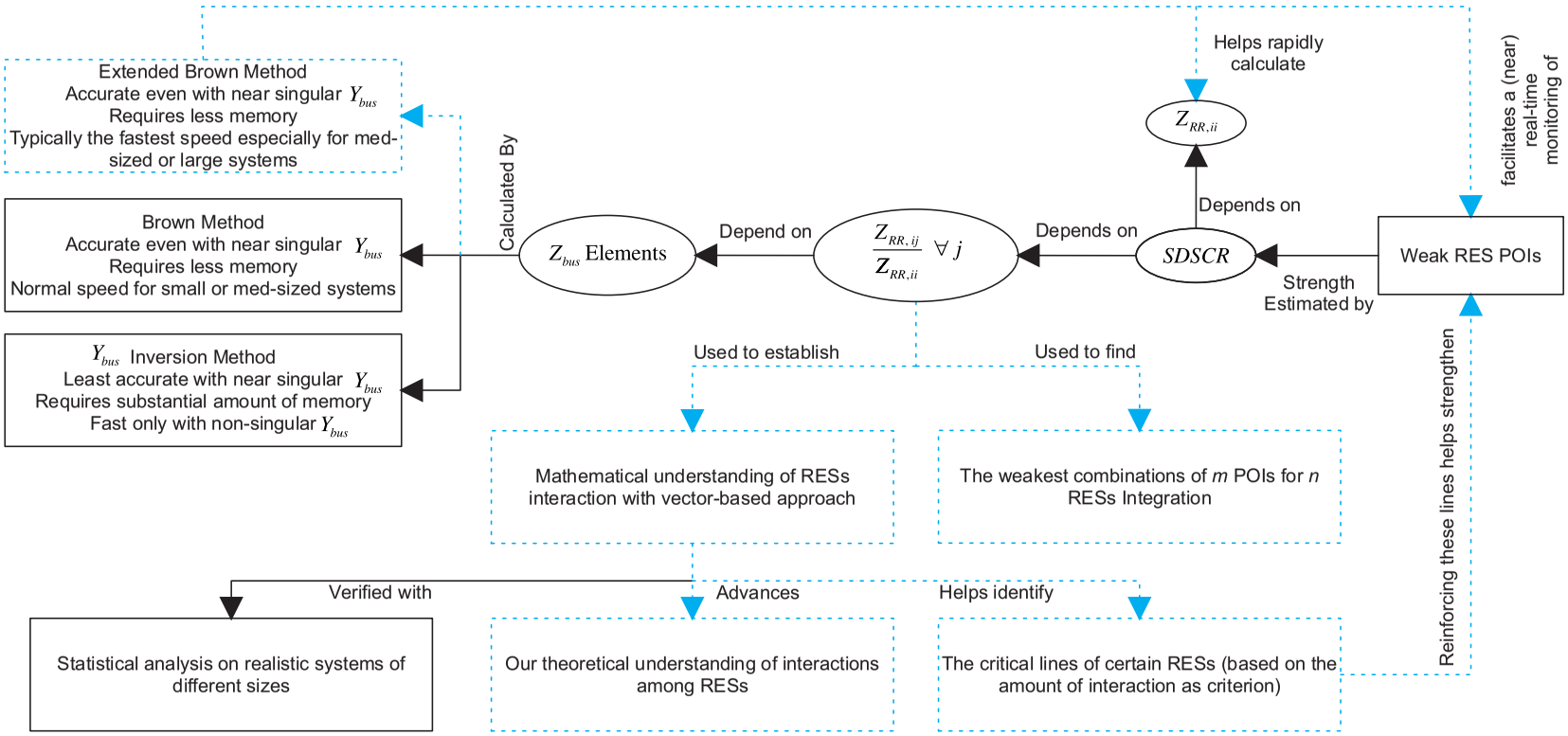

Fig. 1.4. Summary of Some of the Major dissertation Contributions (Actual Contributions are Highlighted by Dashed Blue Lines and Boxes)

range (e.g., 1 is followed by $1 + eps$, where $eps \approx 222.05 \times 10^{-18}$). Thus, if the *exact* result of the calculation is $1 + \frac{eps}{2}$, then a numerical software, say MATLAB, will approximate such result to the nearest available number in the double-format precision, which is 1. For well-conditioned matrices, these approximations still provide correct results with minor errors. By contrast, when a matrix is ill-conditioned, the round-off errors in the double-format precision causes an *error propagation* which, according to Eq. (1.21), substantially changes the values of some or all of the inverted matrix entries.

'Checking' the inverted matrix for abnormal values of entries may seem to be an efficient way to verify its accuracy. However, when a matrix is ill-conditioned, it could sometimes be inverted using the IEEE double-format precision, and the results would be erroneous but reasonable. For instance, assume that a specific impedance in $\boldsymbol{Z}_{bus}$ has a correct value of $j0.700$ p.u. If the Bus Admittance Matrix ($\boldsymbol{Y}_{bus}$) is well-conditioned, the error propagation will not cause too much of deviation in its inverse (i.e., $\boldsymbol{Z}_{bus}$), and the predicted value could be very close to the original one, say $j0.703$. By contrast, if $\boldsymbol{Y}_{bus}$ is ill-conditioned, the result could be much different from the correct one, but its inaccuracy cannot be detected easily, that is, a value of, say, $j0.750$ is significantly different from $j0.700$. An engineer that looks at an impedance of this value will not 'suspect' that the result is incorrect. Thus, matrix inversion of ill-conditioned matrices can lead to undetected calculation errors.

1.7. Research Questions

Eqs. (1.14) to (1.16) on page 17 help us quantify system strength and estimate the amount of interaction among RESs. However, these equations do not clearly provide pieces of information that could be useful for planning and operation of a power system. Such pieces of information are the ones we investigate in this research, and we summarize them as questions as follows

1. How can we quickly find the weakest combinations of RESs?
2. Since $\boldsymbol{Z}_{bus}$ is important in determining the system strength, how can we reduce the calculation burden when we modify the system structure and calculate the new strength?
3. In a given power system, what line influences the strength of a bus or interaction among RESs more than others? Why does this line have a strong influence on the strength of this bus?

Even though these questions may initially look as distinct ones, they still tie together to provide a significant contribution to the field of RES integration. The way they relate to each other is illustrated in Fig. 1.4.

1.8. References

[1] C. Moné, A. Smith, B. Maples, and M. Hand, "Essential Reliability Services Task Force Measures Framework Report," NERC, Tech. Rep., Nov. 2015.

[2] Y. Zhang, S. F. Huang, *et al.*, "Evaluating system strength for large-scale wind plant integration," in *2014 IEEE PES General Meeting | Conference Exposition*, Jul. 2014, pp. 1–5.

[3] J. Z. Zhou and A. M. Gole, "VSC transmission limitations imposed by AC system strength and AC impedance characteristics," 2012.

[4] Y. Zhou, D. Nguyen, P. Kjaer, and S. Saylors, "Connecting wind power plant with weak grid-Challenges and solutions," in *Power and Energy Society General Meeting (PES), 2013 IEEE*, IEEE, 2013, pp. 1–7.

[5] J. Schmall, S.-H. Huang, *et al.*, "Voltage stability of large-scale wind plants integrated in weak networks: An ERCOT case study," in *Power & Energy Society General Meeting, 2015 IEEE*, IEEE, 2015, pp. 1–5.

[6] S. L. Lorenzen, A. B. Nielsen, and L. Bede, "Control of a grid connected converter during weak grid conditions," in *Power Electronics for Distributed Generation Systems (PEDG), 2016 IEEE 7th International Symposium on*, IEEE, 2016, pp. 1–6.

[7] S. Grunau and F. W. Fuchs, "Effect of wind-energy power injection into weak grids," in *Proc. EWEA*, 2012, pp. 1–7.

[8] H. Urdal, R. Ierna, *et al.*, "System strength considerations in a converter dominated power system," *IET Renewable Power Generation*, vol. 9, no. 1, pp. 10–17, 2014.

[9] A. S. Subburaja, N. Shamim, and S. B. Bayne, "Battery Connected DFIG Wind System Analysis for Strong/Weak Grid Scenarios," in *Green Technologies Conference (GreenTech), 2016 IEEE*, IEEE, 2016, pp. 112–117.

[10] Y. Wang, X. Li, C. Wen, and Y. He, "Impact of AC System Strength on Commutation Failure at HVDC Inverter Station," in *2012 Asia-Pacific Power and Energy Engineering Conference*, Mar. 2012, pp. 1–4.

[11] A. Gavrilovic, "AC/DC system strength as indicated by short circuit ratios," in *AC and DC Power Transmission, 1991., International Conference on*, IET, 1991, pp. 27–32.

[12] P. Krishayya, R. Adapa, M. Holm, *et al.*, "IEEE guide for planning DC links terminating at AC locations having low short-circuit capacities, part I: AC/DC system interaction phenomena," *IEEE Std. France: CIGRE*, 1997.

[13] Grant, "Report in the Matter of Integration and Transmission Study for the Future Renewable Energy Standard," Minnesota Department of Commerce, Tech. Rep., Nov. 2014.

[14] M. Eremia and M. Shahidehpour, *Handbook of Electrical Power System Dynamics: Modeling, Stability, and Control*. John Wiley & Sons, 2013, vol. 92.

[15] R. Fernandes, S. Achilles, and J. MacDowell, "Report to NERC ERSTF for Composite Short Circuit Ratio (CSCR) Estimation Guideline," GE, Tech. Rep., Jan. 2015.

[16] J. Schmall, S.-H. Huang, *et al.*, "Voltage stability of large-scale wind plants integrated in weak networks: An ERCOT case study," in *Power & Energy Society General Meeting, 2015 IEEE*, IEEE, 2015, pp. 1–5.

[17] Y. Zhou, D. Nguyen, P. Kjaer, and S. Saylors, "Connecting wind power plant with weak grid-Challenges and solutions," in *Power and Energy Society General Meeting (PES), 2013 IEEE*, IEEE, 2013, pp. 1–7.

[18] S. Achilles, A. Isaacs, J. MacDowell, and C. Smith, "Integrating Inverter-Based Resources into Low Short Circuit Strength Systems," NERC, Tech. Rep., Dec. 2017.

[19] P. Bousseau, F. Fesquet, R. Belhomme, S. Nguefeu, and T. C. Thai, "Solutions for the grid integration of wind farms—A survey," *Wind Energy*, vol. 9, no. 1-2, pp. 13–25, 2006.

[20] D. Wu, G. Li, *et al.*, "Assessing Impact of Renewable Energy Integration on System Strength Using Site-Dependent Short Circuit Ratio," *IEEE Transactions on Sustainable Energy*, 2017.

[21] H. E. Brown, *Solution of Large Networks by Matrix Methods*. Wiley New York et al., 1985.

[22] J. J. Grainger and W. D. Stevenson, *Power System Analysis*. McGraw-Hill New York, 1994, vol. 621.

[23] E. B. Makram and A. A. Girgis, "A generalized computer technique for the development of the three-phase impedance matrix for unbalanced power systems," *Electric power systems research*, vol. 15, no. 1, pp. 41–50, 1988.

[24] E. Makram and A. Girgis, "Development of a three-phase bus impedance matrix in the complex frequency domain for transient analysis in unbalanced distribution systems," *Electric Power Systems Research*, vol. 16, no. 3, pp. 183–193, 1989.

[25] A. R. Bergen, *Power Systems Analysis*. Pearson Education India, 2009.

[26] S. M. Rump, "Inversion of extremely ill-conditioned matrices in floating-point," *Japan Journal of Industrial and Applied Mathematics*, vol. 26, no. 2-3, pp. 249–277, 2009.

CHAPTER 2. A FAST METHOD TO IDENTIFY WEAK POINTS OF INTERCONNECTION OF RENEWABLE ENERGY RESOURCES [1]

2.1. Introduction

The electric power grid is undergoing a rapid change driven by the increasing penetration of Renewable Energy Resources (RERs). The increasing penetration of RERs can change the system's characteristics. Therefore, grid planners and operators are facing new challenges of integrating conventional and renewable resources while maintaining essential reliability services. The RERs are connected to a power grid through power electronic interfaces. While the power electronic controls provide the flexibility for the RERs integration, they also add complexity to ensuring grid reliability services. For instance, when the RERs are connected to a weak grid, fast dynamic responses from the inverter controllers within RERs may have high sensitivity voltages with respect to small disturbances associated to normal operation such as power output variability, line switching, and capacitor/reactor operation [1]–[3]. Such disturbances may trigger oscillatory behaviors of fast controls in RERs interacting with each other [4]–[6]. These oscillatory behaviors result in growing or erratic oscillations that have negative consequences to grid reliability such as unit tripping, flicker or power quality concerns, and ultimately potential

1. The material in this chapter (doi: https://doi.org/10.1016/j.ijepes.2019.03.003) was authored by Di Wu and co-authored by Al-Motasem Aldaoudeyeh.
Di Wu was the principal investigator who was responsible for analysis, math derivation, data collection, code writing, simulation, and writing the bulk of the manuscript.
Al-Motasem Aldaoudeyeh verified the soundness of results, revised and edited the manuscript, and answered reviewers' questions.

human safety concerns or damage to equipment [7], [8]. Urdal *et al.* [9] argue that low grid strength can lead to angular stability issues after faults. This was also confirmed (but for voltage rather than the angle) by [10] whose study shows that with weaker grids, Doubly-Fed Induction Generators (DFIG) stabilizes slower after a fault happens and clears. Further, since distance protection is based on calculated fault impedance, the fault impedance of VSC and RES converters will appear to be higher than it really is, which could eventually cause mal-operation [9]. Given that manufacturers design their controllers under the assumption that the grid is very strong, usually $SCR > 5$, the issues mentioned above become more relevant in real-life situations.

Weakness analysis based on grid strength assessment is useful for grid operators and planners to understand and identify the potential weak grid the weak areas or points of interconnection (POIs) of RERs. Grid strength describes how stiff or rigid the grid is to small perturbations such as changes in load or switching of equipment. While strong grids provide a strong source for resources to connect to, weak grids can pose challenges for connecting new resources and particularly for connecting inverter-based resources [1]. Short circuit ratio (SCR) is an index recommended by the North American Electric Reliability Corporation (NERC) to quantify the grid strength [7], [11]. In the past, SCR was used to analyze the impact of the AC/DC system interactions on the AC-side grid strength involving power electronics interface [9], [12]–[16]. More recently, SCR has been used to analyze the strength of the power grid at POIs of RERs [10], [17]–[23]. The commonly used SCR calculation method ignores the interactions among RERs and thus may lead to an inaccurate estimation of grid strength at the POIs when multiple RERs need to be considered [24]. To take into account the effect of RERs interactions on grid strength, several new methods have been developed, such as the weighted short-circuit ratio (WSCR) method developed by the Electric Reliability Council of Texas (ERCOT) [24], [25] and the Composite

Short-Circuit Ratio (CSCR) method developed by General Electric (GE) [26], [27]. But both CSCR and WSCR calculation methods do not take into account the real electrical network connections among RERs; and therefore, they may not reflect the actual grid strength at the POIs. Also, both CSCR and WSCR methods only provide the aggregated strength of a power grid in the area where the RERs are interconnected electrically close, but they do not calculate the strength of the grid at each individual POIs in the specific area. To overcome those shortcomings, the Site-Dependent Short-Circuit Ratio (SDSCR) method is proposed in [28] by analyzing the relationship between grid strength and voltage stability.

However, it may be computationally challenging for the application of the SDSCR method in large-scale power grids. For instance, at the planning stage of renewable energy integration, considering there are m potential POIs for n RERs integration, there are $\frac{m!}{n!\,(m-n)!}$ combinations of POIs to integrate these RERs. Due to the interactions of RERs, different combinations may have different impacts on grid strength at each POI of those RERs. To identify the weakest combination of those POIs, the SDSCR needs to screen all possible combinations. If m is much larger than n in a realistic power grid (such as $m = 50$ and $n = 5$), there will be a large number of the combinations ($2{,}118{,}800$), which is difficult to be solved within a reasonable amount of time due to the combination nature. This problem could become more prominent if different grid conditions need to be evaluated.

Thus, it is apparent that there is a need for a more efficient and faster method to identify the weakest combinations of POIs without the need to check all of them. In this dissertation, we show that the angle of the impedance ratio plays a critical role in helping us determine which RESs combinations are relevant based on the angle of such an impedance ratio (which will be defined mathematically in Section 2.3.).

2.2. Weakness Analysis Based on Grid Strength Assessment

2.2.1. Grid Strength Assessment

The strength of a power grid at a POI can be evaluated with SCR, which is the ratio of the short circuit capacity at a specific POI to the rated capacity of the RER [26], [29]. When an RER is connected to the power system at POI i, SCR at POI i can be represented as

$$SCR_i = \frac{|S_{ac,\,i}|}{P_{d,\,i}} = \frac{|V_i|^2}{P_{d,\,i}} \frac{1}{|Z_i|} \tag{2.1}$$

Where $|S_{ac,\,i}|$ is the short-circuit capacity of the grid at POI i, $|V_i|$ is the voltage magnitude at POI i, $|Z_{th,\,ii}|$ is the magnitude of Thevenin equivalent impedance at POI i, and $P_{d,\,i}$ is the power injected into POI i. The larger SCR_i, the stronger the grid at POI i. In general, the strength of the power grid at a POI can be quantified using the following SCR ranges: the grid is considered to be strong at a POI if its SCR is larger than 3; the grid is weak at a POI if its SCR is in the range between 2 and 3; and the grid is very weak at a POI if its SCR is smaller than 2 [10], [16], [20].

In the power grid, RERs interact with each other when they are electrically close. As such, their interactions can affect the grid strength of the POIs. However, the effect of the interactions has not been considered in the SCR_i defined in Eq. (2.1). To take into account the effect of the interactions, SDSCR is proposed in [28] by analyzing the relationship between the grid strength and voltage stability in a power grid with a single RER integration and extending the relationship to the power grid with the integration of multiple RERs. The SDSCR is represented as [28]

$$SDSCR_i = \frac{|V_{R,\,i}|^2}{\left| P_{R,\,i} + \sum_{j \in \boldsymbol{R},\, j \neq i} P_{R,\,j}\, w_{ij} \right| |Z_{RR,\,ii}|} \tag{2.2}$$

Where $V_{R,\,i}$ is the voltage at POI i; $|V_{R,\,i}|$ is the magnitude of voltage $V_{R,\,i}$; $P_{R,\,i}$ is the power injected into POI i; $Z_{RR,\,ij}$ is the $(i,\,j)\text{th}$ element in node impedance matrix $\boldsymbol{Z}_{RR}$, which is only related to the nodes connected to RESs; and $\boldsymbol{R}$ is the set of POIs connected with RERs. The weight w_{ij} indicates the interaction among the RER at POI i and other RERs at the remaining POIs. The weight w_{ij} is defined as

$$w_{ij} = \frac{Z_{RR,\,ij}}{Z_{RR,\,ii}} \left(\frac{V_{R,\,i}}{V_{R,\,j}} \right)^{*} \tag{2.3}$$

The SDSCR as defined by Eq. (2.2) has the following features [28]: (1) It takes into account the interactions among RERs through the weight in Eq. (2.3). The effect of other RERs on the grid strength at bus i depends on the ratio of electrical distance $Z_{RR,\,ij}/Z_{RR,\,ii}$ and the ratio of voltages $V_{R,\,i}/V_{R,\,j}$. (2) The SDSCR is the generalized representation of SCR in Eq. (2.1). When only one RER is connected to the power grid, the definition of the SDSCR is the same as that of SCR defined in Eq. (2.1). Thus, it can be concluded that SCR is a special case of SDSCR. Similar to SCR, SDSCR allows for evaluation of the grid strength at each POI when multiple RERs are electrically close in a network area. The ranges of SCR used for system strength evaluation can also be applied to SDSCR.

2.2.2. Challenges of Weakness Analysis Based on Grid Strength Assessment

At the planning stage of renewable energy integration, the SDSCR-based exhaustive search method may need to identify weak POIs to avoid potential weak grid issues. When there are m potential POIs for n RERs integration, there are $\frac{m!}{n!\,(m-n)!}$ combinations of POIs. To identify the weakest combination of POIs from all $\frac{m!}{n!\,(m-n)!}$ combinations, the SDSCR-based exhaustive search method first selects a combination, and in this selected combination the SDSCR at each POI is evaluated. Then, the minimum ratio SDSCR value at all POIs under this selected combination is

used to quantify the weakness of the combination. After all combinations have been screened, the weakest combination of POIs can be identified by ranking all combinations in terms of their weakness. Specifically, the main steps of the exhaustive search method can be briefly summarized as follows

(1) Select the i^{th} combination from $\frac{m!}{n!\,(m-n)!}$ combinations of POIs to conduct grid strength assessment on

(2) Evaluate SDSCR at each POI under the i^{th} combination

(3) Quantify the weakness of the ith combination using the minimum SDSCR value at all POIs under the ith combination

(4) Record the weakness of the i^{th} combination, and let $i = i + 1$. If $i > \frac{m!}{n!\,(m-n)!}$, go to Step (5); otherwise, go back to Step (1)

(5) Identify the weak combination by ranking all combinations of POIs according to their weakness quantified in Step (4)

However, such exhaustive search method becomes computationally challenging when there is a very large number of combinations to be screened in a real power grid (i.e., when m is much larger than n in a realistic power grid). As mentioned in Section 2.5., if $m = 64$ and $n = 5$, the exhaustive search method needs to screen $7{,}624{,}500$ combinations of POIs. As such, this problem is difficult to solve within a reasonable amount of time due to the nature of the combinations. The computational challenge would become more significant when different scenarios need to be evaluated at the planning stage.

To improve the efficiency of this SDSCR-based weakness analysis, we analyze the impact of network structure on grid strength using a vector-based approach then propose a new method for fast weakness analysis based on a simplification of SDSCR (Sections 2.2. and 2.4.).

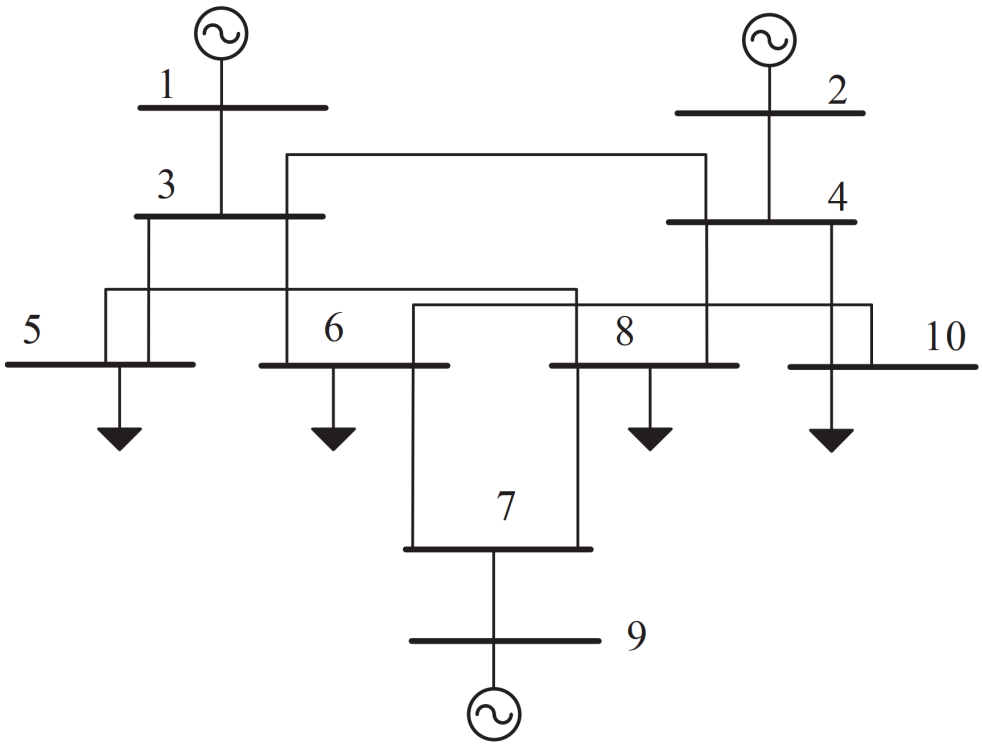

Fig. 2.1. Oneline Diagram of 10-bus System.

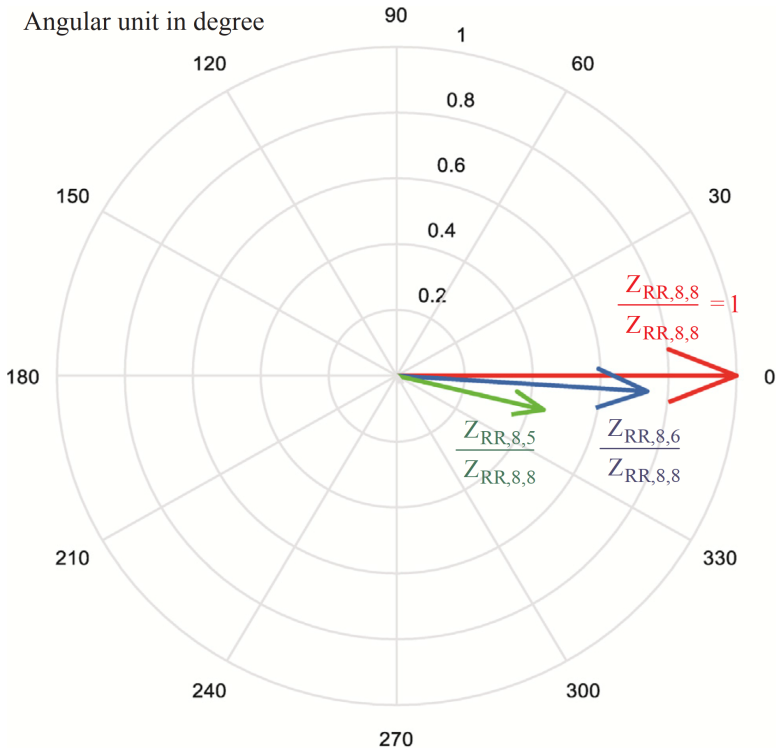

Fig. 2.2. Illustration of impedance ratios $\frac{Z_{RR,ij}}{Z_{RR,ii}}$ at buses 5 and 6 with respect to reference bus 8 in the 10-bus system.

2.3. Impact Analysis of Power Network Structure and its Effect on Grid Strength

To reveal the impact of power network structure on grid strength, SDSCR in Eq. (2.2) is simplified. We assume that renewable energy integration is studied in the stage of power system transmission planning, where it is usual to use normal operating conditions. Thus, the voltage at each POI is close to its nominal value. Under this condition, the voltages at different POIs are close to each other (i.e., $V_{R,i}$ is close to $V_{R,j}$ in Eq. (2.2)). When the same amount of power injections is applied at all potential POIs (i.e., $P_{R,i} = P_{R,j}$ in Eq. (2.2)), we may rewrite SDSCR in Eq. (2.2) as

$$SDSCR_i = \frac{1}{\left|1 + \sum_{j \in \boldsymbol{R},\, j \neq i} \frac{Z_{RR,ij}}{Z_{RR,ii}}\right| P_{R,i} \left|Z_{RR,ii}\right|} \tag{2.4}$$

$$= \frac{1}{\left|\frac{Z_{RR,ii}}{Z_{RR,ii}} + \sum_{j \in \boldsymbol{R},\, j \neq i} \frac{Z_{RR,ij}}{Z_{RR,ii}}\right| P_{R,i} \left|Z_{RR,ii}\right|} \tag{2.5}$$

Eq. (2.4) shows that at a given reference i, grid strength mainly depends on the sum of impedance ratios. Since at the reference i, the Thevenin impedance ratio is a constant equal to 1 (i.e., $\frac{Z_{RR,ii}}{Z_{RR,ii}} = 1$), grid strength actually depends on the sum of the ratios of the transfer impedances $Z_{RR,ij}$ at other POIs to the Thevenin impedance $Z_{RR,ii}$ at the reference i (i.e., $\sum_{j \in \boldsymbol{R},\, j \neq i} \frac{Z_{RR,ij}}{Z_{RR,ii}}$). The larger the sum of impedance ratios (i.e., $1 + \sum_{j \in \boldsymbol{R},\, j \neq i} \frac{Z_{RR,ij}}{Z_{RR,ii}}$) is, the smaller grid strength at given reference i is. Thus, the POIs that have significant impacts on grid strength at the reference i are those that can maximize the sum of impedance ratios regarding the reference i. In other words, a weak combination of POIs regarding this reference POI consists of the reference one itself and all the others that can maximize the sum of the impedance ratios with respect to the reference POI.

To further illustrate the identification method based on impedance ratios, let us consider the example on a 10-bus system as shown in Fig. 2.1. Suppose 2 RERs will be integrated into this grid, and buses 5, 6, and 8 are potential POIs for consideration. To identify the weakest combination of POIs, we can first use the impedance ratios to identify the weakest combinations regarding each reference POI. Then, the top weakest one can be identified by ranking these weakest combinations regarding different reference POIs in terms of their weakness. For example, when bus 8 is chosen as a reference POI, the main steps of the identification method based on impedance ratios can be summarized as follows

(1) Choose a potential POI as a reference such as bus 8

(2) Identify the weakest combination regarding reference bus 8 by comparing the summation of impedance ratios between reference bus 8 and bus 5 (i.e., $1 + \frac{Z_{RR,\,8,\,5}}{Z_{RR,\,8,\,8}}$) with the one between reference bus 8 and bus 6 (i.e., $1 + \frac{Z_{RR,\,8,\,6}}{Z_{RR,\,8,\,8}}$). The weakest combination has the larger summation of impedance ratios

(3) Quantify the weakness of the weakest combination regarding bus by evaluating SDSCR at bus 8

(4) Select another reference bus and repeat Steps (1)–(3) until all 3 potential POIs have been chosen as the reference individually

(5) Identify the top weakest combination by ranking all those weakest combinations regarding each reference buses 8, 5, and 6 in terms of their weakness recorded in Step (3)

In Step (2) as mentioned above, to determine the weak combination of POIs regarding a reference POI, a vector diagram can be used to analyze the impact of impedance ratios on grid strength. For example, Fig. 2.2. shows the vector diagram in which bus 8 is chosen as the reference and each impedance ratio can be represented with a vector: the vector of impedance ratio at the reference bus 8 has magnitude equal to one (i.e., $\frac{Z_{RR,\,8,\,8}}{Z_{RR,\,8,\,8}} = 1$); at the other POIs, the vectors

of impedance ratios have the magnitudes less than one (i.e, $\left|\frac{Z_{RR,8,5}}{Z_{RR,8,8}}\right| < 1$ and $\left|\frac{Z_{RR,8,6}}{Z_{RR,8,8}}\right| < 1$). By analyzing the relative position of these vectors in the diagram, we can identify which POIs have a significant impact on grid strength at reference bus 8. It can be observed from Fig. 2.2. that compared with bus 5, the summation of the impedance ratios at reference bus 8 and bus 6 (i.e. $1 + \frac{Z_{RR,8,6}}{Z_{RR,8,8}}$), has larger magnitude since adding this vector of impedance ratio at bus 6 to the reference vector at bus 8 produces a vector that has a larger magnitude. Thus, the weak combination regarding the bus 8 consists of buses 8 and 6.

As shown in Fig. 2.2., when impedance ratios regarding different POIs are represented with vectors in a diagram, the weakest combination of POIs regarding a reference POI can be identified by analyzing the angles and magnitudes of these vectors in the diagram.

2.3.1. Impact of Impedance Ratio Angles

For impedance ratios with the same magnitudes and different angles, an impedance ratio has a more significant impact on grid strength at reference POI if this impedance ratio has a smaller angular difference to the impedance ratio at the reference POI. This conclusion can be illustrated with Figs. 2.3. and 2.4. In Fig. 2.3., there are four subfigures, in each of which the impedance ratio at the reference POI has the same magnitude (equal to one) and the same angle (equal to zero) due to $\frac{Z_{RR,ii}}{Z_{RR,ii}} = 1$. In addition to the impedance ratio at the reference POI, there are four impedance ratios in these four subfigures of Fig. 2.3. These four impedances located in Quadrants I–IV, respectively, and they have the same magnitude, but different angles. Fig. 2.4. also has four subfigures, in each of which the impedance ratio at the reference POI still has the same magnitude (equal to one) and the same angle (equal to zero) due to $\frac{Z_{RR,ii}}{Z_{RR,ii}} = 1$. In addition, there are eight impedance ratios in these four subfigures of Fig. 2.4. Each two in a subfigure are in the same quadrant with the same magnitude but with different angles.

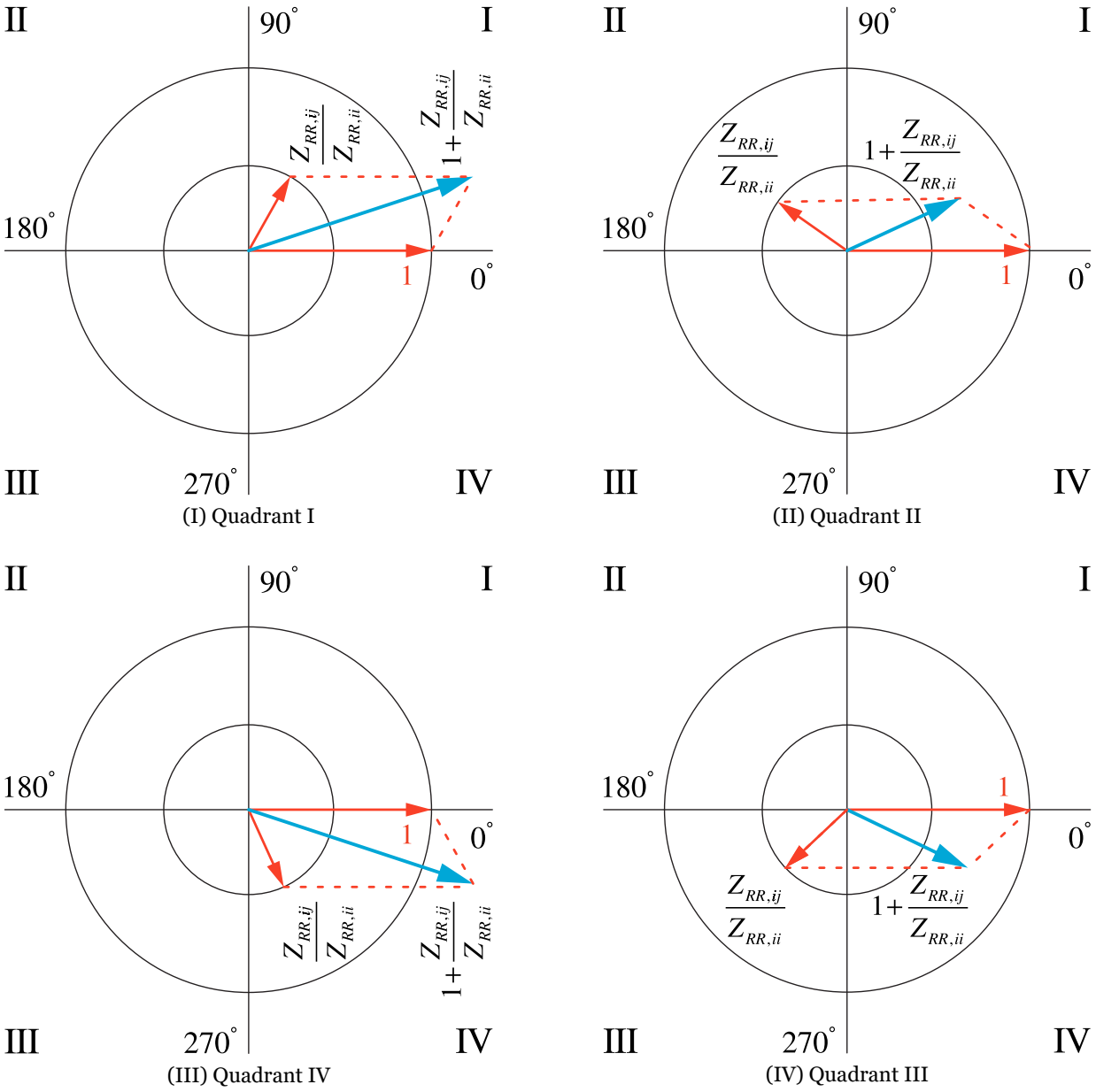

(I) Quadrant I (II) Quadrant II

(III) Quadrant IV (IV) Quadrant III

Fig. 2.3. Impact of an impedance ratio with different angles in different quadrants on grid strength at the reference POI

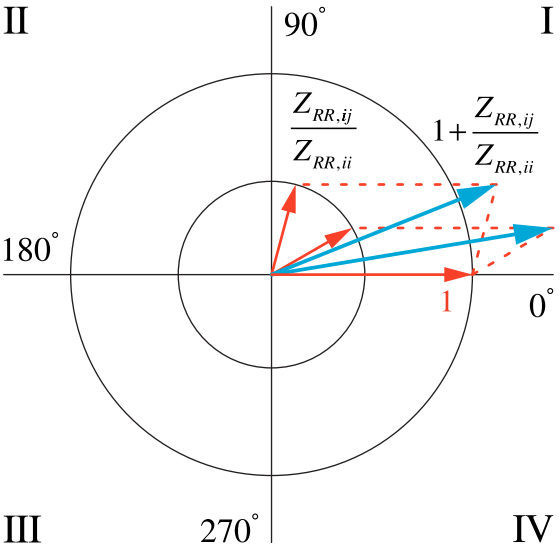

(I) Quadrant I. Varying $\angle\frac{Z_{RR,ij}}{Z_{RR,ii}}$ makes minor differences in $\left|1+\frac{Z_{RR,ij}}{Z_{RR,ii}}\right|$

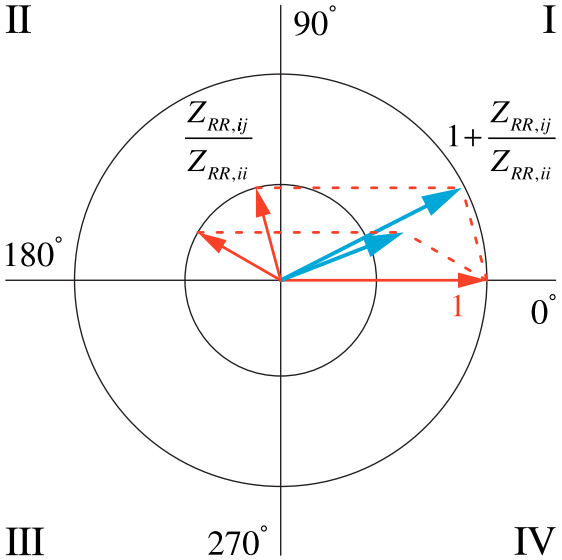

(II) Quadrant II. Varying $\angle\frac{Z_{RR,ij}}{Z_{RR,ii}}$ makes significant differences in $\left|1+\frac{Z_{RR,ij}}{Z_{RR,ii}}\right|$

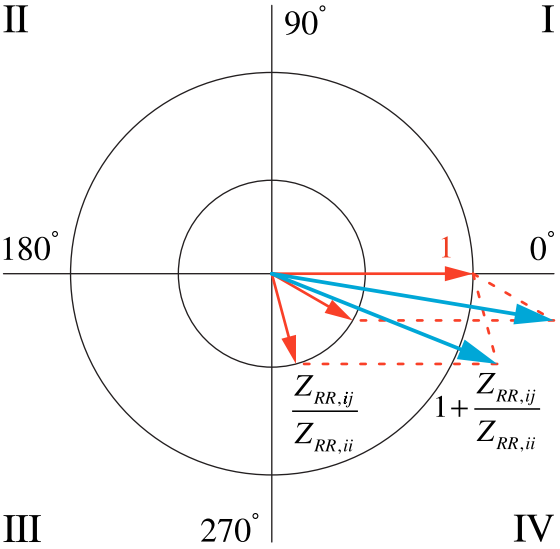

(III) Quadrant IV. Varying $\angle\frac{Z_{RR,ij}}{Z_{RR,ii}}$ makes minor differences in $\left|1+\frac{Z_{RR,ij}}{Z_{RR,ii}}\right|$

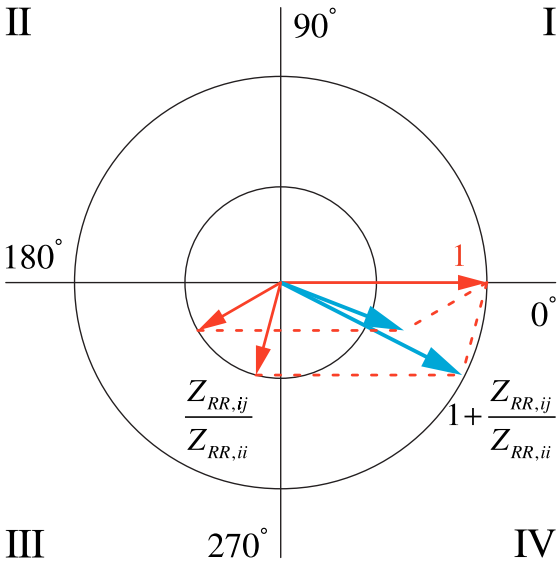

(IV) Quadrant III. Varying $\angle\frac{Z_{RR,ij}}{Z_{RR,ii}}$ makes significant differences in $\left|1+\frac{Z_{RR,ij}}{Z_{RR,ii}}\right|$

Fig. 2.4. Impact of impedance ratios with different angles in the same quadrant on grid strength at the reference POI. Note that in all subfigures, the vector whose angle with respect to the reference is smaller will have larger impact (i.e., the smaller $\angle\frac{Z_{RR,ij}}{Z_{RR,ii}}$ the larger $\left|1+\frac{Z_{RR,ij}}{Z_{RR,ii}}\right|$, thus the larger the (negative) impact on grid strength)

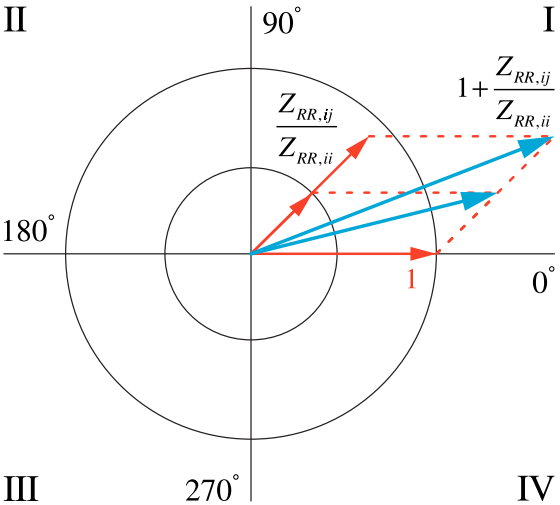

(I) Quadrant I. Varying $\left|\frac{Z_{RR,ij}}{Z_{RR,ii}}\right|$ makes significant differences in $\left|1+\frac{Z_{RR,ij}}{Z_{RR,ii}}\right|$

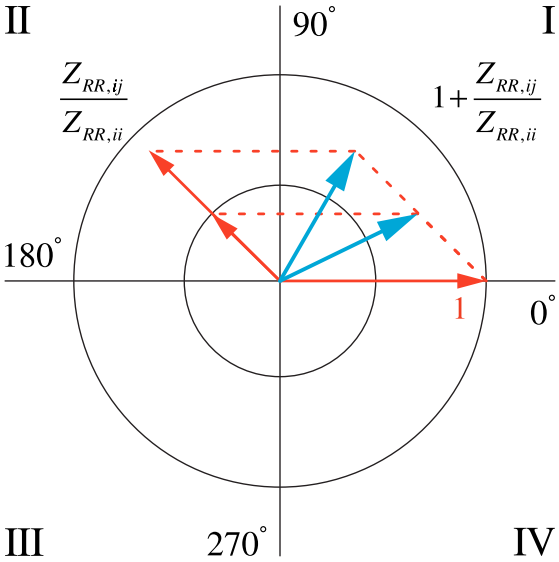

(II) Quadrant II. Varying $\left|\frac{Z_{RR,ij}}{Z_{RR,ii}}\right|$ makes minor differences in $\left|1+\frac{Z_{RR,ij}}{Z_{RR,ii}}\right|$

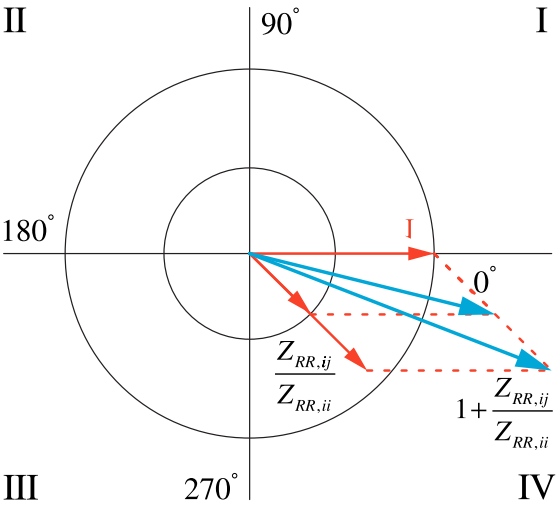

(III) Quadrant IV. Varying $\left|\frac{Z_{RR,ij}}{Z_{RR,ii}}\right|$ makes significant differences in $\left|1+\frac{Z_{RR,ij}}{Z_{RR,ii}}\right|$

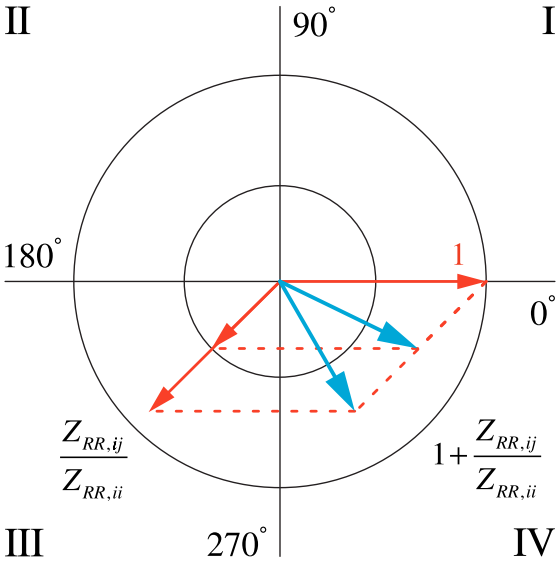

(IV) Quadrant III. Varying $\left|\frac{Z_{RR,ij}}{Z_{RR,ii}}\right|$ makes minor differences in $\left|1+\frac{Z_{RR,ij}}{Z_{RR,ii}}\right|$

Fig. 2.5. Impact of impedance ratios with different magnitudes in the same quadrants on grid strength at the reference POI. The impact varies depending on what quadrant we are in. (i.e., the smaller $\angle\frac{Z_{RR,ij}}{Z_{RR,ii}}$ the larger $\left|1+\frac{Z_{RR,ij}}{Z_{RR,ii}}\right|$, thus the larger the (negative) impact on grid strength)

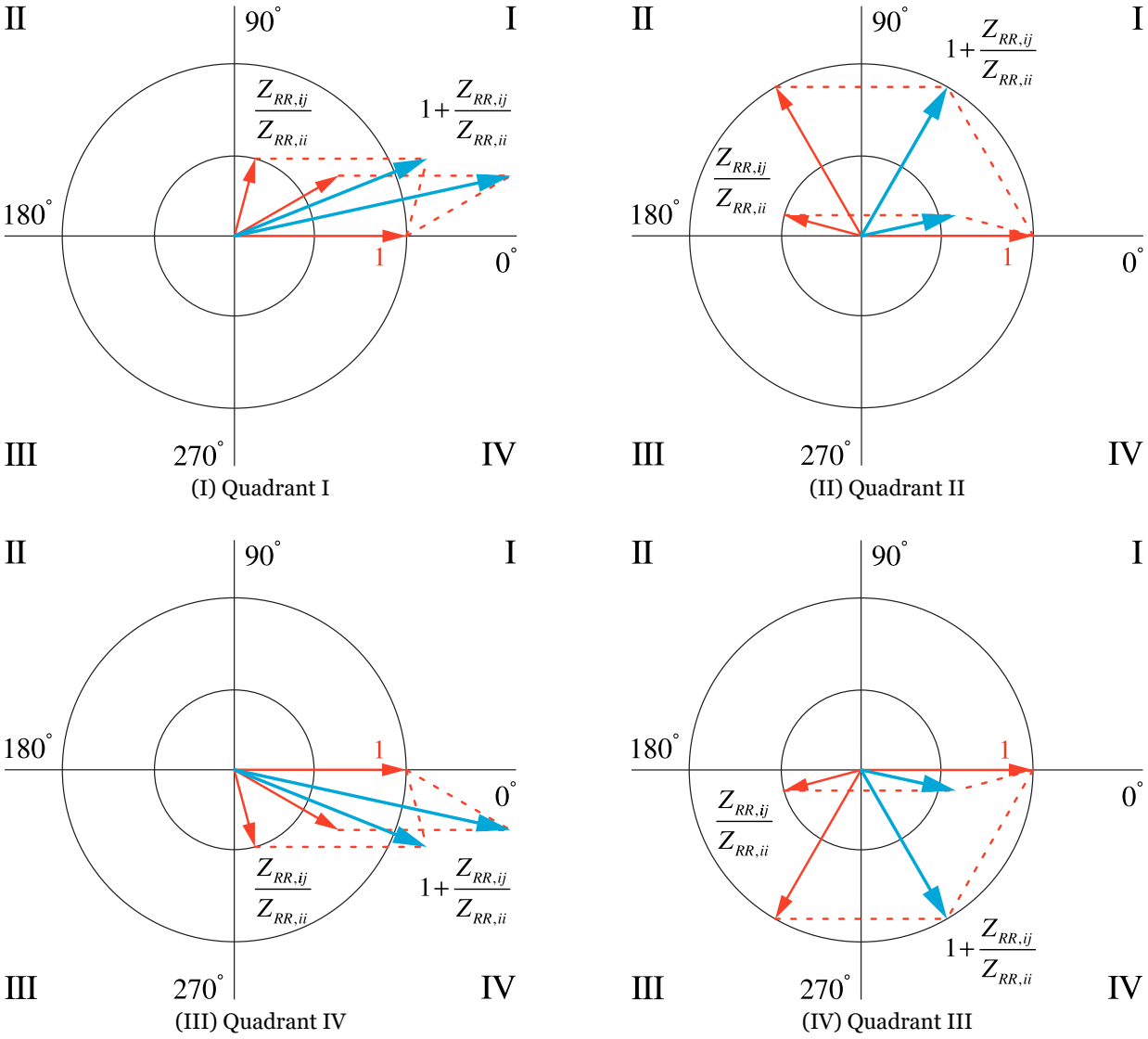

Fig. 2.6. Impact of impedance ratios with different magnitudes and angles in the same quadrants on grid strength at the reference POI.

It can be seen from Fig. 2.3. that compared to the impedance ratio in Quadrants II or III, an impedance ratio in Quadrant I or IV has a smaller angular difference to the impedance ratio at the reference POI. Thus, the impedance ratio in Quadrants I or IV has a more significant impact on grid strength at the reference POI than the one in Quadrants II or III. When the vector of impedance ratio with its angle in Quadrants I or IV is added to the vector of impedance ratio at the reference POI, the sum of the two vectors has larger magnitude.

Furthermore, from Fig. 2.4., we see that vector diagrams in Quadrants I and IV are mirrors of each other around the x-axis. Likewise, the vector diagrams in Quadrants II and III are also mirrors of each other around the x-axis. Thus, whatever applies to Quadrant I also applies to Quadrant IV, while whatever applies to Quadrant II also applies to Quadrant III. However, using Quadrants I and II for illustration is more convenient for most people.

2.3.2. Impact of Impedance Ratio Magnitudes

For impedance ratios with the same angles but different magnitudes in the same quadrant, an impedance ratio in Quadrants I or IV has a more significant impact on grid strength at the reference POI if this impedance ratio has a larger magnitude; an impedance ratio in Quadrants II or III has a more significant impact on grid strength at the reference POI if this impedance ratio has a smaller magnitude. These conclusions can be demonstrated in Fig. 2.5. In Fig. 2.5., there are four subfigures, and each subfigure has the same impedance ratio at the reference POI with the same magnitude (equal to one) and the same angle (equal to zero) due to $\frac{Z_{RR,ii}}{Z_{RR,ii}} = 1$. In addition, there are eight impedance ratios in these four subfigures. In each subfigure, two impedance ratios are located in Quadrants I–IV, respectively.

It can be seen from Fig. 2.5. that in the Quadrant I or IV, an impedance ratio with larger magnitude has a more significant impact on grid strength at reference POI. In the Quadrant I or

IV, when adding this vector of impedance ratio with larger magnitude to the vector of impedance ratio at the reference POI, the resultant vector sum has a larger magnitude. Also, it can be seen from Fig. 2.5. in the Quadrant II or III, an impedance ratio with larger magnitude has a more significant impact on grid strength at reference POI. In the Quadrant II or III, when adding this vector of impedance ratio with smaller magnitude to the vector of impedance ratio at the reference POI, the resultant vector sum has a larger magnitude.

Furthermore, from Fig. 2.5., we see that vector diagrams in Quadrants I and IV are mirrors of each other around the x-axis. Likewise, the vector diagrams in Quadrants II and III are also mirrors of each other around the x-axis. Thus, whatever applies to Quadrant I also applies to Quadrant IV, while whatever applies to Quadrant II also applies to Quadrant III. However, using Quadrants I and II for illustration is more convenient for most people.

2.3.3. Impact of Impedance Ratio Magnitude and Angle

For impedance ratios with different angles and magnitudes, an impedance ratio in Quadrants I or IV has a more significant impact on grid strength at the reference POI than the one in Quadrants II or III. Moreover, in the same quadrant, an impedance has a more significant impact on grid strength at the reference POI if this impedance has a larger magnitude and smaller angular difference to the impedance ratio at the reference POI. These conclusions can be illustrated shown in Fig. 2.6. In Fig. 2.6., there are four subfigures, and each subfigure has the same impedance ratio at the reference POI with the same magnitude (equal to one) and the same angle (equal to zero). In addition, there are eight impedance ratios in these four subfigures. In each subfigure, two impedance ratios are located in Quadrant I–IV respectively, and in the same quadrant, one impedance ratio has larger magnitude and small angular difference to the reference impedance ratio than the other.

It can be seen from Fig. 2.6. that in Quadrants I or IV, an impedance ratio has a more significant impact on grid strength at the reference POI than the impedance ratio in Quadrants II or III. In Quadrants I or IV, even though an impedance ratio has a smaller magnitude, it also has a more significant impact on grid strength at the reference POI than an impedance ratio with larger magnitude in Quadrants II or III. When adding the vector of the impedance ratio with smaller magnitude Quadrants I or IV to the vector of impedance ratio at the reference POI, the resultant vector sum has a larger magnitude.

Also, we see from Fig. 2.6. that in the same quadrant, an impedance with larger magnitude and smaller angular difference to the impedance ratio at the reference POI has a more significant impact on grid strength at the reference POI. In the same quadrant, when adding this vector of impedance ratio with larger magnitude and smaller angular difference into the vector of impedance ratio at the reference POI, the resultant vector sum has a larger magnitude.

Based on the analysis of impedance ratios in vector diagrams, we further investigate the features of impedance ratios at different POIs at different voltage levels in realistic power grids. Typical results are demonstrated in Fig. 2.7.

Criterion I: for POIs that have impedance ratio angles in Quadrants I and IV, the weakest combination of POIs regarding a reference POI can be identified only using the magnitudes of impedance ratios, since in these two quadrants an impedance ratio has a larger magnitude while it has a smaller angular difference to the vector of impedance ratio at the reference POI. As a result, the weakest combination consists of the impedance ratio with larger magnitude and reference impedance ratio. In other words, when the vector of the impedance ratio with a larger magnitude is added to the vector at the reference POI, the vector sum has a larger magnitude, which yields a significant impact on grid strength at the reference POI.

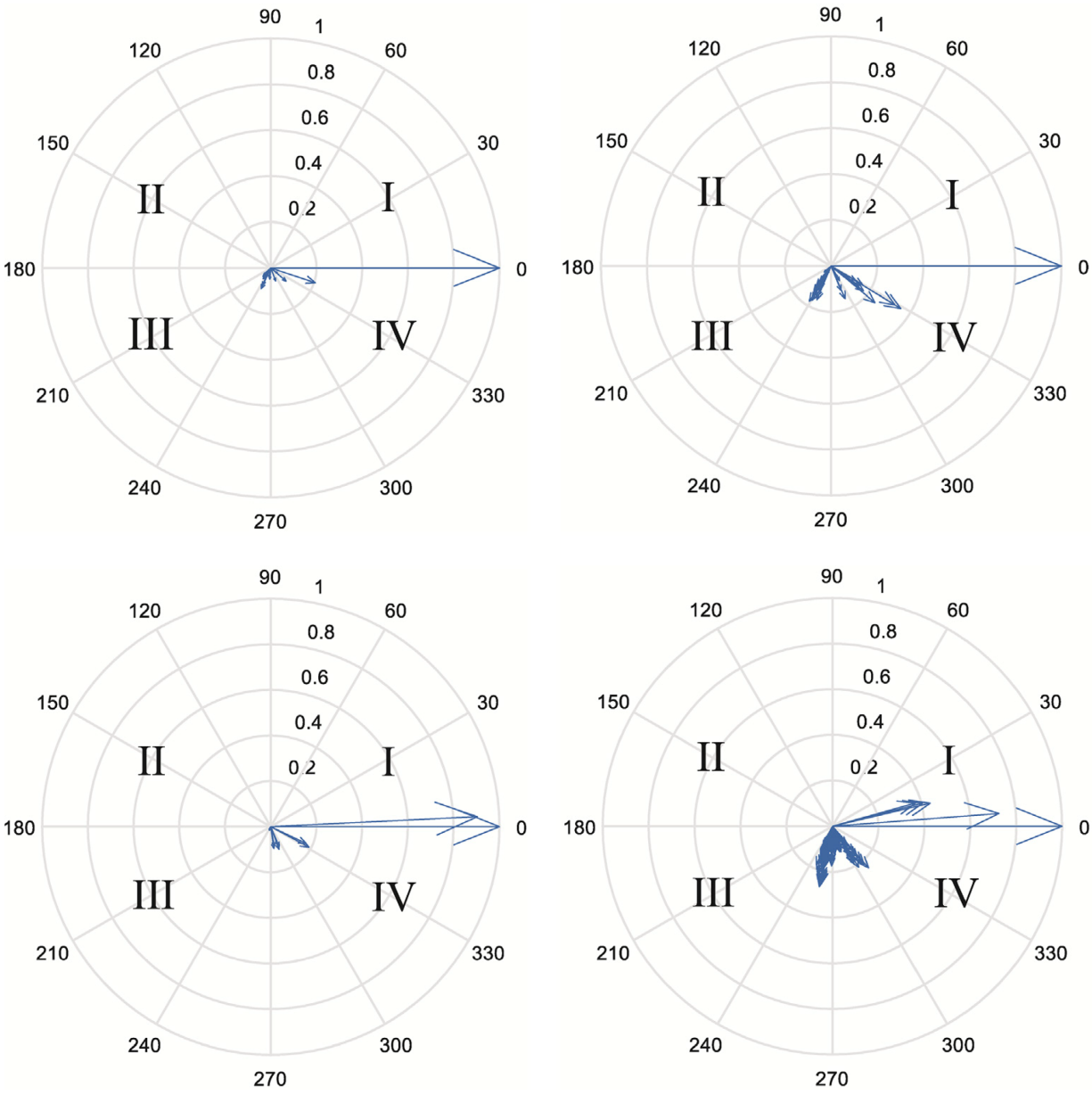

Fig. 2.7. Vector diagrams of the impedance ratios at different POIs with different voltage levels in a realistic power grid.

Criterion II: for POIs that have angles of impedance ratios in Quadrants II and III, the weakest combination of POIs regarding a reference POI can be identified mainly using the impedance ratio angular difference to the impedance ratio at the reference POI, since in the two quadrants the vectors of these impedance ratios have similar magnitudes. Thus, the weakest combination is composed of the impedance ratio with a smaller angular difference to reference impedance ratio. In other words, when the vector of impedance ratio with the smaller angular difference is added to the vector of impedance ratio at the reference POI, the vector sum has a larger magnitude, which has a significant impact on grid strength at the reference POI.

2.4. Proposed Method for Structural Weakness Analysis

Based on the criteria I and II as mentioned above, we propose a recursive method for identifying the weak combination of POIs in a power grid. In the method, the weak combination of POIs regarding each reference POI is first identified based on the criteria I and II; then, the SDSCR at each reference POI within its weak combination is evaluated using Eq. (2.2); finally, the top weakest combination of POIs in a power grid is identified by ranking the SDSCR for all the weak combinations of POIs regarding different reference POIs.

Fig. 2.8. shows the flowchart of the proposed method. It is worth noting that when Criterion I is applied, all impedance ratios of POIs of the weakest combination are located in Quadrants I or IV. However, when Criterion II is applied, impedance ratios of POIs of the weakest combinations contain all the ones in Quadrant I or IV with some others in Quadrant II or III. Considering there are m potential POIs for integrating n RERs $(m > n)$, the main steps of the flowchart are described as follows

Step (1) Select POI i from m potential POIs as the reference POI (note that all m POIs will eventually be selected as references by looping over all of them. This happens in Step (7) where all

candidate POIs must be checked as reference POIs); **Step (2)** Calculate the ratio of the impedance at each of the other POIs to the impedance at the reference POI (i.e., $\frac{Z_{RR,ij}}{Z_{RR,ii}}\ j = 1, 2, \cdots, m$); **Step (3)** Identify the number of POIs that have the angle of impedance ratio in the range $\left[-\frac{\pi}{2},\ \frac{\pi}{2}\right]$ (i.e., in Quadrants I or IV). Let this number be k. If $k \geq (n-1)$, record the identified POIs and then go to Step (4); otherwise, go to Step (5); **Step (4)** According to Criterion I, rank k POIs in terms of the magnitudes of impedance ratios in the order from the largest to the smallest. The weak combination of POIs regarding the reference POI i consists of the top $(n-1)^{th}$ ranked POIs. Then go to Step (7); **Step (5)** According to Criterion II, rank the remaining $(m-k-1)$ POIs in terms of their angles of impedance ratios in the order from the smallest to the largest. Then, go to Step (6); **Step (6)** Identify the weak combination of POIs regarding the reference POI i by combining the k POIs as determined in Step (3) with the top $(n-k-1)$ ranked POIs as determined in Step (4). Then, go to Step (7); **Step (7)** Record the weak combination of POIs for reference POI i and its SDSCR value. If there is still candidate POI needs to be checked, and then go back to Step (1); otherwise, go to Step (8), and **Step (8)** Identify the weakest combination of POIs from the recorded weak combinations of POIs regarding each reference POI i by ranking the SDSCR values as calculated in Step (7) in the order from the smallest to the largest.

Such a procedure is verified in the next sections with a standard power system (IEEE 39-bus) and a realistic one (with 1030 buses).

2.5. Numerical Studies

In this section, the proposed method is validated and compared with the exhaustive search method described in Section 2.3. on the modified IEEE 39-bus system and a realistic power grid. The validation and comparison are carried out on a 2.3-GHz, Intel Core i5-6200U processor on 8GB RAM laptop.

2.5.1. IEEE 39-bus System

To validate the efficacy and efficiency of the proposed method, we consider different cases of RER integration including the integrations of 3 RERs, 4 RERs, and 5 RERs into this system as shown in Fig. 2.8. In these cases, the following 10 buses are chosen as the potential POIs: buses 5, 9, 11, 14, 31, 32, 33, 34, 35, and 36, which are shown with WT symbols connected to them in Fig. 2.9. The generators connected to buses 3136 are removed from this system when these buses are chosen as potential POIs. The original slack generator at bus 31 is replaced with the generator at bus 39. For each case of RER integration, the proposed method is compared with the exhaustive search method in terms of their identification results and computational times. Note that when the exhaustive search method is used to identify the weakest combination, it requires to screen all possible combinations of POIs for each case of RER integration.

TABLE 2.1. shows the total number of all possible combinations of POIs for different cases of RER integration. TABLEs 2.2. to 2.4. present the top five weakest combinations of POIs identified with the exhaustive method and the proposed method for different cases of RER integration.

TABLEs 2.2. to 2.4. also provide the computational times of using those two methods to identify the weakest combinations for each case of RER integration.

TABLE 2.1.
TOTAL COMBINATION NUMBER OF POIS SCREENED USING THE EXHAUSTIVE SEARCH METHOD FOR DIFFERENT CASES OF RER INTEGRATION.

Case No.	Case 1	Case 2	Case 3
Number of integrated RERs	3	4	5
Number of potential POIs	10	10	10
Number of Screened Combinations of POIs	120	210	252

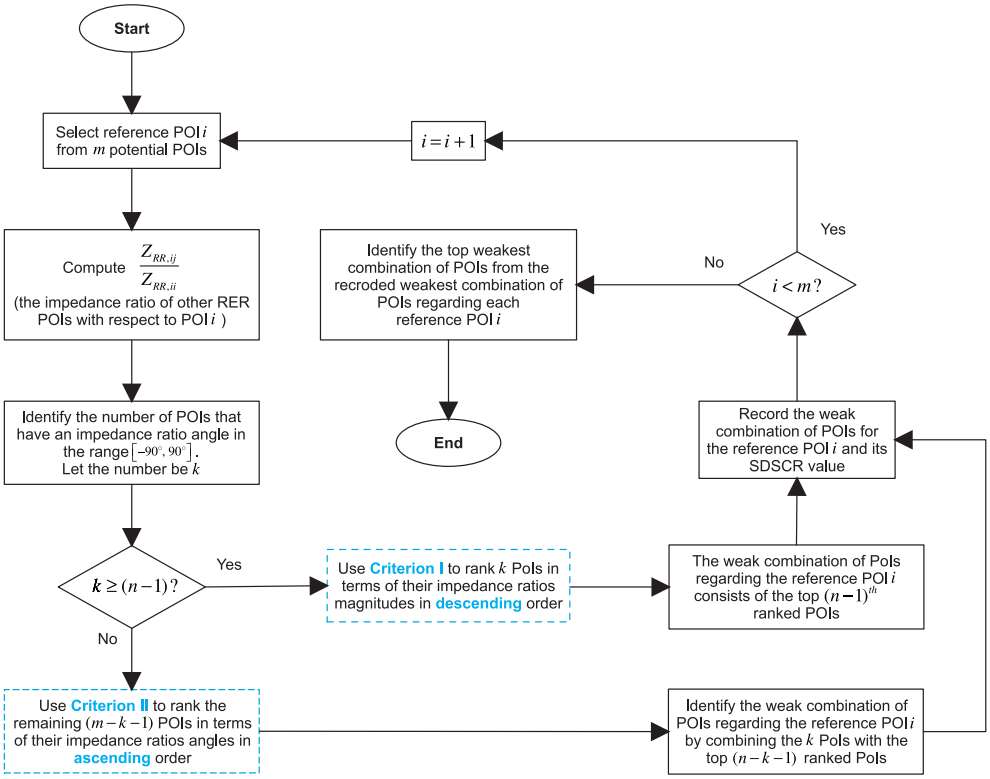

Fig. 2.8. Flowchart of the Proposed Method for Fast Weakness Analysis

TABLE 2.2.
TOP FIVE WEAKEST COMBINATIONS OF POIS IDENTIFIED WITH THE EXHAUSTIVE SEARCH METHOD AND THE PROPOSED METHOD FOR CASE 1.

Exhaustive Search Method				Proposed Method				
Combination of POIs			$SDSCR_{\min}$	Combination of POIs			$SDSCR_{\min}$	Ref. POI
33	**36**	**35**	**4.90**	**33**	**36**	**35**	**4.90**	**36**
34	33	35	5.23	34	33	35	5.23	34
11	5	31	5.63	11	5	31	5.63	11
33	14	35	5.73	33	14	35	5.73	33
14	5	31	5.76	14	5	31	5.76	14
Time 8.80 s				**Time** 0.460 s				

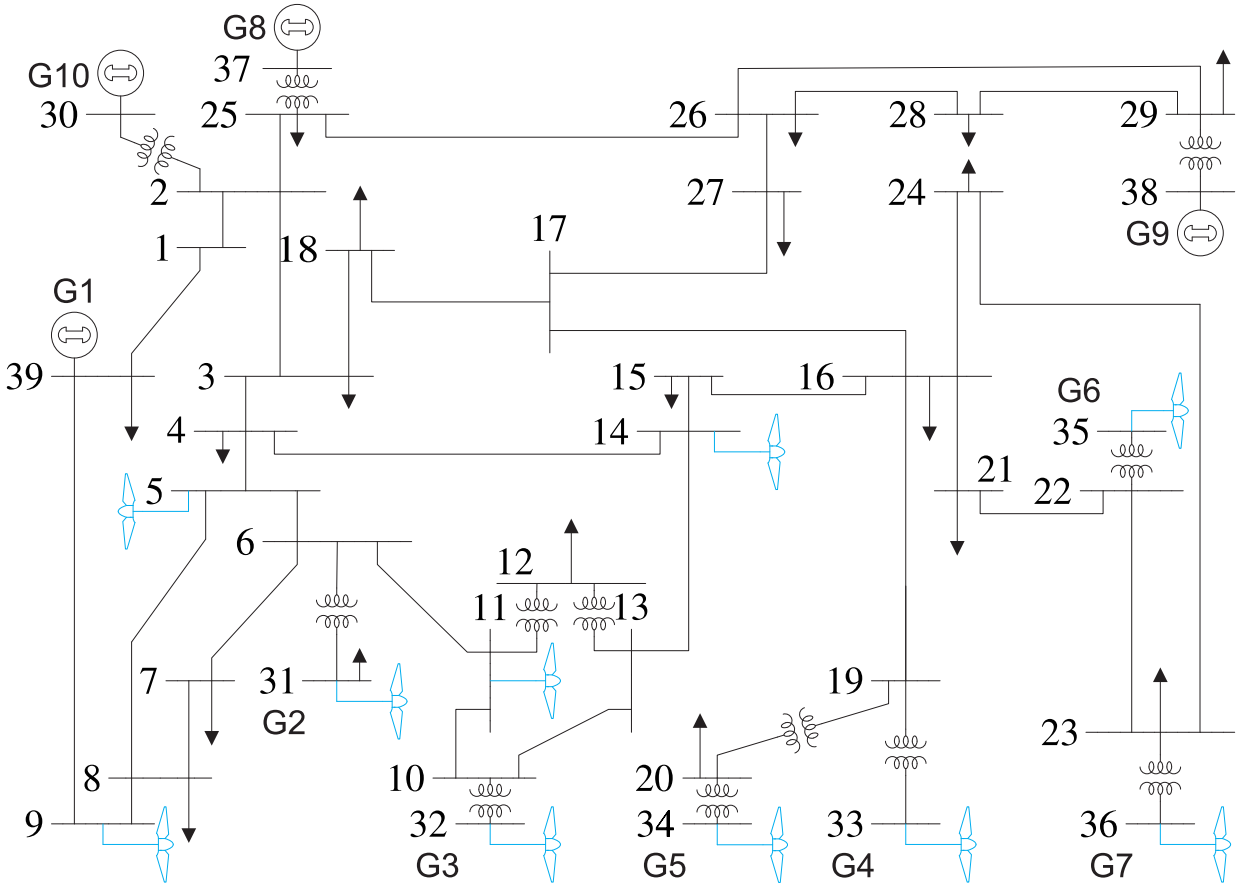

Fig. 2.9. One-line Diagram of the IEEE 39-bus System.

TABLE 2.3.
TOP FIVE WEAKEST COMBINATIONS OF POIS IDENTIFIED WITH THE EXHAUSTIVE SEARCH METHOD AND THE PROPOSED METHOD FOR CASE 2.

Exhaustive Search Method					Proposed Method					
Combination of POIs				$SDSCR_{\min}$	Combination of POIs				$SDSCR_{\min}$	Ref. POI
33	**36**	**14**	**35**	**4.36**	**33**	**36**	**14**	**35**	**4.36**	**36**
34	33	14	35	4.68	34	33	14	35	4.68	34
11	14	32	5	4.86	11	14	32	5	4.86	32
11	5	31	9	4.96	11	5	31	9	4.96	31
33	11	14	35	4.98	33	11	14	35	4.98	35
Time 13.400 s					**Time** 500 ms					

TABLE 2.4.
TOP FIVE WEAKEST COMBINATIONS OF POIS IDENTIFIED WITH THE EXHAUSTIVE SEARCH METHOD AND THE PROPOSED METHOD FOR CASE 3.

Exhaustive Search Method						Proposed Method						
Combination of POIs					$SDSCR_{\min}$	Combination of POIs					$SDSCR_{\min}$	Ref. POI
33	**36**	**14**	**32**	**35**	**4.02**	**33**	**36**	**14**	**32**	**35**	**4.02**	**36**
34	33	14	32	35	4.32	34	33	14	32	35	4.32	34
11	14	32	5	35	4.41	11	14	32	5	35	4.41	32
11	14	5	35	9	4.44	11	14	5	35	9	4.44	11
11	14	5	31	9	4.46	11	14	5	31	9	4.46	31
Time 14.500 s						**Time** 640 ms						

TABLE 2.5.
TOTAL COMBINATION NUMBER OF POIS SCREENED USING THE EXHAUSTIVE SEARCH METHOD FOR DIFFERENT CASES OF RER INTEGRATION.

Voltage Level	69 kV	34.5 kV	13.8 kV
Number of integrated RERs	5	5	5
Number of potential POIs	64	50	46
Number of Screened Combinations of POIs	7,620,000	2,120,000	1,370,000

TABLE 2.6.
TOP FIVE WEAK COMBINATIONS OF POIS AT DIFFERENT VOLTAGE LEVELS IDENTIFIED USING THE EXHAUSTIVE SEARCH METHOD

	Reference POI	Combinations of POIs				$SDSCR_{\min}$	Time
69 kV	**80**	**84**	**76**	**81**	**78**	**1.77**	22 h
	86	84	76	81	78	1.79	
	86	80	84	81	78	1.80	
	86	80	76	81	78	1.83	
	86	80	84	76	78	1.85	
34.5 kV	**1008**	**926**	**925**	**885**	**884**	**2.65**	6 h
	1008	926	917	885	884	2.68	
	1008	926	916	885	884	2.76	
	1008	925	917	885	884	2.85	
	1008	925	916	885	884	3.06	
13.8 kV	**969**	**998**	**1001**	**1003**	**1000**	**1.20**	4 h
	969	939	1017	1003	1020	1.22	
	969	939	1017	1003	1022	1.42	
	969	939	1017	1003	1001	1.60	
	969	939	1017	1003	976	1.82	

TABLE 2.7.
TOP FIVE WEAK COMBINATIONS OF POIS AT DIFFERENT VOLTAGE LEVELS IDENTIFIED USING THE PROPOSED SEARCH METHOD

	Reference POI	Combinations of POIs				$SDSCR_{\min}$	Time
69 kV	**78**	**81**	**84**	**76**	**80**	**1.77**	2.50 h
	76	81	84	86	78	1.79	
	80	78	84	86	81	1.80	
	86	76	80	78	81	1.83	
	84	76	80	78	86	1.85	
34.5 kV	**1008**	**885**	**884**	**926**	**925**	**2.65**	0.830 h
	917	885	1008	926	884	2.68	
	926	1008	885	884	916	2.76	
	925	917	885	884	1008	2.85	
	916	925	885	884	1008	3.06	
13.8 kV	**969**	**1003**	**1000**	**1001**	**998**	**1.20**	0.530 h
	1020	1003	1017	969	939	1.22	
	1022	939	969	1003	1017	1.42	
	1001	1003	1017	939	969	1.60	
	976	1017	939	1003	969	1.82	

It can be observed from TABLEs 2.2. to 2.4. that the proposed method and the exhaustive method have the same identification results for various cases of RER integration. For example, when 5 RERs are integrated into this system, the exhaustive search method evaluates SDSCR at every POI under each of all 252 combinations (as shown in TABLE 2.1.); then, the method quantifies the weakness of each combination using the minimum SDSCR evaluated at all POIs under the same combination; finally, the top weakest combination is identified by ranking the weakness of all combinations. As shown in TABLE 2.4., the top weakest combination is the one consisting of buses 33, 36, 14, 32, and 35 since its weakness (i.e., the minimum SDSCR at all POIs under this combination) is 4.02, which is smaller than the other fours. The proposed method also identifies the same weakest combination of POIs and provides the same SDSCR for this combination. However, the procedure of the proposed method is different from the exhaustive search method. The proposed method first identifies the weakest combinations regarding each reference POI using the impedance ratios based on the two criteria summarized in Section 2.3.; then, the method quantifies the weakness of each weakest combination regarding a reference POI in term of the SDSCR evaluated at the reference; finally, the top weakest combination is identified by ranking the weakness of all weakest combination regarding each reference POI. As shown in TABLE 2.4., the top weakest combination consists of buses 33, 36, 14, 32, and 35, and its weakness (i.e., the SDSCR evaluated at the reference bus 36 under this combination) is 4.02, which is smaller than the other four weakest combinations at the other reference buses. From TABLEs 2.2. to 2.4., the same observation can be obtained for the other cases of RER integration.

More importantly, it can be seen from TABLEs 2.2. to 2.4. that the proposed method is more efficient than the exhaustive search method from the computational perspective. For example, for the case of 5 RER integration, the exhaustive method needs to screen all 252 (as shown

in TABLE 2.1.) combinations of POIs to identify the top weakest combination. Moreover, under the same combination, the SDSCR at each POI needs to be evaluated so that the weakness of the combination can be quantified with the minimum SDSCR at all POIs for the weakest combination identification. As shown in TABLE 2.4., the exhaustive search method takes 14.5 s to identify the top weakest combination. The time is much greater than 0.64 s taken by the proposed method. The proposed method takes less time since it can avoid screening all 252 combination using impedance ratios. Moreover, it only evaluates SDSCR at reference POI for quantifying the weakness of the corresponding weakest combination. When considering the other cases of RER integration, it can be also seen from TABLEs 2.2. to 2.4. that the proposed method takes much less computational times than the exhaustive method.

2.5.2. A Real Power Grid

To further validate the efficacy and efficiency of the proposed method, we compare the proposed method with the exhaustive method in a realistic power grid consisting of 1334 lines and 1030 buses. It is assumed that a total of 15 RERs are integrated into this grid at different POIs with different voltage levels: 5 RERs are connected to $69\,\mathrm{kV}$ POIs, 5 RERs are connected to $34.5\,\mathrm{kV}$ POIs, and the remaining 5 RERs are connected to $13.2\,\mathrm{kV}$ POIs. Total numbers of potential POIs for the RERs integration at each voltage level are 64, 50, and 46. TABLE 2.5. shows the total number of all possible combinations of POIs required to be screened using the exhaustive search method. TABLEs 2.6. and 2.7. present the identification results and computational times of the exhaustive search method and the proposed method, respectively. Similar to the observation from the IEEE 39-bus system, we observe from TABLEs 2.6. and 2.7. that both exhaustive search method and the proposed method identify the same the weakest combinations of POIs at different voltage levels. As shown in TABLE 2.6., at $69\,\mathrm{kV}$ voltage level, the exhaustive

search method identifies the weakest combination of POIs consisting of buses 80, 84, 76, 81 and 78, and its weakness (i.e., the minimum SDSCR at all POIs under this combination) is 1.77. As shown in TABLE 2.7., at the same $69\,\mathrm{kV}$ voltage level, the proposed method also identifies the same weakest combination and provides the same SDSCR at the reference bus 78 under the same combination. From TABLEs 2.6. and 2.7., the same observation can be obtained for POIs at the other two voltage levels $34.5\,\mathrm{kV}$ and $13.8\,\mathrm{kV}$.

More clearly, it can be seen from TABLEs 2.6. and 2.7. that the proposed method is much more efficient than the exhaustive search method in such a large power grid. As shown in TABLE 2.6., the exhaustive method needs to screen a large number of combinations of POIs at each voltage level, but the proposed method can avoid screening such a large number of combinations by taking the advantage of the information derived from power network structure. For example, at $69\,\mathrm{kV}$ voltage level, the exhaustive search method needs to screen $7{,}620{,}000$ combinations of POIs to identify the weakest combination; while the proposed method can avoid screening such a large number of combinations. As a result, to identify the same weakest combination, the proposed method only needs $2.50\,\mathrm{h}$, which are much less than $22\,\mathrm{h}$ consumed by the exhaustive search method.

2.6. Conclusions

In this dissertation, we investigated the impact of power network structure on grid strength while taking into account the interactions among RERs interconnected through power networks. It is found that the impact of the interactions among RERs through power network structure on grid strength at a POI mainly depends on the ratios of two types of impedances: **a)** the transfer impedances between the reference POI and each of the remaining POIs in the power grid and, and **b)** the Thevenin impedance at the reference POI. Furthermore, the identification of a weak

combination of POIs regarding a reference POI can be implemented by searching POIs that can maximize the sum of impedance ratios regarding the reference POI.

It is found that the magnitudes and angles of the impedance ratios have different impacts on grid strength, and those impacts can be summarized as two criteria for fast identifying the weak combination of POIs. Based on the two criteria, a recursive method was developed for fast weakness analysis. The efficacy of the proposed method is demonstrated on the IEEE 39-bus system and a realistic power grid.

2.7. References

[1] S. Achilles, A. Isaacs, J. MacDowell, and C. Smith, "Integrating Inverter-Based Resources into Low Short Circuit Strength Systems," NERC, Tech. Rep., Dec. 2017.

[2] F. Zhou, G. Joos, and C. Abbey, "Voltage stability in weak connection wind farms," in *Power Engineering Society General Meeting, 2005. IEEE*, IEEE, 2005, pp. 1483–1488.

[3] R. Piwko, N. Miller, *et al.*, "Integrating large wind farms into weak power grids with long transmission lines," in *Power Electronics and Motion Control Conference, 2006. IPEMC 2006. CES/IEEE 5th International*, IEEE, vol. 2, 2006, pp. 1–7.

[4] S.-H. Huang, J. Schmall, *et al.*, "Voltage control challenges on weak grids with high penetration of wind generation: ERCOT experience," in *Power and Energy Society General Meeting, 2012 IEEE*, IEEE, 2012, pp. 1–7.

[5] L. Wang, C.-J. Yeh, M.-H. Hsieh, C.-T. Wu, and C.-L. Lu, "Analysis of voltage variations and short-circuit ratios of a large-scale offshore wind farm connected to a practical power system," in *Power and Energy Society General Meeting (PES), 2013 IEEE*, IEEE, 2013, pp. 1–5.

[6] Lovelace, Will. (Nov. 11, 2015). Low SCR Wind Integration and Mitigation, Minnkota Power Cooperative, [Online]. Available: http://www.cce.umn.edu/documents/CPE-Conferences/MIPSYCON-PowerPoints/2015/PGLowSCRWindGenerationInstabilityIdentificationandMitigation.pdf (visited on 05/20/2019).

[7] C. Moné, A. Smith, B. Maples, and M. Hand, "Essential Reliability Services Task Force Measures Framework Report," NERC, Tech. Rep., Nov. 2015.

[8] *Connection of Wind Farms to Weak AC Networks*, CIGRE Brochure, Dec. 2016. [Online]. Available: https://e-cigre.org/publication/671-connection-of-wind-farms-to-weak-ac-networks (visited on 05/20/2019).

[9] H. Urdal, R. Ierna, *et al.*, "System strength considerations in a converter dominated power system," *IET Renewable Power Generation*, vol. 9, no. 1, pp. 10–17, 2014.

[10] A. S. Subburaja, N. Shamim, and S. B. Bayne, "Battery Connected DFIG Wind System Analysis for Strong/Weak Grid Scenarios," in *Green Technologies Conference (GreenTech), 2016 IEEE*, IEEE, 2016, pp. 112–117.

[11] NERC, "Short-Circuit Modeling and System Strength," NERC, Tech. Rep., Feb. 2018.

[12] P. Krishayya, R. Adapa, M. Holm, *et al.*, "IEEE guide for planning DC links terminating at AC locations having low short-circuit capacities, part I: AC/DC system interaction phenomena," *IEEE Std. France: CIGRE*, 1997.

[13] A. Gavrilovic, "AC/DC system strength as indicated by short circuit ratios," in *AC and DC Power Transmission, 1991., International Conference on*, IET, 1991, pp. 27–32.

[14] J. Chen-chen, W. Jun, and B. Xiao-yu, "Study of the effect of AC system strength on the HVDC startup characteristics," 2012.

[15] S. L. Lorenzen, A. B. Nielsen, and L. Bede, “Control of a grid connected converter during weak grid conditions,” in *Power Electronics for Distributed Generation Systems (PEDG), 2016 IEEE 7th International Symposium on*, IEEE, 2016, pp. 1–6.

[16] *Integration of large Scale Wind Generation using HVDC and Power Electronics*, CIGRE Brochure, 2009. [Online]. Available: https://e-cigre.org/publication/370-integration-of-large-scale-wind-generation-using-hvdc-and-power-electronics (visited on 06/02/2019).

[17] S. Grunau and F. W. Fuchs, “Effect of wind-energy power injection into weak grids,” in *Proc. EWEA*, 2012, pp. 1–7.

[18] Y. Zhou, D. Nguyen, P. Kjaer, and S. Saylors, “Connecting wind power plant with weak grid-Challenges and solutions,” in *Power and Energy Society General Meeting (PES), 2013 IEEE*, IEEE, 2013, pp. 1–7.

[19] G. Liu, X. Cao, *et al.*, “Adaptive control strategy to enhance penetration of PV power generations in weak grid,” in *Power Electronics and Application Conference and Exposition (PEAC), 2014 International*, IEEE, 2014, pp. 1217–1221.

[20] M. Bassini, M. Horita, J. Jardini, and M. Davies, “Assessment of enabling technologies for the connection of wind farms to weak AC networks,” *CIGRE Science and Engineering*, vol. 6, 2016.

[21] M. Hong, H. Xin, *et al.*, “Critical Short Circuit Ratio Analysis on DFIG Wind Farm with Vector Power Control and Synchronized Control,” *Journal of Elctrical Engineering Technology*, vol. 11, 2016.

[22] N. W. Miller, B. Leonardi, R. D'Aquila, and K. Clark, "Western wind and solar integration study phase 3a: Low levels of synchronous generation," National Renewable Energy Lab.(NREL), Golden, CO (United States), Tech. Rep., 2015.

[23] Y. Zhu and D. Brown, "Prepare to meet the challenges in regional transmission planning and development," in *2015 IEEE Power Energy Society General Meeting*, Jul. 2015, pp. 1–5.

[24] Y. Zhang, S.-H. F. Huang, *et al.*, "Evaluating system strength for large-scale wind plant integration," in *PES General Meeting| Conference & Exposition, 2014 IEEE*, IEEE, 2014, pp. 1–5.

[25] J. Schmall, S.-H. Huang, *et al.*, "Voltage stability of large-scale wind plants integrated in weak networks: An ERCOT case study," in *Power & Energy Society General Meeting, 2015 IEEE*, IEEE, 2015, pp. 1–5.

[26] R. Fernandes, S. Achilles, and J. MacDowell, "Report to NERC ERSTF for Composite Short Circuit Ratio (CSCR) Estimation Guideline," GE, Tech. Rep., Jan. 2015.

[27] Grant, "Report in the Matter of Integration and Transmission Study for the Future Renewable Energy Standard," Minnesota Department of Commerce, Tech. Rep., Nov. 2014.

[28] D. Wu, G. Li, *et al.*, "Assessing Impact of Renewable Energy Integration on System Strength Using Site-Dependent Short Circuit Ratio," *IEEE Transactions on Sustainable Energy*, 2017.

[29] J. Schmall, S.-H. Huang, *et al.*, "Voltage stability of large-scale wind plants integrated in weak networks: An ERCOT case study," in *Power & Energy Society General Meeting, 2015 IEEE*, IEEE, 2015, pp. 1–5.

CHAPTER 3. MODELING SERIES COMPENSATION EFFECT ON THE BUS IMPEDANCE MATRIX FOR ONLINE APPLICATIONS [1]

3.1. Introduction

The Bus Impedance Matrix ($\boldsymbol{Z}_{bus}$) is a matrix that characterizes the relationship between current injections and voltages in a system. $\boldsymbol{Z}_{bus}$ contains diagonal elements called *driving point impedances* or *self impedances*. These are the equivalent impedances between each bus and the reference bus [1], and they are the same as the Thevenin impedances of each bus. Thus, the diagonal elements reflect important characteristics of the entire system as seen from each corresponding bus [2]. The off-diagonal elements are called *transfer impedances*, and they are less intuitive to understand. They are parameters for every possible combination of two buses of the system (excluding any combination that has the reference bus in it) which are defined as the ratio of the voltage at certain bus over the current injection into another bus (say bus m) when all current injections, except the one at m, are set to zero [1].

The conventional use of $\boldsymbol{Z}_{bus}$ is calculation of fault current in interconnected systems. More recent works show that $\boldsymbol{Z}_{bus}$ contains very useful structural characteristics information that

---

1. The material in this chapter (doi: https://doi.org/10.1016/j.epsr.2019.105890) was authored by Al-Motasem Aldaoudeyehand co-authored by Di Wu.
Al-Motasem Aldaoudeyehwas responsible for math derivation, analyzing math results, data collection, code writing, simulation, writing the bulk of the manuscript, and answering reviewers' questions.
Di Wuprovided intellectual input, checked the integrity of math derivations, checked soundness of reasoning, revised and edited the manuscript, and answered reviewers' questions.

we could employ in loss allocation in deregulated environments [3], voltage stability margin estimation [4], determination of system strength of Renewable Energy Sources (RESs) buses [5], contribution of generators participation levels to the voltage of buses [6], real time overload relief of transmission lines [7], fault location in transmission networks [8], [9], modeling voltage controllers in load flow [10], and harmonic sources identification [11].

The motivation of the paper is summarized in short here. Then we follow up with examples from the literature 1. many researchers develop methods that employ $\boldsymbol{Z}_{bus}$ or a part of its elements in the analysis, identification, allocation, etc. Some of these achievements can be more beneficial if an online version of them is developed and deployed, 2. clearly, in real-life operation of a power system, the structure of the system changes, and one these changes could be the continuous variation of the series impedance of branches (e.g., using thyristor controlled series capacitor), 3. as a result, the methods developed before must update $\boldsymbol{Z}_{bus}$ as they work in real--time, 4. the change of the series impedance of a line requires too much of computational effort and time with the existing methods to find the new $\boldsymbol{Z}_{bus}$ which slows down making estimations, corrective actions, preparing for vulnerabilities, etc, 5. thus, developing a new method to increase the speed of constructing $\boldsymbol{Z}_{bus}$ would help mitigate these computational impediments.

Su and Liu [4] express the voltage of a given bus i with an expression that includes what they label as "coupling term" that depicts the effect of other loads (and generation) on bus i voltage. Such coupling term includes the transfer impedance of each bus with respect to bus i. The authors then develop their method to identify the stability margin based on the impedance matching concept. If such a method of stability margin is to be deployed for real-time monitoring of stability margin, then it must calculate $\boldsymbol{Z}_{bus}$ again each time the series compensation of a line varies during a real-life operation of power systems.

However, present methods take a long time to find $\boldsymbol{Z}_{bus}$. After a few minutes of calculations, the load levels may change. Thus we end up not being able to find the stability margin in a timely manner. It is also possible that series compensation changes again, which makes it hard to get an accurate estimation for a long time. Wu *et al.* [5] develop Site-Dependent Short Circuit Ratio (SDSCR) to estimate system strength at RES buses while incorporating the effect of interactions among RESs. The SDSCR is an index that includes $\boldsymbol{Z}_{bus}$ elements related to RES buses, and real-time application of SDSCR may face the same impediment (as we calculate the new $\boldsymbol{Z}_{bus}$, RESs power injections change and series compensation changes, preventing us from getting strength estimation in a timely manner). We could face similar situations in the real-time application of finding contributions of generators to bus voltages [6], and real-time overload relief of transmission lines [7]. This is not to say that the previously cited solutions are deficient. It is just an explanation as to why computational difficulties could limit our ability to attain the benefits of these techniques and fulfill their purpose by lifting computational impediments.

Building $\boldsymbol{Z}_{bus}$ by direct construction rather than by inverting $\boldsymbol{Y}_{bus}$ dates earlier than the 1960s [12]. The method is summarized rigorously by Homer Brown in 1985 [1]. Since then, to our best knowledge, there has been little efforts to advance the theoretical knowledge of such an important aspect. Makram and Girgis [13] develop $\boldsymbol{Z}_{bus}$ building technique that expands the work in [1] to account for the unequal mutual coupling of feeders, making it suitable for unbalanced fault calculations. Makram and Girgis [13] expand their work in [14] by introducing a formulation amenable to use in the presence of harmonic distortion.

Saxena and Rao [15] devise a new algorithm to calculate $\boldsymbol{Z}_{bus}$ based on rearranging the numbers of buses and classifying branches into two types (i.e, branches and chords) and some cluster of branches, buses, and impedances into what is called ‘cantilever sub-networks’. Similar

to Brown method, the method proposed here begins with one bus connected to the reference node, but the proposed algorithm carefully selects the branches to add such that it reduces the number of the needed arithmetic calculations.

Ou and Lin [16] define variations of $\boldsymbol{Z}_{bus}$ to make the work amenable for certain applications. It provides a mathematical formulation of current-voltage relationships in terms of currents flowing in lines (compared to currents injections into buses in the traditional definition of $\boldsymbol{Z}_{bus}$). The matrix is denoted as $\boldsymbol{Z}_{\mathrm{V-BC}}$. Ou and Lin [16] then describe how to construct $\boldsymbol{Z}_{\mathrm{V-BC}}$ using the same four types of modifications in Brown's method, but with some differences on how each type is handled mathematically. Load flow analysis is then done to show the benefit of such formulation in making the solution robust against divergence.

One contribution of this dissertation is to develop a new technique to modify $\boldsymbol{Z}_{bus}$ of a network after a change in the series impedance of a line connected between a particular pair of buses. Such changes in line impedances often take place during system operation, and hence, one needs to have a $\boldsymbol{Z}_{bus}$ re-computation that is both fast and accurate. A new idea we present in this dissertation is to account for series compensation effect on $\boldsymbol{Z}_{bus}$. We do this by inserting a new impedance in parallel with the preexisting branch of interest. After some mathematical formulation, we get a new expression where the change in the impedance of the preexisting branch is given explicitly in the equations. The aforementioned helps us calculate changes in $\boldsymbol{Z}_{bus}$ on an element-by-element basis. However, we also provide vector-based formation that is more amenable to modify the entire $\boldsymbol{Z}_{bus}$ without re-building it from scratch to model the effect of series compensation on it. Such a vector-based formation is amenable for numerical softwares such as MATLAB. Thus, engineers who are familiar with such softwares can easily employ it in their analysis or design.

3.2. Brown Method for Constructing Bus Impedance Matrix

A conceptually simple method to find $\boldsymbol{Z}_{bus}$ is by inverting $\boldsymbol{Y}_{bus}$. Such a method has two major drawbacks: 1. matrix inversion is computationally intensive and requires a lot of memory and 2. ill-conditioning and round-off errors. Thus, for large systems, it is almost always better to build $\boldsymbol{Z}_{bus}$ by analyzing the relationship between currents and voltages. Even though it is utterly impossible to build $\boldsymbol{Z}_{bus}$ directly for a pre-existing system, it is still possible to build it by 1) starting from one bus connected to the reference node (usually the ground) via a shunt admittance, 2) expanding $\boldsymbol{Z}_{bus}$ by adding one series impedance or shunt admittance at a time, and 3) each time we add a new element, we augment or modify the preceding matrix to an updated one. Such procedure is used in Brown's method, which finds $\boldsymbol{Z}_{bus}$ by direct construction and is described in detail in [1], [2], [13], [14], [17]. Brown's method depends on a careful examination of the current-voltage relationship changes for possible modifications in the system. Four basic cases are defined in Brown's method, all of which include adding a branch whose impedance is Z_b as follows: **a)** From a new bus k to the reference node; **b)** From an existing bus k to a new bus p; **c)** From an existing bus k to the reference node, and **d)** From an existing bus k to an existing bus p.

In some cases (e.g., series compensation of transmission lines), the reactance of the line changes. In Brown modeling technique, the network sees this as a change of the impedance of a branch between two existing buses. However, none of the previously mentioned cases in Brown's method provides means to modify a pre-existing $\boldsymbol{Z}_{bus}$ to account for the change of the series impedance of a branch. Thus, we must reconstruct $\boldsymbol{Z}_{bus}$ all over again. In this dissertation, we extend Brown's method to include a fifth case: the change of existing branch Z_b^{old} between two existing buses k and p. To our best knowledge, even the most recent works that extensively use

$\boldsymbol{Z}_{bus}$ (such as [6], [18], [19]) do not address the previously mentioned case. Filling a gap in the literature, we do that in Section 3.3.

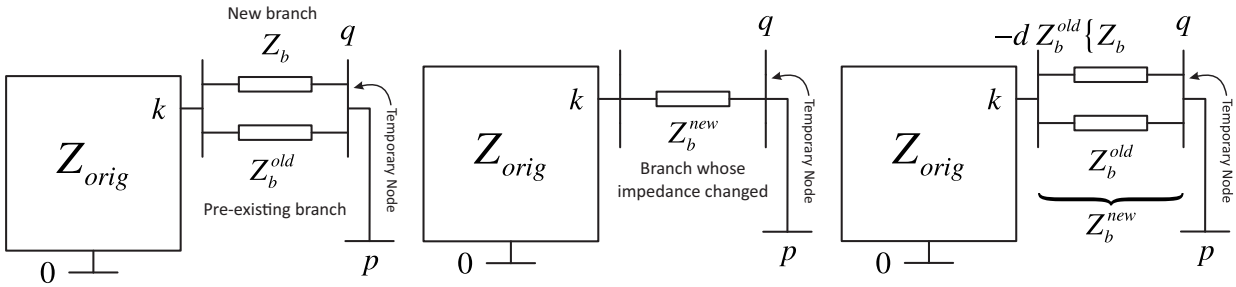

(I) Modeling the addition of branch Z_b between two existing buses (k and p) in Brown's method

(II) The desired type of modification that cannot be modeled with any of the four cases in conventional Brown's method (branch impedance change between two existing buses)

(III) Illustration of the needed modeling and our approach to addressing it

Fig. 3.1. Modeling the Modification of Z_{bus} due to Change in the Impedance Between Buses k and p (Node 0 is the Reference Node)

3.3. Proposed Method to Update $\boldsymbol{Z}_{bus}$ to Account for Changes in the Series Impedance of a Branch

We describe the essential strategy verbally here . Afterwards, we implement it mathematically. Fig. 3.1.(I) shows the fourth case in Brown's method, connecting a branch between two existing buses. Here, the equivalent impedance between k and p will simply be the combination of the two impedances in parallel which can be denoted as Z_b^{new} as in Fig. 3.1.(II). Thus, in principle, we can account for the change of a branch impedance by starting with the fourth case in Brown's method. Mathematically, we start with connecting a branch $Z_b = -d\,Z_b^{old}$ in parallel with a pre-existing Z_b^{old}, and their equivalent is denoted as Z_b^{new} (Fig. 3.1.(III)). According to [1], [2], [17], the effect of adding such branch is modeled by augmenting $\boldsymbol{Z}_{bus}$ with a new row and column that correspond to a temporary node q whose voltage with respect to the reference is zero

(reason $V_q = 0$ is in [1], [2], [17]). To sum up, we desire to transfer the effect of adding a new branch between k and p (i.e., Fig. 3.1.(I)) to its equivalent of modifying the series impedance of preexisting branch impedance (i.e., Fig. 3.1.(II)) by using the equivalent of adding an impedance of $Z_b = -d\, Z_b^{old}$ (i.e., Fig. 3.1.(III)).

Eq. (3.1) (derived in Section A.1.) shows summarized mathematical form of how such augmentation works. Since $V_q = 0$, we may remove node q by Kron reduction which changes every element in the older $\boldsymbol{Z}_{bus}$ (i.e., Z_{lm}^{old}) to a new value Z_{lm}^{new} as shown below

$$\left[\begin{array}{c} V_1 \\ \vdots \\ V_k \\ \vdots \\ V_p \\ \vdots \\ \hline V_q = 0 \end{array}\right] = \left[\begin{array}{c|c} & \\ \boldsymbol{Z}_{orig} & col.\,k - col.\,p \\ & \\ \hline row.\,k - row.\,p & Z_{th,\,kp} - d\, Z_b^{old} \end{array}\right] \left[\begin{array}{c} I_1 \\ \vdots \\ I_k \\ \vdots \\ I_p \\ \vdots \\ \hline I_b \end{array}\right] \tag{3.1}$$

$$Z_{lm}^{new} = Z_{lm}^{old} - \frac{(Z_{lk} - Z_{lp})(Z_{km} - Z_{pm})}{Z_{th,kp} - d\, Z_b^{old}} \tag{3.2}$$

$$Z_{th,kp} = Z_{kk} + Z_{pp} - Z_{kp} - Z_{pk} \tag{3.3}$$

Where l and m are any two buses, k and p are two pre-existing buses that connected with each other with a branch whose impedance is Z_b^{old} and changed to Z_b^{new}, and $Z_{th,kp}$ is known as

the electric distance between buses k and p. Taking only the reactive component of impedances in Eq. (3.2) and isolating for d yields

$$d = \frac{(X_{lk} - X_{lp})(X_{km} - X_{pm})}{\Delta X_{lm}} y_b^{old} + X_{th,kp}\, y_b^{old} \tag{3.4}$$

Here, d is independent of the choice of the node index values l and m. y_b^{old} is the inverse of X_b^{old}. The new value of the series reactance of line $k - p$, X_b^{new}, and the required change its reactance, ΔX_b, are

$$X_b^{new} = -\frac{X_b^{old}\, \frac{d}{y_b^{old}}}{X_b^{old} - \frac{d}{y_b^{old}}} \tag{3.5}$$

$$\Delta X_b = X_b^{new} - X_b^{old} \tag{3.6}$$

By substituting Eq. (3.4) in Eq. (3.5), we get

$$X_b^{new} = -\frac{X_b^{old}\, \left(\frac{\chi_{lm}}{\Delta X_{lm}} + X_{th,kp}\right)}{X_b^{old} - \left(\frac{\chi_{lm}}{\Delta X_{lm}} + X_{th,kp}\right)} \tag{3.7}$$

Where

$$\chi_{lm} = (X_{lk} - X_{lp})(X_{km} - X_{pm}) \tag{3.8}$$

It is worth noting that χ_{lm} is dependent on the choice of the node index values l and m. Solving Eq. (3.7) for ΔX_{lm}

$$\Delta X_{lm} = \frac{\chi_{lm}\, (X_b^{new} - X_b^{old})}{X_{th,kp}\, (X_b^{old} - X_b^{new}) + X_b^{new}\, X_b^{old}} \tag{3.9}$$

Define

$$X_b^{new} = (1 - \beta)\, X_b^{old} \tag{3.10}$$

Where β is the compensation factor, a coefficient that represents the fraction of line $k-p$ reactance being compensated (e.g., $\beta = 0.3$ means 30% compensation of X_b^{old}). Substitute Eq. (3.10) in Eq. (3.9)

$$\Delta X_{lm} = -\frac{\beta\, \chi_{lm}}{\beta X_{th,kp} + (1-\beta) X_b^{old}} \tag{3.11}$$

After applying the same analysis above can be repeated for Z_{bus} without neglecting the real part, the equivalent impedance would be

$$Z_b^{new} = -\frac{Z_b^{old}\left(\frac{\zeta_{lm}}{\Delta Z_{lm}} + Z_{th,kp}\right)}{Z_b^{old} - \left(\frac{\zeta_{lm}}{\Delta Z_{lm}} + Z_{th,kp}\right)} \tag{3.12}$$

Where

$$\zeta_{lm} = (Z_{lk} - Z_{lp})(Z_{km} - Z_{pm}) \tag{3.13}$$

Like in Eq. (3.8), ζ_{lm} is dependent on the choice of the node index values l and m. Solving Eq. (3.12) for ΔZ_{lm}

$$\Delta Z_{lm} = \frac{\zeta_{lm}\,(Z_b^{new} - Z_b^{old})}{Z_{th,kp}\,(Z_b^{old} - Z_b^{new}) + Z_b^{new}\, Z_b^{old}} \tag{3.14}$$

Define

$$Z_b^{new} = R_b + j(1-\beta) X_b^{old} \tag{3.15}$$

$$Z_b^{old} = R_b + j X_b^{old} \tag{3.16}$$

Substitute Eq. (3.15) in Eq. (3.14)

$$\Delta Z_{lm} = -\zeta_{lm} \frac{j\beta\; X_b^{old}}{j\beta\, X_b^{old}\,(Z_{th,\,kp} - (R_b + j X_b^{old})) + (R_b + j X_b^{old})^2} \tag{3.17}$$

Replace $R_b + jX_b$ with Z_b^{old} in Eq. (3.17)

$$\Delta Z_{lm} = -\zeta_{lm} \frac{j\beta\, X_b^{old}}{j\beta\, X_b^{old}\,(Z_{th,\,kp} - Z_b^{old}) + \left(Z_b^{old}\right)^2} \tag{3.18}$$

Eqs. (3.9), (3.11), (3.14) and (3.18) shows the change in X_{lm} (or Z_{lm}) in an element-by-element manner. Eqs. (3.9) and (3.11) can be written in vectorized format by using sparse matrix multiplications with $\boldsymbol{X}_{bus}^{old}$, which leads to only selecting the relevant value of $\boldsymbol{X}_{bus}^{old}$ elements (only the elements related to $X_{lk},\, X_{lp},\, X_{km},$ and X_{pm} in Eq. (3.8). In a formal mathematical form, this is written as

$$\boldsymbol{X}_{bus}^{new} = \boldsymbol{X}_{bus}^{old} + \varepsilon_X \left[\boldsymbol{X}_{bus}^{old}(\boldsymbol{e}_k - \boldsymbol{e}_p)(\boldsymbol{e}_k - \boldsymbol{e}_p)^T \boldsymbol{X}_{bus}^{old}\right] \tag{3.19}$$

$$\boldsymbol{X}_{bus}^{new} = \boldsymbol{X}_{bus}^{old} + \varepsilon_\beta \left[\boldsymbol{X}_{bus}^{old}(\boldsymbol{e}_k - \boldsymbol{e}_p)(\boldsymbol{e}_k - \boldsymbol{e}_p)^T \boldsymbol{X}_{bus}^{old}\right] \tag{3.20}$$

$$\varepsilon_X = \frac{(X_b^{new} - X_b^{old})}{X_{th,kp}\,(X_b^{old} - X_b^{new}) + X_b^{new}\, X_b^{old}} \tag{3.21}$$

$$\varepsilon_X^\beta = -\frac{\beta}{\beta X_{th,kp} + (1-\beta) X_b^{old}} \tag{3.22}$$

Likewise, Eqs. (3.14) and (3.18) can be written in vectorized format by using sparse matrix multiplications with $\boldsymbol{X}_{bus}^{old}$, which leads to only selecting the relevant value of $\boldsymbol{X}_{bus}^{old}$ elements (only the elements related to $X_{lk},\, X_{lp},\, X_{km},$ and X_{pm} in Eq. (3.8). In a formal mathematical form, this is written as

$$\boldsymbol{Z}_{bus}^{new} = \boldsymbol{Z}_{bus}^{old} + \varepsilon_Z \left[\boldsymbol{Z}_{bus}^{old}(\boldsymbol{e}_k - \boldsymbol{e}_p)(\boldsymbol{e}_k - \boldsymbol{e}_p)^T \boldsymbol{Z}_{bus}^{old}\right] \tag{3.23}$$

$$\boldsymbol{Z}_{bus}^{new} = \boldsymbol{Z}_{bus}^{old} + \varepsilon_\beta \left[\boldsymbol{Z}_{bus}^{old}(\boldsymbol{e}_k - \boldsymbol{e}_p)(\boldsymbol{e}_k - \boldsymbol{e}_p)^T \boldsymbol{Z}_{bus}^{old}\right] \tag{3.24}$$

$$\varepsilon_Z = \frac{(Z_b^{new} - Z_b^{old})}{Z_{th,kp}\,(Z_b^{old} - Z_b^{new}) + Z_b^{new}\, Z_b^{old}} \tag{3.25}$$

$$\varepsilon_Z^\beta = -\frac{j\beta\, X_b^{old}}{j\beta\, X_b^{old}\,(Z_{th,\,kp} - Z_b^{old}) + \left(Z_b^{old}\right)^2} \tag{3.26}$$

Where Eqs. (3.21), (3.22), (3.25) and (3.26) are called the *common scaling factors*, $\boldsymbol{e}_k$ and $\boldsymbol{e}_p$ are two vectors (i.e, columns) whose k^{th} and p^{th} elements are 1 while the rest are zeros. The lengths $\boldsymbol{e}_k$ and $\boldsymbol{e}_p$ are equal to the number of buses in the system.

Some remarks on Eqs. (3.19) to (3.26): **a)** They help us find the new $\boldsymbol{Z}_{bus}$ *explicitly* in terms of Z_b^{new} and Z_b^{old}. Thus, Eqs. (3.19), (3.20), (3.23) and (3.24) represent a *fifth* modification of $\boldsymbol{Z}_{bus}$ and distinguished case that is different from previously mentioned four cases: changing the series impedance of a branch between two existing buses, k and p. Eqs. (3.20) and (3.24) are a variation of Eqs. (3.19) and (3.23), respectively. The main difference is that Eqs. (3.20) and (3.24) allow us to find the change in Z_{lm} and X_{lm} explicitly in terms of the compensation factor β; **b)** Calculating $\boldsymbol{X}_{bus}^{new}$ and $\boldsymbol{Z}_{bus}^{new}$ depends solely on data we can obtain from the existing $\boldsymbol{X}_{bus}$ and $\boldsymbol{Z}_{bus}$ as well as the new and old values of the branch impedance or reactance (or β). Thus, we do not need to re-construct $\boldsymbol{Z}_{bus}$ after modifying the series impedance of a line. To our best knowledge, there is no paper or research in the literature that derives similar analytical expressions before writing this dissertation, and **c)** When $X_b^{new} = X_b^{old}$ ($Z_b^{new} = Z_b^{old}$), there is no change in any $\boldsymbol{X}_{bus}$ ($\boldsymbol{Z}_{bus}$) element since both of Eqs. (3.19) and (3.23) reduce to $\boldsymbol{X}_{bus}^{new} = \boldsymbol{X}_{bus}^{old}$ ($\boldsymbol{Z}_{bus}^{new} = \boldsymbol{Z}_{bus}^{old}$). Likewise, if $X_b^{new} = X_b^{old}$ ($Z_b^{new} = Z_b^{old}$) then $\beta = 0$, which also reduces Eqs. (3.20) and (3.24) to $\boldsymbol{X}_{bus}^{new} = \boldsymbol{X}_{bus}^{old}$ ($\boldsymbol{Z}_{bus}^{new} = \boldsymbol{Z}_{bus}^{old}$). In other words, if nothing changes in the system structure, then its bus reactance (impedance) matrix stays the same. Such results are expected and are successfully predicted by Eqs. (3.19), (3.20), (3.23) and (3.24), adding evidence to soundness of results.

In matrix algebra, it is known that Sherman-Morrison identity is a generalized identity in calculating the inverse of a perturbed matrix by using the elements of the original inverse and the amount of perturbations. In the next sections, we will further verify Eqs. (3.19) to (3.26) by showing that they are a special form of Sherman-Morrison identity applied to power networks.

3.4. Relationship Between The Proposed Method and Sherman-Morrison Identity

According to Sherman-Morrison identity, we can calculate the inverse of a perturbed matrix without having to invert it again (given that we know the inverse of the matrix before perturbing it). If we have a non-singular matrix $\boldsymbol{A}$, then we can find the inverse of perturbed $\boldsymbol{A}$ by correcting the original inverse as follows [20], [21]

$$\left(\boldsymbol{A}+\boldsymbol{C}\boldsymbol{D}^{T}\right)^{-1}=\boldsymbol{A}^{-1}-\frac{1}{\alpha}\boldsymbol{A}^{-1}\boldsymbol{C}\boldsymbol{D}^{T}\boldsymbol{A}^{-1} \tag{3.27}$$

Where

$$\alpha=1+\boldsymbol{D}^{T}\boldsymbol{A}^{-1}\boldsymbol{C} \tag{3.28}$$

Eq. (3.27) holds as long as $\boldsymbol{A}$ is invertible and $\alpha=1+\boldsymbol{D}^{T}\boldsymbol{A}^{-1}\boldsymbol{C}\neq 0$. Here, $\boldsymbol{C}$, and $\boldsymbol{D}$ are any two vectors whose length is equal to the rows (or columns) number of $\boldsymbol{A}$. To understand the relationship between our work and Sherman-Morrison identity, we need to modify its original form given in Eqs. (3.27) and (3.28) to a form equivalent to Eqs. (3.19) to (3.26). Since Sherman-Morrison identity does not impose any restriction on the contents of $\boldsymbol{C}$ and $\boldsymbol{D}$ vectors (except that $\alpha=1+\boldsymbol{D}^{T}\boldsymbol{A}^{-1}\boldsymbol{C}\neq 0$), we can set any $\boldsymbol{C}$ and $\boldsymbol{D}$ as we desire and the identity would still be valid. Here, we substitute $\boldsymbol{C}=\frac{1}{\gamma}\bar{\boldsymbol{C}}$, $\boldsymbol{D}^{T}=\bar{\boldsymbol{D}}^{T}$, and $\boldsymbol{A}=\bar{\boldsymbol{A}}$ in Eqs. (3.27) and (3.28)

$$\left(\bar{\boldsymbol{A}}+\frac{1}{\gamma}\bar{\boldsymbol{C}}\bar{\boldsymbol{D}}^{T}\right)^{-1}=\bar{\boldsymbol{A}}^{-1}-\frac{1}{\bar{\alpha}}\bar{\boldsymbol{A}}^{-1}\frac{1}{\gamma}\bar{\boldsymbol{C}}\bar{\boldsymbol{D}}^{T}\bar{\boldsymbol{A}}^{-1} \tag{3.29}$$

$$\bar{\alpha}=1+\bar{\boldsymbol{D}}^{T}\bar{\boldsymbol{A}}^{-1}\frac{1}{\gamma}\bar{\boldsymbol{C}} \tag{3.30}$$

When $\bar{\alpha}\gamma=-1$, then

$$\left(\bar{\boldsymbol{A}}+\frac{1}{\gamma}\bar{\boldsymbol{C}}\bar{\boldsymbol{D}}^{T}\right)^{-1}=\bar{\boldsymbol{A}}^{-1}+\bar{\boldsymbol{A}}^{-1}\bar{\boldsymbol{C}}\bar{\boldsymbol{D}}^{T}\bar{\boldsymbol{A}}^{-1} \tag{3.31}$$

Thus, for a certain value of γ, Eq. (3.31) is correct. To find γ for which $\bar{\alpha}\gamma = -1$ we multiply Eq. (3.30) by γ and set it to -1

$$\bar{\alpha}\gamma = \left(1 + \bar{\boldsymbol{D}}^T \bar{\boldsymbol{A}}^{-1} \frac{1}{\gamma} \bar{\boldsymbol{C}}\right) \gamma = -1 \tag{3.32}$$

$$\Rightarrow \gamma = -\left(1 + \bar{\boldsymbol{D}}^T \bar{\boldsymbol{A}}^{-1} \bar{\boldsymbol{C}}\right) \tag{3.33}$$

Thus, Eq. (3.31) is a variation of the Sherman-Morrison identity given in Eq. (3.27) and is valid as long as $\gamma \neq 0$. To show that Eqs. (3.19), (3.20), (3.23) and (3.24) are a special case of Sherman-Morrison identity, we assign the values of $\bar{\boldsymbol{A}}$ to $\boldsymbol{Y}_{bus}^{old}$, $\bar{\boldsymbol{C}}$ to $\boldsymbol{u}_{k-p}$, and $\bar{\boldsymbol{D}}^T$ to $\boldsymbol{u}_{k-p}^T$. Afterwards we substitute these values in Eqs. (3.31) and (3.33), which yields

$$\boldsymbol{Y}_{bus}^{new\,-1} = \boldsymbol{Y}_{bus}^{old\,-1} + \boldsymbol{Y}_{bus}^{old\,-1} \boldsymbol{u}_{k-p} \boldsymbol{u}_{k-p}^T \boldsymbol{Y}_{bus}^{old\,-1} \tag{3.34}$$

$$\boldsymbol{Y}_{bus}^{new} = \boldsymbol{Y}_{bus}^{old} + \boldsymbol{Y}_{bus}^{mod} \tag{3.35}$$

$$\boldsymbol{Y}_{bus}^{mod} = \frac{\boldsymbol{u}_{k-p} \boldsymbol{u}_{k-p}^T}{\gamma} \tag{3.36}$$

$$\gamma = -\left(1 + \boldsymbol{u}_{k-p}^T \boldsymbol{Y}_{bus}^{old\,-1} \boldsymbol{u}_{k-p}\right) \tag{3.37}$$

Since $\boldsymbol{Y}_{bus}{}^{-1} = \boldsymbol{Z}_{bus}$

$$\boldsymbol{Z}_{bus}^{new} = \boldsymbol{Z}_{bus}^{old} + \boldsymbol{Z}_{bus}^{old} \boldsymbol{u}_{k-p} \boldsymbol{u}_{k-p}^T \boldsymbol{Z}_{bus}^{old} \tag{3.38}$$

$$\boldsymbol{u}_{k-p} = \sqrt{\varepsilon_{k-p}}\,(\boldsymbol{e}_k - \boldsymbol{e}_p) \tag{3.39}$$

Where ε_{k-p} can be obtained from one of Eqs. (3.21), (3.22), (3.25) and (3.26), a selection that depends on whether we want to neglect the real part of $\boldsymbol{Z}_{bus}$ elements and whether we want to modify the series impedance of line $k-p$ to a value of interest or just compensate its reactance by a certain fraction (i.e., β).

It is noteworthy that Eqs. (3.38) and (3.39) are a generalization of Eqs. (3.19) to (3.26) using Sherman-Morrison identity. However, our method is still original and substantial because we determined the correct values of $\bar{\boldsymbol{C}}$ and $\bar{\boldsymbol{D}}$ that we must substitute in Eq. (3.31) to model the effect of changing the series impedance of line $k-p$, a pertinent and weighty task. Some remarks on Eqs. (3.34) to (3.39): **a)** It may seem that since Eq. (3.34) contains an inverted matrix then it holds only if $\boldsymbol{Y}_{bus}^{old}$ is invertible. However, the inverse of $\boldsymbol{Y}_{bus}^{old}$ could be obtained even if $\boldsymbol{Y}_{bus}^{old}$ is singular, which is attributed to the fact that Brown's method can be used to construct $\boldsymbol{Y}_{bus}^{old\,-1}$ (i.e., $\boldsymbol{Z}_{bus}^{old}$) without having to actually invert $\boldsymbol{Y}_{bus}^{old}$. Afterwards, our method can be used to quickly find the new $\boldsymbol{Z}_{bus}$ whenever the series impedance of a line is modified (which is not feasible with Brown's method); **b)** Since the Left-Hand Side (L.H.S) of Eq. (3.34) must be the new $\boldsymbol{Y}_{bus}$ and since we know that the L.H.S is a perturbed $\boldsymbol{Y}_{bus}^{old}$, then the matrix given by $\frac{\boldsymbol{u}_{k-p}\boldsymbol{u}_{k-p}^{T}}{\gamma}$ must be equal to the amount of perturbations in $\boldsymbol{Y}_{bus}^{old}$ if the series impedance of line $k-p$ changes. Thus, by calculating $\boldsymbol{Y}_{bus}^{mod}$ using Eqs. (3.36) and (3.37) and comparing it with $\boldsymbol{Y}_{bus}^{new} - \boldsymbol{Y}_{bus}^{old}$ as found by direct construction of $\boldsymbol{Y}_{bus}$, we could get an evidence to confirm the validity of our method (as shown in Section 3.5.). In fact, Eq. (3.36) is an elegant, vector-based method to find the change in $\boldsymbol{Y}_{bus}$ in terms $\boldsymbol{Z}_{bus}$ elements, and **c)** Eq. (3.36) is valid only if $\gamma \neq 0$, but even if $\gamma = 0$, our method would still succeed in finding $\boldsymbol{Z}_{bus}^{new}$ since Eq. (3.38) does not contain γ or a matrix inversion.

3.5. Numerical Results

In this section, we compare three methods to construct $\boldsymbol{Z}_{bus}$, namely, $\boldsymbol{Y}_{bus}$ inversion, Brown's method, and extended Brown's method. Our method is called 'extended' since it adds a fifth case to the formation of $\boldsymbol{Z}_{bus}$, the modification of a series impedance of a line. We obtain the data of seven systems of different sizes ranging from 39 bus to 3120 bus systems. The data of these systems are available in MATPOWER package in MATLAB (available online at

www.pserc.cornell.edu/matpower).The calculations are done with a desktop with AMD Ryzen 7 2700X processor and 64GB/3000MHz RAM.

The results are obtained for systems with pre-existing $\boldsymbol{Z}_{bus}$, but we want to modify the series impedance of one of their lines and recalculating $\boldsymbol{Z}_{bus}$.

3.5.1. Comparison of Accuracy

The accuracy of Eqs. (3.38) and (3.39) is verified by checking if they predict the new $\boldsymbol{Z}_{bus}$ correctly. We compare the results obtained from these equations with the ones obtained by Brown's method. Root Mean Square Error (RMSE) is used to measure the accuracy of the results. The reason why we choose Brown's method to compare our results with is that $\boldsymbol{Y}_{bus}$ inversion may return inaccurate results if the condition number of $\boldsymbol{Y}_{bus}$ is too large.

The RMSEs are summarized in TABLE 3.1. The fact that RMSEs are infinitesimally small confirms that our modeling approach is accurate in calculating $\boldsymbol{Z}_{bus}^{new}$. Moreover, another column is added which compares $\boldsymbol{Y}_{bus}^{mod}$ with $\boldsymbol{Y}_{bus}^{new} - \boldsymbol{Y}_{bus}^{old}$ as found by direct construction of $\boldsymbol{Y}_{bus}$. The accurate prediction of $\boldsymbol{Y}_{bus}^{mod}$ using Eq. (3.36) further confirms the validity of our work. This validity confirmation is explained as follows: since modifying the series impedance of a line perturbs $\boldsymbol{Y}_{bus}$ and given that Eq. (3.34) contains $\boldsymbol{Y}_{bus}^{old}$ with the matrix $\frac{\boldsymbol{u}_{k-p}\boldsymbol{u}_{k-p}^{T}}{\gamma}$ added to it, then this matrix should be exactly equal to the difference $\boldsymbol{Y}_{bus}^{new} - \boldsymbol{Y}_{bus}^{old}$, which what we could see in TABLE 3.1. The errors are too small that they are safely and convincingly attributed to the rounding errors in MATLAB double-format precision.

It is worth noting that RMSEs are clearly independent of system size proving that our method is accurate for small or large systems (an advantage of Brown's method that is still retained in our method).

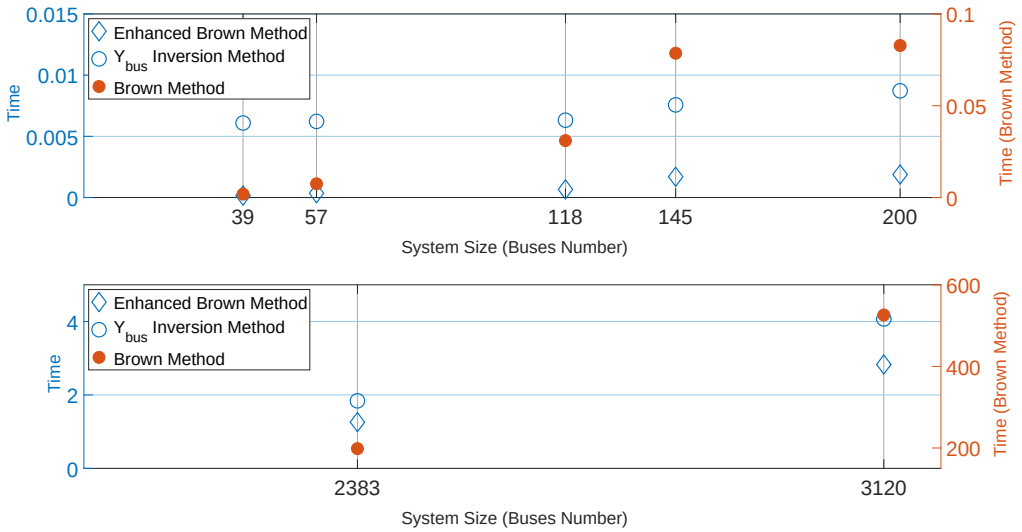

(I) Well-Conditioned Systems

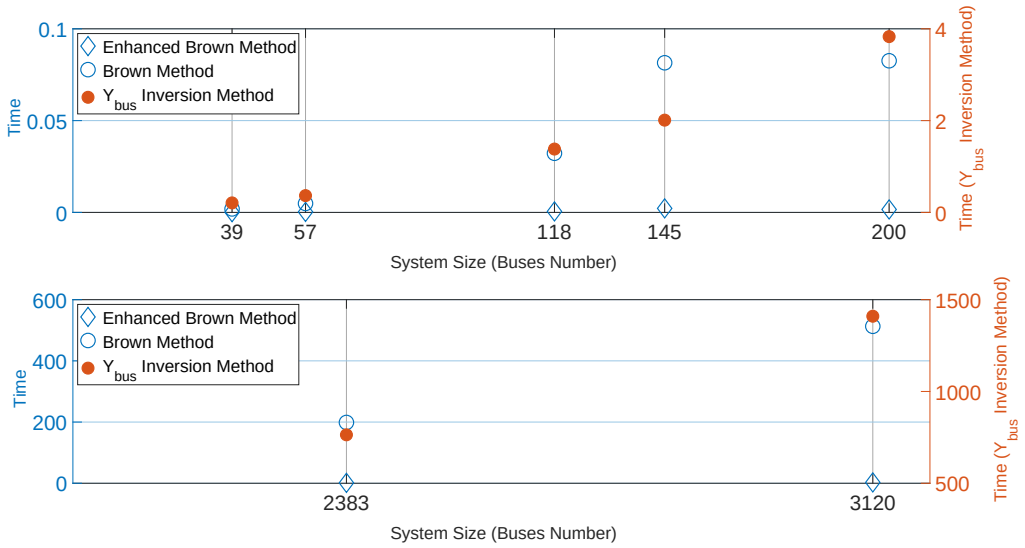

(II) Ill-Conditioned Systems

Fig. 3.2. Speed Comparison of Our Method Against Brown Method and $\boldsymbol{Y}_{bus}$ Inversion

TABLE 3.1.
ROOT MEAN SQUARE ERRORS OF THE PROPOSED METHOD AGAINST BROWN METHOD

System Size	$RMSE$ for $\boldsymbol{Y}_{bus}^{mod}$ in Eq. (3.36)	$RMSE$ for $\boldsymbol{Z}_{bus}^{new}$ in Eq. (3.38)
39	970×10^{-15}	96×10^{-18}
57	16×10^{-15}	84×10^{-15}
118	18.1×10^{-15}	6.13×10^{-15}
145	2.69×10^{-15}	115×10^{-15}
200	3.57×10^{-15}	3.87×10^{-15}
2383	61.6×10^{-15}	219×10^{-15}
3120	12.4×10^{-15}	1.36×10^{-12}

TABLE 3.2.
ATTRIBUTES COMPARISON OF OUR METHOD (EXTENDED BROWN METHOD), BROWN METHOD, AND $\boldsymbol{Y}_{bus}$ INVERSION METHOD

	$\boldsymbol{Y}_{bus}$ Inversion	Our Method	Brown Method
Vulnerability to $\boldsymbol{Y}_{bus}$ Singularity	Yes	No	No
Accuracy When $\boldsymbol{Y}_{bus}$ is Near Singular	Low	Very High	Very High
Calculation Speed for Large Systems with Well-Conditioned $\boldsymbol{Y}_{bus}$	In Between	Fastest	Slowest
Calculation Speed for Large Systems with Ill-Conditioned $\boldsymbol{Y}_{bus}$	Slowest	Fastest	In Between
Memory Requirement for Large Systems	Very High	Low	Low

3.5.2. Comparison of Speed

Here, we present results showing the speed improvement we get from using the fifth case in $\boldsymbol{Z}_{bus}$ formation. Fig. 3.2. shows the speed of finding $\boldsymbol{Z}_{bus}$ for systems of different sizes. In Fig. 3.2.(I) we see that all methods offer a very fast speed (less than $0.100\,\mathrm{s}$). However, when system sizes reaches thousands of buses, our method and $\boldsymbol{Y}_{bus}$ inversion finish the calculations

within seconds, while Brown's method takes $198\,\mathrm{s}$ for the 2383-bus system and $526\,\mathrm{s}$ for the 3120-bus systems (compared to $1.30\,\mathrm{s}$ and $2.90\,\mathrm{s}$ with extended Brown's method). Thus, our extended Brown's method retains the original feature of Brown's method (requiring less memory) while still being faster than $\boldsymbol{Y}_{bus}$ inversion method.

The previously mentioned is for systems with well-conditioned $\boldsymbol{Y}_{bus}$. If the system has an ill-conditioned $\boldsymbol{Y}_{bus}$, its inversion can be inaccurate, and the inaccuracy is hard to detect. Thus, if we still want a correct result by inverting an ill-conditioned $\boldsymbol{Y}_{bus}$, we must increase the variable precision. We doubled the number of significant decimal digits in MATLAB and recalculated $\boldsymbol{Z}_{bus}$ with the results presented in Fig. 3.2.(II). It is easy to see here that $\boldsymbol{Y}_{bus}$ inversion takes substantially longer time, reaching $764\,\mathrm{s}$ for 2383-bus system and $1410\,\mathrm{s}$ for 3120-bus system (compared to $1.35\,\mathrm{s}$ and $2.70\,\mathrm{s}$ with extended Brown's method), which clearly shows that the time of $\boldsymbol{Y}_{bus}$ inversion exponentially grows when we try to invert an ill-conditioned $\boldsymbol{Y}_{bus}$ and still expect accurate results (because this necessitates increasing the floating-point accuracy).

3.5.3. Summary of Methods Attributes

TABLE 3.2. compares the three methods in terms of their speed, accuracy, and memory requirement. Our method is clearly the fastest among the methods compared but without sacrificing the accuracy due to ill-conditioning of $\boldsymbol{Y}_{bus}$. Further, since our method does not require a matrix inversion, it is more economical in its memory use. Thus, the speed, accuracy, and low memory requirement of our method make it more suitable for online applications. One more advantage of our method is that it can obtain certain elements of the new $\boldsymbol{Z}_{bus}$ without having to calculate the entire $\boldsymbol{Z}_{bus}$ (see Eqs. (3.13), (3.14) and (3.18)). Many of the recently developed techniques in power system analysis can take advantage of this feature [4], [10], [11]. For instance, Saxena *et al.* [11] need only $\boldsymbol{Z}_{bus}$ elements related only to non-linear current sources. Thus, if

we would like to repeat the analysis of [11] with different series compensation levels in different lines, we need to modify $\boldsymbol{Z}_{bus}$ elements related only to these sources. If the number of non-linear sources is 30 and the number of system's buses is 2383, then we need $30 \times 2383 = 71{,}490$ elements from $\boldsymbol{Z}_{bus}$. With $\boldsymbol{Y}_{bus}$ inversion and Brown's method, we cannot rapidly obtain $\boldsymbol{Z}_{bus}$ elements related to these 30 sources but we rather need to find $2383 \times 2383 = 5{,}678{,}700$ elements. Džafić *et al.* [10] present a power flow algorithm to simulate the local voltage controllers in a meshed distribution network. The authors use "sensitivity matrix" approach aimed at representing the effect of Load Tap Changer (LTC) in each load flow iteration, which is done by modeling LTCs as fictitious current injections. In such a method, only $\boldsymbol{Z}_{bus}$ elements related to PV buses are needed. Thus, if a change happens in the system, we do not need to reconstruct $\boldsymbol{Z}_{bus}$ from scratch, but rather only $\boldsymbol{Z}_{bus}$ elements related to PV buses. Thus, reconstructing all of $\boldsymbol{Z}_{bus}$ in such case wastes computational capacity.

3.6. Conclusions

This dissertation explains how to extend Brown's method to account for a fifth case in modifying the structure of a power system: the change of a series impedance of an existing branch between two existing buses. With the conventional Brown's method, such change is not accounted for by any type of $\boldsymbol{Z}_{bus}$ modification case discussed briefly in Section 3.2.

Our modeling approach retains the same desirable features of Brown's method (low memory requirement and high accuracy even with near-singular $\boldsymbol{Y}_{bus}$) while offering substantially faster speed. The modification of a series impedance of a line frequently happens in power systems to increase the controllability. Our work allows for a fast, accurate and less demanding solution to find $\boldsymbol{Z}_{bus}$ when lines compensation varies in real-time which facilitate the online application of many solutions that rely on $\boldsymbol{Z}_{bus}$ elements.

We also discovered in this dissertation that the perturbations in $\boldsymbol{Y}_{bus}$ elements due to changing the series reactance of a line could be written explicitly in terms of $\boldsymbol{Z}_{bus}$ elements and the new impedance of that line. In the future, such discovery could potentially be used to further understand the relationship between $\boldsymbol{Y}_{bus}$ and $\boldsymbol{Z}_{bus}$ or how the system characteristics vary when the impedance of a line is modified.

3.7. References

[1] H. E. Brown, *Solution of Large Networks by Matrix Methods*. Wiley New York et al., 1985.

[2] J. J. Grainger and W. D. Stevenson, *Power System Analysis*. McGraw-Hill New York, 1994, vol. 621.

[3] A. S. Alayande, A. A. Jimoh, and A. A. Yusuff, "An alternative algorithm for solving generation to load matching and loss allocation problems," *International Transactions on Electrical Energy Systems*, vol. 27, no. 8, e2347, 2017.

[4] H.-Y. Su and C.-W. Liu, "Estimating the voltage stability margin using PMU measurements," *IEEE Transactions on Power Systems*, vol. 31, no. 4, pp. 3221–3229, 2016.

[5] D. Wu, G. Li, *et al.*, "Assessing Impact of Renewable Energy Integration on System Strength Using Site-Dependent Short Circuit Ratio," *IEEE Transactions on Sustainable Energy*, 2017.

[6] D. H. A. Lee, "Voltage stability assessment using equivalent nodal analysis," *IEEE Transactions on Power Systems*, vol. 31, no. 1, pp. 454–463, 2016.

[7] B. Gou and H. Zhang, "Fast real-time corrective control strategy for overload relief in bulk power systems," *IET Generation, Transmission & Distribution*, vol. 7, no. 12, pp. 1508–1515, 2013.

[8] N. Kang and Y. Liao, "Double-circuit transmission-line fault location with the availability of limited voltage measurements," *IEEE transactions on power delivery*, vol. 27, no. 1, pp. 325–336, 2012.

[9] Q. Jiang, X. Li, B. Wang, and H. Wang, "Pmu-based fault location using voltage measurements in large transmission networks," *IEEE transactions on power delivery*, vol. 27, no. 3, p. 1644, 2012.

[10] I. Džafić, R. A. Jabr, E. Halilovic, and B. C. Pal, "A sensitivity approach to model local voltage controllers in distribution networks," *IEEE Transactions on Power Systems*, vol. 29, no. 3, pp. 1419–1428, 2014.

[11] D. Saxena, S. Bhaumik, and S. Singh, "Identification of multiple harmonic sources in power system using optimally placed voltage measurement devices," *IEEE Transactions on Industrial Electronics*, vol. 61, no. 5, pp. 2483–2492, 2014.

[12] H. E. Brown, C. E. Person, L. K. Kirchmayer, and G. W. Stagg, "Digital calculation of 3-phase short circuits by matrix method," *Transactions of the American Institute of Electrical Engineers. Part III: Power Apparatus and Systems*, vol. 79, no. 3, pp. 1277–1281, Apr. 1960, ISSN: 0097-2460.

[13] E. B. Makram and A. A. Girgis, "A generalized computer technique for the development of the three-phase impedance matrix for unbalanced power systems," *Electric power systems research*, vol. 15, no. 1, pp. 41–50, 1988.

[14] E. Makram and A. Girgis, "Development of a three-phase bus impedance matrix in the complex frequency domain for transient analysis in unbalanced distribution systems," *Electric Power Systems Research*, vol. 16, no. 3, pp. 183–193, 1989.

[15] A. Saxena and D. A. Rao, “A new approach to bus impedance matrix building,” *Computers & Electrical Engineering*, vol. 29, no. 1, pp. 55–65, 2003.

[16] T.-C. Ou and W.-M. Lin, “A novel z-matrix algorithm for distribution power flow solution,” in *2009 IEEE Bucharest PowerTech*, IEEE, 2009, pp. 1–8.

[17] A. R. Bergen, *Power Systems Analysis*. Pearson Education India, 2009.

[18] M. B. Wafaa and L.-A. Dessaint, “Approach to dynamic voltage stability analysis for DFIG wind parks integration,” *IET Renewable Power Generation*, vol. 12, no. 2, pp. 190–197, 2017.

[19] M. Javadi, “New Implication of Short Circuit Analysis in Assessing Impact of Renewable Energy Resources on System Strength of a Power Grid,” PhD thesis, University of Oklahoma, 2017.

[20] X. He, M. Holm, and M. Neytcheva, “Parallel Implementation of the Sherman-Morrison Matrix Inverse Algorithm,” in *International Workshop on Applied Parallel Computing*, Springer, 2012, pp. 206–219.

[21] C. Wang, H. Li, and D. Zhao, “Preconditioning Toeplitz-plus-diagonal linear systems using the Sherman–Morrison–Woodbury formula,” *Journal of Computational and Applied Mathematics*, vol. 309, pp. 312–319, 2017.

CHAPTER 4. VECTOR-BASED APPROACH TO ANALYZE TRANSMISSION NETWORK EFFECT ON INTERACTION AMONG RENEWABLES

4.1. Introduction

The increasing integration of RESs, such as wind and solar, is challenging grid planning and operation. Most RESs interface with the power grid through power electronic inverters. While these inverters offer faster and more advanced control as well as additional flexibility, they also add a layer of complexity to ensuring their reliable operation. For instance, RESs do not contribute to the short-circuit capacity at their buses, meaning that they do not contribute to smaller Thevenin impedance to nearby buses [1]. Further, these interfaces depend on stable voltage reference from the grid. When the grid becomes weaker, the voltage reference is less stable and control dynamics and tuning becomes more influential on the system voltage at RES POIs [2]. The difficulties include poor signal tracking with a potential loss of stability due to gain increases [3] and poor oscillation damping [4], [5].

These challenges become even more relevant when manufacturers assume a very strong grid when designing their controllers, which is usually the case [4]. Manufacturers usually assume a Short-Circuit Ratio (SCR) of more than 5, which is overly optimistic considering that stable and persistent wind gust exist away from load centers. Thus, the RESs are usually connected to unfavorable locations from a structural perspective, making it very likely that the SCR is substantially less than 5. Even if the system is strong at the Point-of-Interconnection (POI) of an RES, the fact that it is located in these unfavorable locations could mean a significant drop in

SCR when a power line outage occurs. For instance, Zhang *et al.* [4] mention a real-life example of a Wind Power Plant (WPP) connected to the ERCOT grid through $69\,\mathrm{kV}$ transmission lines with $SCR \approx 4$. When one of these lines disconnected, the SCR dropped to less than 2 resulting in poorly damped or un-damped voltage oscillations. Investigations revealed that aggressive voltage control (e.g., increasing the gain when system strength decreases) was the reason for such undesired behavior.

Thus, it is clear that system operators must be aware of any potential weakness in the grid. This awareness would help operators prepare for contingencies and procure necessary ancillary services. Further, information about system strength can be beneficial for expansion planning. The SCR was devised by [6] and the IEEE [7] as a measure of system weakness for High Voltage DC (HVDC) integration which, since then, has been used for that purpose [8] and even for other types of power electronic interfaces such as the Voltage Source Converter [9]. Another use of SCR is to evaluate the strength of a power grid at the POIs of RESs [1], [4], [5], [10]–[13].

One major drawback of the commonly used SCR calculation method is that it ignores the interactions among RESs. Thus it may lead to inaccurate estimation of grid strength at the POIs when the combined effect of RES must be accounted for [4], [11], [14]. Motivated by overcoming the shortcoming of the conventional SCR, a modified version of is proposed by General Electric (GE) [12] and Minnesota Department of Commence [1]. This index is called Composite Short-Circuit Ratio (CSCR) and is based on the assumption of neglecting all electric distances among RESs and calculating a 'unified' SCR for all of them. Another extension to the conventional SCR is the Weighted Short-Circuit Ratio (WSCR) method developed by ERCOT [4], [13]. WSCR is the same as the CSCR with one significant difference: it gives a 'weight' for each bus short-circuit MVA capacity based on the rating of the wind plant at that bus. Both the CSCR and

the WSCR calculation methods do not take into account the real electrical network connections among RERs; and therefore, they may not reflect the actual grid strength at the POIs. Both the CSCR and WSCR methods mainly provide the aggregated strength of a power grid in the area where the RERs are interconnected electrically close, but they do not calculate the strength of the grid at each individual POI in the specific area. To overcome those shortcomings, Wu *et al.* [14] devise the Site-Dependent Short-Circuit Ratio (SDSCR) index by analyzing the relationship between grid strength and voltage stability.

Despite all the progress made in estimating RES POIs strength [1], [5], [10]–[12], [14], [15], discussing or analyzing issue arising from weak grids [3], [5], [9], [10], [15]–[20], or improving system strength by control/compensation means [3], [9], [10], there is still a lack of literature on the theoretical understanding of the relationship between system structure and the strength at certain POIs. Thus, this dissertation addresses such topic. More on this and the motivation is discussed in Section 4.2.

4.2. Background and Description of Motivation

4.2.1. Grid Strength Assessment

The strength of a power grid at a POI can be evaluated with SCR, which is the ratio of the short-circuit capacity at a specific POI to the rated capacity of the RES [12], [13]. When an RES is connected to a power system at POI i, SCR at POI i can be represented as

$$SCR_i = \frac{|S_{ac,\,i}|}{P_{d,\,i}} = \frac{|V_i|^2}{P_{r,\,i}} \frac{1}{|Z_{th,\,ii}|} \tag{4.1}$$

where $S_{ac,\,i}$ is the short-circuit capacity of the grid at POI i, $|V_i|$ is the voltage magnitude at POI i, $Z_{th,\,ii}$ is the magnitude of Thevenin equivalent impedance at POI i, and $P_{r,\,i}$ is the rated power at the RES connected to POI i.

In a power grid, RESs interact with each other when they are electrically close. As such, their interactions can affect the grid strength at their POIs. However, SCR does no take into account the effect of such interactions. Hence, Wu *et al.* [14] devise SDSCR by analyzing the relationship between the grid strength and voltage stability in a power grid with a single RES integration and extending the relationship to the power grid with the integration of multiple RESs. For an RES at POI i, SDSCR is

$$SDSCR_i = \frac{|V_{R,i}|^2}{\left|S^*_{eq,i}\right| |Z_{RR,ii}|} \tag{4.2}$$

Where

$$S^*_{eq,i} = P_{R,i} + \sum_{j \in \boldsymbol{R},\, j \neq i} P_{R,j}\, w_{ij} \tag{4.3}$$

$$w_{ij} = \frac{Z_{RR,ij}}{Z_{RR,ii}} \left(\frac{V_{R,i}}{V_{R,j}}\right)^* \tag{4.4}$$

Here, $P_{R,i}$ is the power injected from RES at POI i, $\boldsymbol{R}$ is a set of RES buses (or POIs), $Z_{RR,ij}$ is the transfer impedance between POI i and POI j, $Z_{RR,ii}$ is the self-impedance at POI i. $V_{R,i}$ and $V_{R,j}$ are voltages at POI i and POI j, respectively.

SDSCR has the following features: **a)** it takes into account the interactions among RESs in terms of electrical connectivity which is depicted in $\sum_{j \in \boldsymbol{R},\, j \neq i} P_{R,j}\, w_{ij}$. Unlike CSCR or WSCR, SDSCR does not assume full interaction, nor absence of interaction in SCR, and **b)** SDSCR is a generalized representation of SCR (i.e., if $w_{ij} = 0 \quad \forall\, j$, Eq. (4.2) gets reduced to Eq. (4.1)). Hence, SDSCR is a more accurate index of system strength at certain POI. Detailed discussion on the features and physical interpretation of SDSCR as well as a numerical study demonstrating its accuracy is available in [14].

4.2.2. Motivation

A substantial part of power system operation depends on the current-voltage relationship; that is, voltages at all buses in the system are the result of (equivalent) current injections by generators (whether conventional or renewable). However, current injections need to flow in the transmission network components, which include transmission lines, transformers, shunt capacitors, series compensators, etc.

Because of this, it is natural to think that these components play some role in influencing voltage level (or its sensitivity for specific variations in operating conditions). More importantly, however, is that some of these components have more influence on the system operation than others. For instance, if we have only one Extra High Voltage (EHV) line connecting the only major generator in the area to the largest load center, then it is natural to expect that such line is important for the voltage of the load center bus. Such importance, however, could be influenced by the specific structure of the network; if the load center contains highly meshed lines with five $69\,\mathrm{kV}$ subtransmission lines working in parallel between two nodes then the EHV line is most certainly more important than any of these sub-transmission lines (because these lines are less heavily loaded than EHV lines and their number, 5, allow for better redistribution of power if one is disconnected).

The previously mentioned example can be a result of the engineer's experience or 'intuition'. However, a systematic analysis and theoretical understanding of reasons behind the importance of certain lines need a mathematical approach that closely aligns with the aspect of interest. Thus, the motivation of this dissertation is to develop a mathematical approach that provides a *theoretical justification* as to why certain lines are more relevant to the interaction among RESs than other lines. To our best knowledge, the literature either discusses the problems that

arise due to weak POIs (as in [3], [5], [9], [10], [15]–[20]), estimates the strength at POIs (as in [1], [5], [10]–[12], [14], [15]), and/or proposes some control/compensation based solutions (as in [3], [9], [10]), but did not address the previously mentioned motivation.

The contribution of this work is furnishing a theoretical connection between interaction among RESs and the structure of a power system. More specifically, our work answers the question: *why are certain lines more important to RESs interaction than others*? Such theoretical connection allows for more in-depth insight into RES POIs weakness and more systematic methods to identify system expansions or changes in operating conditions that could improve the system strength at weak POIs. The actual implementation of these methods is not demonstrated rigorously in this dissertation. However, we still provide an in-depth analysis in Section 4.4. with its verification in Section 4.5. then follow with short example some some potential benefits of the concepts we develop in Section 4.6.

Benefits of such work may include, for instance, the inclusion of Operational Interaction Operators (it will be derived in Section 4.3.), in defining the fitness function of swarm intelligence algorithms when used to optimize power system operation. This is plausible since there is a strong correlation between the Operational Interaction Operators and the overall amount change interaction among RESs due to structural changes in the system (Section 4.5.).

4.3. Operational Transfer Impedances and Operational Interaction Operators

The term $\sum_{j\in\boldsymbol{R},\, j\neq i} P_{R,\,j}\, w_{ij}$ in Eqs. (4.2) and (4.3) is a sum of terms whose number is equal to the number of RESs less one. Each term contains a real number (i.e., $P_{R,\,j}$) multiplied by a complex one (i.e., w_{ij}). The final result of this summation of complex numbers is added to $P_{R,\,i}$ resulting in an 'effective' complex power that the system will 'see' at POI i. The variable w_{ij} is called *interaction operator* since it scales $P_{R,\,j}$ and change its angle (making it a complex

power rather than pure active one). When the system contains multiple RESs, we will have multiple interaction operators, each of which has a different magnitude and angle. Thus, it would be relatively hard to get a theoretical understanding of interaction even when trying to simplify the analysis (e.g., by setting all RES power injections to one common value).

For instance, in Fig. 4.1.(I), $S_{eq,\,i}$ is drawn. Here, we have 6 RESs in total, and we study RES at bus 1. Thus, we have 5 interaction operators with $\sum_{j\in \boldsymbol{R},\, j\neq i} P_{R,\,j}\, w_{ij}$ being a sum of 5 complex numbers. When we change the structure or operating conditions of the system, all 5 interaction operators will change (in both angle and magnitude) resulting in Fig. 4.1.(II) which shows a significant reduction in $|S_{eq,\,i}|$. In such a case, it is hard to determine which interaction operator had the most influence on $|S_{eq,\,i}|$. Further, even if we specify that a certain interaction operator had the most influence, it is still not clear whether its angle or magnitude change was the one responsible for the significant reduction in $|S_{eq,\,i}|$.

Motivated to simplify such situation, we propose the concepts of *operational transfer impedances*, which are impedances of the system that retain information about other RESs operating conditions, and *operational interaction operators* (same as w_{ij} in Eq. (4.4) except for substituting the operational transfer impedances instead).

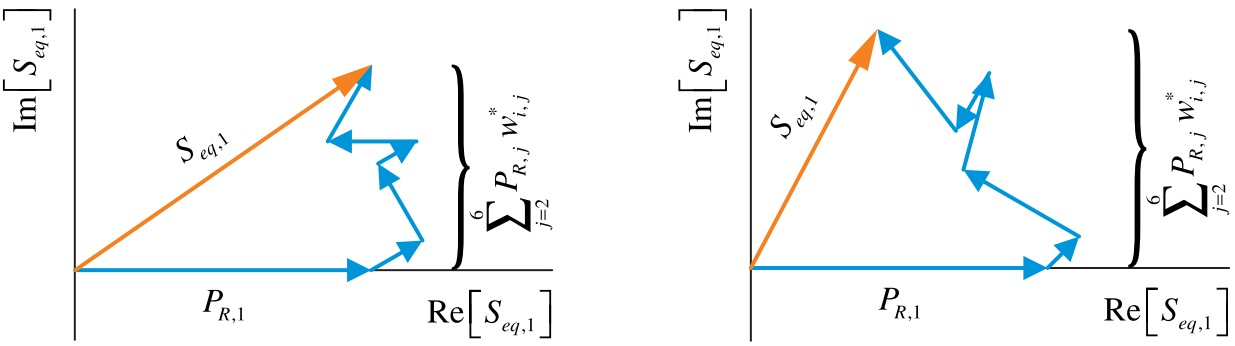

(I) Original Operating Conditions (II) New Operating Conditions

Fig. 4.1. $|S_{eq,\,i}|$ for Two Different Operating Conditions

4.3.1. Operational Transfer Impedances

Wu *et al.* [14] derive the SDSCR by dividing the generation sources of a system into two major types: **a)** conventional generation which is a set of generators denoted as $\boldsymbol{G}$, and **b)** renewable generation which is a set of RESs denoted as $\boldsymbol{R}$ (see Fig. 4.2.). Based on that, we can write the voltage-current relationships as follows

$$\left[\begin{array}{c} \boldsymbol{V}_G \\ \hline \boldsymbol{V}_R \end{array}\right] = \left[\begin{array}{c|c} \boldsymbol{Z}_{GG} & \boldsymbol{Z}_{GR} \\ \hline \boldsymbol{Z}_{RG} & \boldsymbol{Z}_{RR} \end{array}\right] \left[\begin{array}{c} \boldsymbol{I}_G \\ \hline \boldsymbol{I}_R \end{array}\right] \tag{4.5}$$

Where $\boldsymbol{V}_G$, $\boldsymbol{V}_R$, $\boldsymbol{I}_G$, $\boldsymbol{I}_R$ are vectors of conventional generation buses voltages, RES buses voltages, conventional generation buses current injections and RES buses current injections, respectively. $\boldsymbol{Z}_{GG}/\boldsymbol{Z}_{RR}$ are sub-matrices of $\boldsymbol{Z}_{bus}$ elements for the buses of conventional/RES generation. $\boldsymbol{Z}_{GR}$ and $\boldsymbol{Z}_{GR}$ are sub-matrices of $\boldsymbol{Z}_{bus}$ elements corresponding to pairs of buses that one of them belongs to $\boldsymbol{G}$ and the other to $\boldsymbol{R}$.

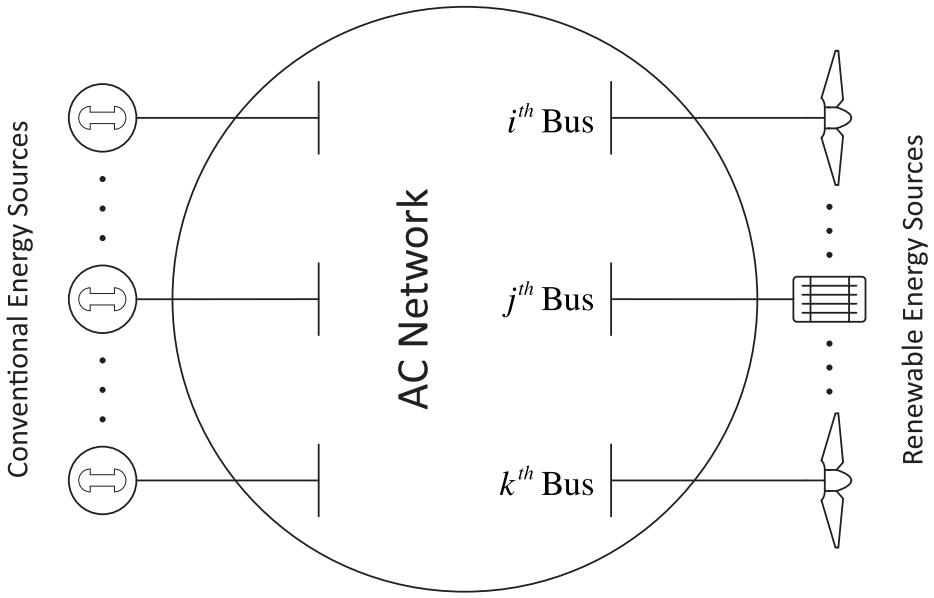

Fig. 4.2. An AC System with Multiple RESs

By replacing all RESs (except for the i^{th} and j^{th} ones) with their equivalent impedances (see Section C.2.), Eq. (4.5) becomes

$$\left[\begin{array}{c} \boldsymbol{V}_G \\ \hline \boldsymbol{V}_R \end{array}\right] = \left[\begin{array}{c|c} \bar{\boldsymbol{Z}}_{GG} & \bar{\boldsymbol{Z}}_{GR} \\ \hline \bar{\boldsymbol{Z}}_{RG} & \bar{\boldsymbol{Z}}_{RR} \end{array}\right] \left[\begin{array}{c} \bar{\boldsymbol{I}}_G \\ \hline \bar{\boldsymbol{I}}_R \end{array}\right] \tag{4.6}$$

Where $\bar{\boldsymbol{Z}}_{GG}$, $\bar{\boldsymbol{Z}}_{GR}$, $\bar{\boldsymbol{Z}}_{RG}$, $\bar{\boldsymbol{Z}}_{RR}$ are similar to $\boldsymbol{Z}_{GG}$, $\boldsymbol{Z}_{GR}$, $\boldsymbol{Z}_{RG}$, $\boldsymbol{Z}_{RR}$ in Eq. (4.5) except that they are modified to account for the replacement of some RESs with equivalent impedances. $\bar{\boldsymbol{I}}_G$ is the same as $\boldsymbol{I}_G$ (because we did not replace any conventional generation). $\bar{\boldsymbol{I}}_R$ is $\boldsymbol{I}_R$ with all elements (except the i^{th} and the j^{th} where both i and j here refer to specific buses) being set to zero. Mathematically, the n^{th} element of $\bar{\boldsymbol{I}}_G$ is

$$\bar{\boldsymbol{I}}_R(n) = \begin{cases} I_{R,\,i} & \text{if} \quad n = i \\ I_{R,\,j} & \text{if} \quad n = j \\ 0 & \text{if} \quad n \neq i \text{ or } j \end{cases} \tag{4.7}$$

Since current injection in Eq. (4.7) is zero for every n^{th} RES (except the i^{th} and the j^{th}), we can remove all rows in Eq. (4.6) that correspond to any n^{th} element (except the i^{th} and the j^{th}) without affecting the overall current voltage relationships or the calculated complex power injected at each bus. Thus, Eq. (4.6) can be reduced further to a more simplified form as

$$\left[\begin{array}{c} \boldsymbol{V}_G \\ \hline V_{R,\,i} \\ V_{R,\,j} \end{array}\right] = \left[\begin{array}{c} \\ \bar{\boldsymbol{Z}}_{bus} \\ \\ \end{array}\right] \left[\begin{array}{c} \bar{\boldsymbol{I}}_G \\ \hline \bar{I}_{R,\,i} \\ \bar{I}_{R,\,j} \end{array}\right] \tag{4.8}$$

Where

$$\bar{\boldsymbol{Z}}_{bus} = \left[\begin{array}{c|cc} \bar{\boldsymbol{Z}}_{GG} & \bar{\boldsymbol{Z}}_{GR_i} & \bar{\boldsymbol{Z}}_{GR_j} \\ \hline \bar{\boldsymbol{Z}}_{R_iG} & \bar{Z}_{RR,\,ii} & \bar{Z}_{RR,\,ij} \\ \bar{\boldsymbol{Z}}_{R_jG} & \bar{Z}_{RR,\,ij} & \bar{Z}_{R,\,jj} \end{array}\right] \tag{4.9}$$

4.3.2. Operational Interaction Operators

Wu *et al.* [14] derive Eqs. (4.2) to (4.4) by determining the boundary condition of stability stability in RES bus i in terms of power injection at that bus, which is then followed by showing the relationship between that boundary condition and system strength. Note that since Wu *et al.* [14] begin with Eq. (4.5) as starting point for its analysis and since Eq. (4.8) is a special case of Eq. (4.5), the concepts of SDSCR and interaction that emerge from Eq. (4.5) still also apply to a system that we reduced its $\boldsymbol{Z}_{bus}$. Thus, Eqs. (4.3) and (4.4) do also have equivalents based on Eq. (4.8) which we write as

$$\bar{S}^{*}_{eq,\,i} = P_{R,\,i} + \bar{w}_{ij} P_{R,\,j} \tag{4.10}$$

$$\bar{w}_{ij} = \frac{\bar{Z}_{RR,\,ij}}{\bar{Z}_{RR,\,ii}} \left(\frac{V_{R,\,i}}{V_{R,\,j}}\right)^{*} \tag{4.11}$$

Here $\bar{w}_{ij}$ is called the *Operational Interaction Operator* (OIO) between RESs i and j, $\bar{Z}_{RR,\,ij}$ and $\bar{Z}_{RR,\,ii}$ are the operational transfer impedance between RES buses i and j and the operational Thevenin impedance at RES bus i, respectively.

Both of Eqs. (4.3) and (4.10) can be used to identify the effect of specific structural change in the transmission system on the impact of interaction on bus i. However, the interaction term in Eq. (4.3) (i.e., $\sum_{j \in \boldsymbol{R},\, j \neq i} P_{R,\,j}\, w_{ij}$) is a summation of multiple complex numbers that are equal to the number of RESs less one, making it hard to apply a vector-based approach to analyzing

the structural effect on the interaction among renewables. For instance, if we have 10 RESs, then the interaction term $\sum_{j \in \boldsymbol{R},\, j \neq i} P_{R,\,j}\, w_{ij}$ will be a summation of 9 complex numbers. It would then be hard to tell which w_{ij} change was responsible for the increase/decrease in interaction. By contrast, in Eq. (4.10), we have only one interaction term (i.e., $\bar{w}_{ij} P_{R,\,j}$), allowing us to do a simple vector-based analysis. Such analysis is primarily based on the location of the angle of the OIO and its importance in determining whether the angle of the OIO or its magnitude has the most significant impact on the magnitude of Eq. (4.3). We describe this in details and with illustrative diagrams in the next section. Afterwards, we draw final conclusions as to when the angle of OIO is more relevant than its magnitude, and when the opposite is true.

4.4. A Mathematical Basis for Understanding the Relationship Between Interaction and Structural Changes in Power Grid

Eqs. (4.10) and (4.11) show that the interaction effect and its relationship with structural changes can be addressed from a vector-based perspective. The impact of interaction on RES bus i is captured in a single operator (i.e., $\bar{w}_{ij}$) that will govern how the 'equivalent' complex power at bus i varies. However, since both angle and magnitude of $\bar{w}_{ij}$ may change because of structural or operating conditions changes, we need to examine some phasor diagrams that help us decide which one (angle or magnitude) is more important under which circumstances. This is the topic of the current section.

In the following subsections, we will use the concept of 'quadrant' to refer to the quadrant at which the angle of $\bar{w}_{ij}$ lies, which significantly influences whether the angle or magnitude of $\bar{w}_{ij}$ will be the most dominant. To understand the concepts we discuss in this section and avoid confusion, the reader is advised to see Figs. 4.4. to 4.6. and read their sublabels since each one contains an important concept we want to emphasize.

4.4.1. Preliminaries

This section furnishes some preliminaries that will be used later. From Eqs. (4.10) and (4.11), the magnitude of $P_{R,i} + \bar{w}_{ij}P_{R,j}$ can be written as

$$|P_{R,i} + \bar{w}_{ij}P_{R,j}| = \sqrt{\left[P_{R,j} + |\bar{w}_{ij}P_{R,j}| \cos\left(\angle P_{R,j}\bar{w}_{ij}\right)\right]^2 + \left[|\bar{w}_{ij}P_{R,j}| \sin\left(\angle P_{R,j}\bar{w}_{ij}\right)\right]^2} \quad (4.12)$$

From Eq. (4.12), it is clear $|\bar{w}_{ij}P_{R,j}| \cos\left(\angle P_{R,j}\bar{w}_{ij}\right)$ is added directly to $P_{R,j}$. By contrast, $|\bar{w}_{ij}P_{R,j}| \sin\left(\angle P_{R,j}\bar{w}_{ij}\right)$ is added in quadrature to $[P_{R,j} + |\bar{w}_{ij}P_{R,j}| \cos\left(\angle P_{R,j}\bar{w}_{ij}\right)]$. It follows that their impact on Eq. (4.12) (hence the interaction amount) can vary. For convenience, we denote the change in $|\bar{w}_{ij}P_{R,j}| \cos\left(\angle P_{R,j}\bar{w}_{ij}\right)$ as $\Delta\Re\left[\bar{w}_{ij}P_{R,j}\right]$ and the change in $|\bar{w}_{ij}P_{R,j}| \sin\left(\angle P_{R,j}\bar{w}_{ij}\right)$ as $\Delta\Im\left[\bar{w}_{ij}P_{R,j}\right]$.

We categorize the changes in $|P_{R,j} + \bar{w}_{ij}P_{R,j}|$ as 'classes'. Each class is used to provide a rough idea of the amount of impact on $|P_{R,j} + \bar{w}_{ij}P_{R,j}|$ due to changes in real or imaginary parts of $\bar{w}_{ij}P_{R,j}$. They are

Class A The change in $|P_{R,j} + \bar{w}_{ij}P_{R,j}|$ is largest when $\Delta\Re\left[\bar{w}_{ij}P_{R,j}\right]$ is *negative (positive)* and significant while $\Delta\Im\left[\bar{w}_{ij}P_{R,j}\right]$ is *negative (positive)* whether moderate or significant

Class B The change in $|P_{R,j} + \bar{w}_{ij}P_{R,j}|$ is large when $\Delta\Re\left[\bar{w}_{ij}P_{R,j}\right]$ is significant (*regardless of sign*) while $\Delta\Im\left[\bar{w}_{ij}P_{R,j}\right]$ is minor (*regardless of sign*)

An example of this is illustrated in Fig. 4.3.(I). When $\Delta\Re\left[\bar{w}_{ij}P_{R,j}\right]$ is significant and negative, the change in $|P_{R,j} + \bar{w}_{ij}P_{R,j}|$ is large despite $\Delta\Im\left[\bar{w}_{ij}P_{R,j}\right]$ being positive and minor

Class C The change in $|P_{R,j} + \bar{w}_{ij}P_{R,j}|$ is moderate when $\Delta\Re\left[\bar{w}_{ij}P_{R,j}\right]$ is *negative (positive)* and significant while $\Delta\Im\left[\bar{w}_{ij}P_{R,j}\right]$ is *positive (negative)* and significant

From Fig. 4.3.(II) we see that $\Delta\Re\left[\bar{w}_{ij}P_{R,\,j}\right]$ is negative while $\Delta\Im\left[\bar{w}_{ij}P_{R,\,j}\right]$ is positive. Despite being of opposite signs with equal magnitudes, $\Delta\Re\left[\bar{w}_{ij}P_{R,\,j}\right]$ had a greater impact and there is a moderate negative change in $|P_{R,\,j}+\bar{w}_{ij}P_{R,\,j}|$

Class D The change in $|P_{R,\,j}+\bar{w}_{ij}P_{R,\,j}|$ is very small when $\Delta\Re\left[\bar{w}_{ij}P_{R,\,j}\right]$ is *negative (positive)* and minor while $\Delta\Im\left[\bar{w}_{ij}P_{R,\,j}\right]$ is *positive (negative)* and significant

From Fig. 4.3.(III) we see that $\Delta\Re\left[\bar{w}_{ij}P_{R,\,j}\right]$ is negative and minor and small while $\Delta\Im\left[\bar{w}_{ij}P_{R,\,j}\right]$ is positive and significant. However, $|P_{R,\,j}+\bar{w}_{ij}P_{R,\,j}|$ did not change that much. This means that $\Delta\Re\left[\bar{w}_{ij}P_{R,\,j}\right]$ had a great impact despite being substantially smaller than $\Delta\Im\left[\bar{w}_{ij}P_{R,\,j}\right]$

Class E The change in $|P_{R,\,j}+\bar{w}_{ij}P_{R,\,j}|$ is smallest when $\Delta\Re\left[\bar{w}_{ij}P_{R,\,j}\right]$ and $\Delta\Im\left[\bar{w}_{ij}P_{R,\,j}\right]$ are of *opposite signs* and both are minor

4.4.2. Angle of $\bar{w}_{ij}$ is in Quadrant I or IV

Fig. 4.4. illustrates the effect of $\angle\bar{w}_{ij}$ when it is between -90° to 90°. Under such condition $|\bar{w}_{ij}|$ is more dominant for one clear reason; $P_{R,\,i}$ is a real positive number, and when the angle of $\bar{w}_{ij}$ is close to 0°, then $\bar{w}_{ij}P_{R,\,j}$ will be mostly real part which significantly increases the magnitude of their summation (Fig. 4.4.(I)). Further, when the magnitude increases, some of its imaginary part will also increase which helps slightly increase the magnitude meaning that changes in imaginary part happen in such a way that their effect *stacks*. Thus, Class A or (at least) Class B applies.

The angle of $\bar{w}_{ij}$ is relevant in these quadrants but not as much as its magnitude. In these quadrants, if the angle of $\bar{w}_{ij}$ deviates away from 0°, its real part decreases while its imaginary part increase (and vice versa for the opposite) meaning that the effect of one *partially offsets* the other (Fig. 4.4.(II)). Thus, Class D or (at most) Class C applies.

Thus, in Quadrants I and IV, it is clear that the effect of $|\bar{w}_{ij}|$ is more dominant than that of $\angle\bar{w}_{ij}$ since the effect of $|\bar{w}_{ij}|$ belongs to higher classes.

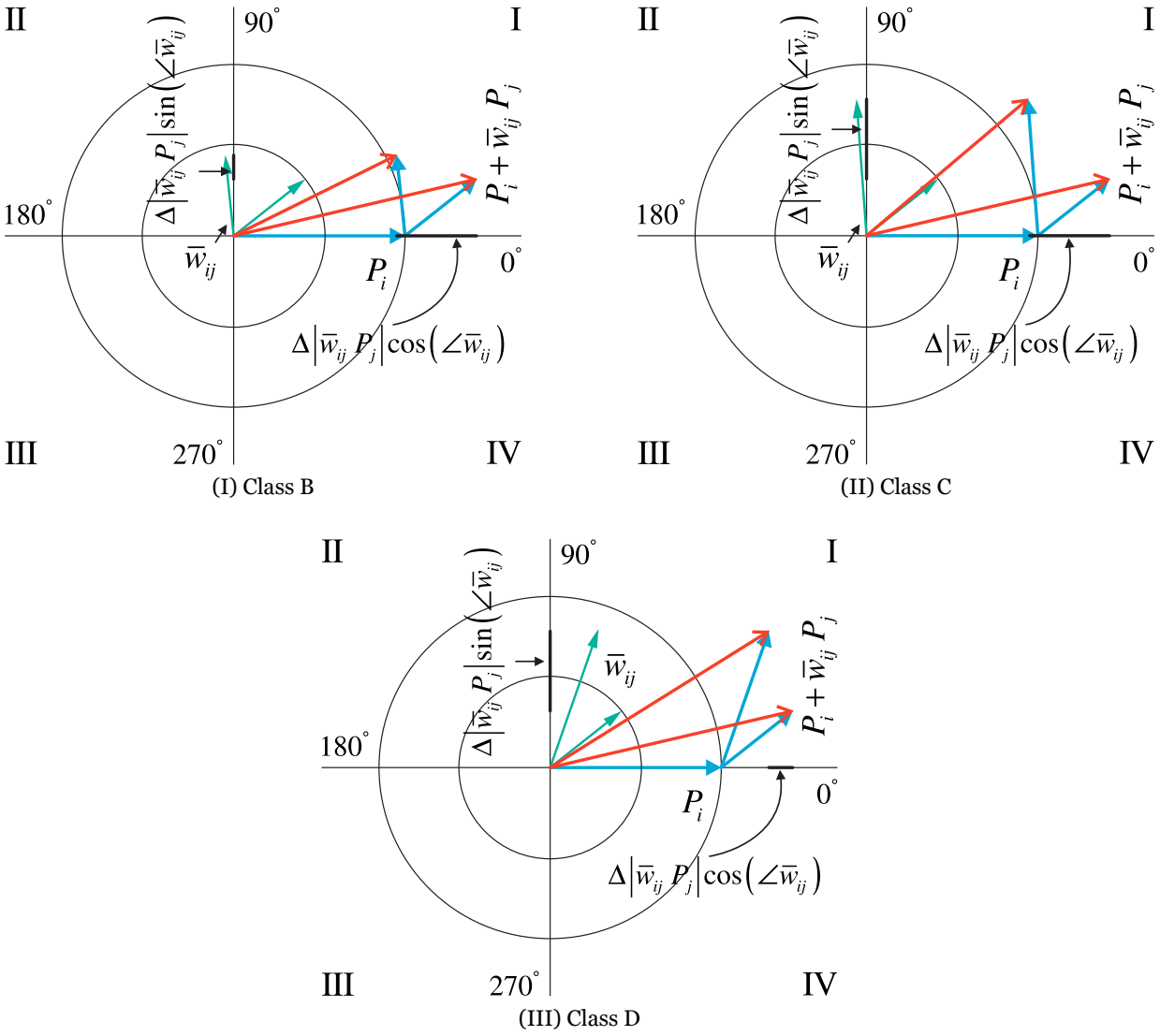

Fig. 4.3. $|P_{R,j}+\bar{w}_{ij}P_{R,j}|$ Changes Classes

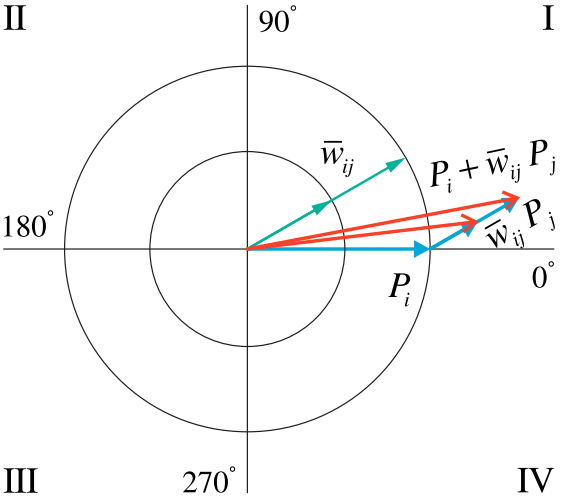

(I) $|\bar{w}_{ij}|$ is most significant in Quadrants I and IV

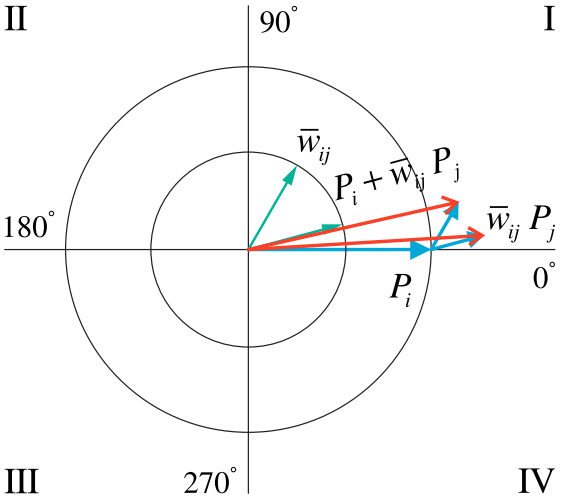

(II) $\angle\bar{w}_{ij}$ is least significant in Quadrants I and IV

Fig. 4.4. The effect of $\bar{w}_{ij}$ Magnitude and Angle Quadrants I and IV. $\bar{w}_{ij}$ is not drawn to scale

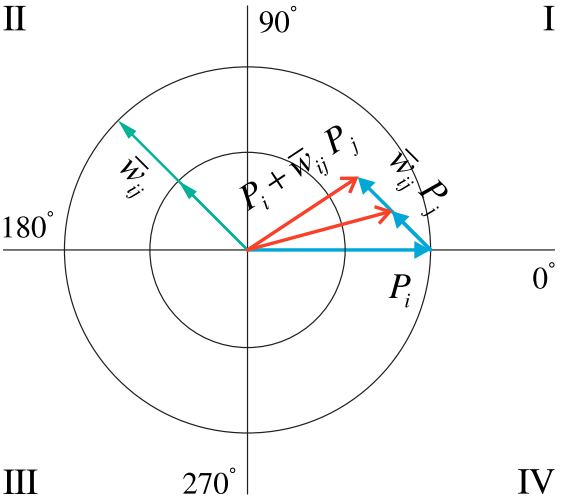

(I) $|\bar{w}_{ij}|$ is least significant in Quadrants II and III

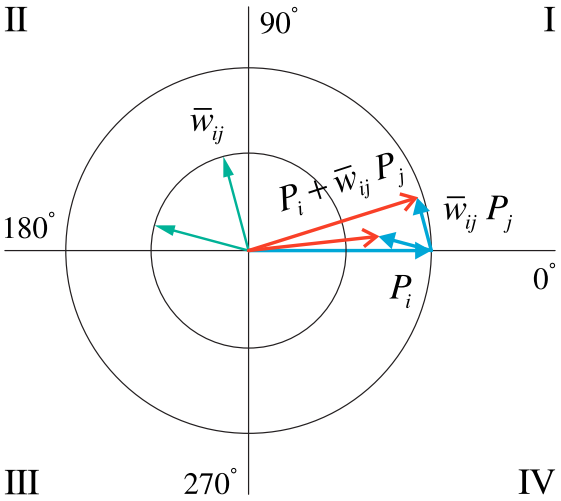

(II) $\angle\bar{w}_{ij}$ is most significant in Quadrants II and III

Fig. 4.5. The effect of $\bar{w}_{ij}$ Magnitude and Angle in Quadrants II and III. $\bar{w}_{ij}$ is not drawn to scale

4.4.3. Angle of $\bar{w}_{ij}$ is in Quadrant II or III

Fig. 4.5. illustrates the effect of $\angle\bar{w}_{ij}$ when it is between 90° to 270°. Under such condition, $\angle\bar{w}_{ij}$ is more dominant. The magnitude of $\bar{w}_{ij}$ is relevant in these quadrants but not as much as its angle. By looking closely at Fig. 4.5.(II), we see that when the angle approaches 180°, then $\bar{w}_{ij}P_{R,\,j}$ will be mostly *negative real part* which subtracts from the real positive number $P_{R,\,i}$. Further, increasing the angle towards 180° decreases the imaginary part which helps further reduce the imaginary part of $\bar{w}_{ij}P_{R,\,j}$ reducing what adds in quadrature to $P_{R,\,j}$. Thus, in these two quadrants, the change of angle happens to lead to changes in real and imaginary part in such a way that their effect *stacks*. Thus, Class A or (at least) Class B applies. By contrast, when increasing the magnitude, the real part of $\bar{w}_{ij}P_{R,\,j}$ becomes more negative than it was, but the imaginary part will increase which *partially offsets* some of the effect of the real part on $|\bar{w}_{ij}P_{R,\,j}|$ (Fig. 4.5.(I)). Similar arguments apply to when the magnitude of $\bar{w}_{ij}$ decreases. Thus, Class D or (at most) Class C applies.

Thus, in Quadrants II and III, it is clear that the effect of $\angle\bar{w}_{ij}$ is more dominant than that of $|\bar{w}_{ij}|$ since the effect of $\angle\bar{w}_{ij}$ belongs to higher classes.

4.4.4. Angle of $\bar{w}_{ij}$ is near $\pm 90^{\circ}$

When the angle of $\bar{w}_{ij}$ is very close to the threshold that separates Quadrants I and II (i.e., 90°) or Quadrants III and IV (i.e., -90° or 270°), we need more analysis than the one done in SubSections 4.4.2. and 4.4.3. Since these areas 'critical' and separate quadrants from each other, the effect of $|\bar{w}_{ij}|$ and $\angle\bar{w}_{ij}$ could stack well (or weakly) or cancel each other significantly (or marginally).

Fig. 4.6.(I) shows three vectors of $P_{R,\,i} + \bar{w}_{ij}P_{R,\,j}$ when $|\bar{w}_{ij}|$ changes from 1 (relative reference) to 1.36 (moderate change) to 1.88 (substantial change). In the figure, we can clearly see

that 36% increase in $|\bar{w}_{ij}|$ increased $|P_{R,\,i} + \bar{w}_{ij}P_{R,\,j}|$ by only 3%, and 12% increase required almost doubling $|\bar{w}_{ij}|$. Thus, the significance of $|\bar{w}_{ij}|$ is relatively small when $\angle\bar{w}_{ij}$ near $\pm 90^{\circ}$. Thus, Class D applies.

Fig. 4.6.(II) shows three vectors of $P_{R,\,i} + \bar{w}_{ij}P_{R,\,j}$ when $|\bar{w}_{ij}|$ changes from 75° (reference) to 90° (moderate change) to 120° (substantial change). In the figure, we can clearly see that 15° increase in $\angle\bar{w}_{ij}$ decreases $P_{R,\,i} + \bar{w}_{ij}P_{R,\,j}$ by only 6%, and 45° increase substantially changed $|P_{R,\,i} + \bar{w}_{ij}P_{R,\,j}|$ by 21%. Thus, the significance of $\angle\bar{w}_{ij}$ is moderate near $\pm 90^{\circ}$. Thus, Class B or (at least) Class C applies.

4.4.5. Combined Effect of $\bar{w}_{ij}$ Angle and Magnitude When its Angle is Near $\pm 90^{\circ}$

It is possible that both $|\bar{w}_{ij}P_{R,\,j}|$ and $\angle\bar{w}_{ij}P_{R,\,j}$ change simultaneously. Under such a case, we still need to determine which one of them is more dominant (if any). Here, we will address such question by checking how much change in the angle we need to (noticeably) influence the effect of magnitude changes. Likewise, we will also check how much change in the magnitude we need to (noticeably) influence the effect of angle changes.

From Fig. 4.6.(I), we learn that moderate amount of change in magnitude caused only 3% increase in $|P_{R,\,i} + \bar{w}_{ij}P_{R,\,j}|$. Such amount of increase can be significantly enhanced by slight change in $\angle\bar{w}_{ij}$ towards 0°, which we can see by looking at Fig. 4.6.(III). A 15° decrease in $\angle\bar{w}_{ij}$ changed the increase in $|\bar{w}_{ij}P_{R,\,j}|$ from 3% to 12%. Similar reasoning applies to substantial changes in $|\bar{w}_{ij}|$ along with slight changes in $\angle\bar{w}_{ij}$ towards 0°. Thus, Class B applies and a slight change in the angle significantly changes the effect of $|\bar{w}_{ij}|$.

Similarly, Fig. 4.6.(IV) illustrates phasor diagrams of $\angle\bar{w}_{ij}P_{R,\,j}$ near $\pm 90^{\circ}$ with both angle and magnitude of $\bar{w}_{ij}$ changing. When $\angle\bar{w}_{ij}$ moves towards 180° by 15°, a moderate change in $|\bar{w}_{ij}P_{R,\,j}|$ is required to slightly offset effect of $\angle\bar{w}_{ij}P_{R,\,j}$ on the reference magnitude. Further,

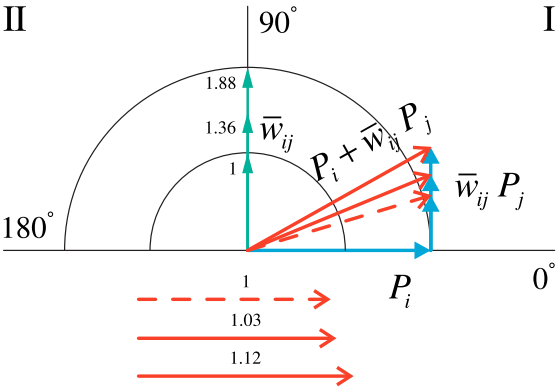

(I) $|\bar{w}_{ij}|$ is slightly significant when $\angle\bar{w}_{ij}$ is near $\pm 90°$

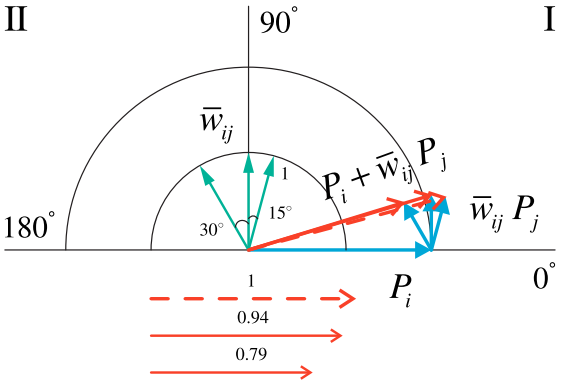

(II) $\angle\bar{w}_{ij}$ is moderately significant when $\angle\bar{w}_{ij}$ is near $\pm 90°$

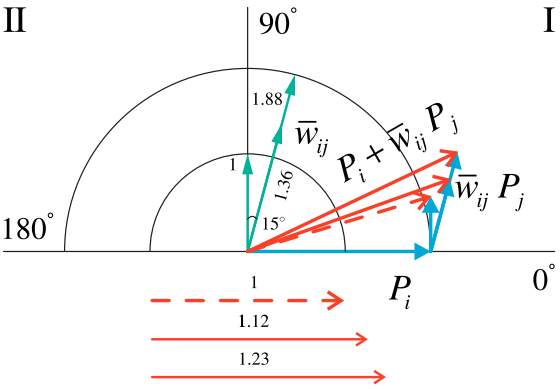

(III) Small changes in $\angle\bar{w}_{ij}$ significantly change the effect of $|\bar{w}_{ij}|$ near $\pm 90°$

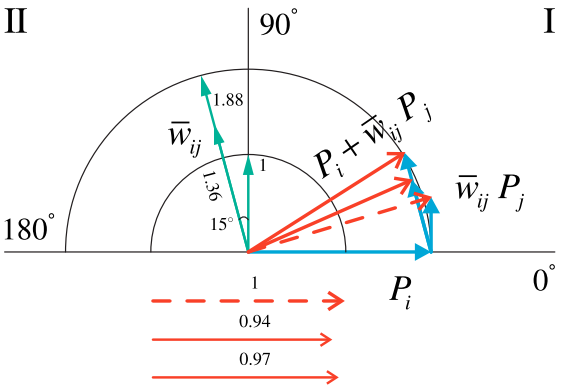

(IV) Substantial changes in $|\bar{w}_{ij}|$ are needed to change effect of $\angle\bar{w}_{ij}$ near $\pm 90°$

1. Figures are drawn to scale except for $\bar{w}_{ij}$. Numbers near $\bar{w}_{ij}$ *do not* represent their actual values, but rather normalized ones for convenience and comparison purposes
2. $|P_{R,i} + \bar{w}_{ij} P_{R,j}|$ that is taken as reference is shown in dashed lines
3. Numbers close to $P_{R,i} + \bar{w}_{ij} P_{R,j}$ show their relative lengths with respect to each other
4. What applies to Quadrant I and II also applies to Quadrant IV and III, respectively
5. The subscript R in $P_{R,i}$ and $P_{R,j}$ is dropped to improve figure readability

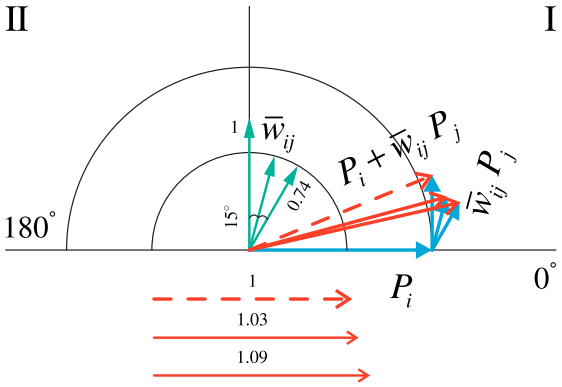

(V) Small to moderate change in $\angle\bar{w}_{ij}$ can offset the effect of moderate change in $|\bar{w}_{ij}|$ near $\pm 90°$

Fig. 4.6. The effect of $\bar{w}_{ij}$ Magnitude and Angle in Different Quadrants. $\bar{w}_{ij}$ is not drawn to scale

from Fig. 4.6.(IV), we see that $|P_{R,i} + \bar{w}_{ij}P_{R,j}|$ is supposed to decrease because of deviation of $\angle\bar{w}_{ij}P_{R,j}$ towards 180°. However, a substantial change in $|\bar{w}_{ij}P_{R,j}|$ still does not entirely offset the decrease in $|P_{R,i} + \bar{w}_{ij}P_{R,j}|$ (there is still 3% decrease). Thus, Class D applies and substantial changes in $|\bar{w}_{ij}P_{R,j}|$ are needed to change the effect of $\angle\bar{w}_{ij}P_{R,j}$ near $\pm 90^{\circ}$.

Finally, Fig. 4.6.(V) illustrates another phasor diagrams of $\angle\bar{w}_{ij}P_{R,j}$ near $\pm 90^{\circ}$ with both angle and magnitude of $\bar{w}_{ij}$ changing. It is clear that when we are close to $\pm 90^{\circ}$ the magnitude of $P_{R,i} + \bar{w}_{ij}P_{R,j}$ should decrease with decreases in $|\bar{w}_{ij}P_{R,j}|$. However, when $|\bar{w}_{ij}P_{R,j}|$ moderately decreases by 26% simultaneously with slight deviation in $\angle\bar{w}_{ij}P_{R,j}$ towards 0°, the magnitude of $P_{R,i} + \bar{w}_{ij}P_{R,j}$ actually increases slightly, which leads us to the conclusion that small to moderate change in $\angle\bar{w}_{ij}P_{R,j}$ can offset the effect of moderate change in $|\bar{w}_{ij}P_{R,j}|$.

4.4.6. Summary on the Effects of $\bar{w}_{ij}$ Angle and Magnitude in Different Quadrants

This SubSection provides remarks based on SubSections 4.4.2. to 4.4.5.: **a)** When $\angle\bar{w}_{ij}$ is in Quadrant I or IV, the effect of changing $|\bar{w}_{ij}P_{R,j}|$ will cause real and imaginary parts of $\bar{w}_{ij}P_{R,j}$ to change in such a way that their effects on $|P_{R,i} + \bar{w}_{ij}P_{R,j}|$ *stack* (i.e., either both real and imaginary cause an increase in $|P_{R,i} + \bar{w}_{ij}P_{R,j}|$ or both will cause a decrease in $|P_{R,i} + \bar{w}_{ij}P_{R,j}|$). This is Class A or (at least) Class B change. By contrast, the effect of changing $\angle\bar{w}_{ij}$ will cause imaginary and real parts to *partially offset each other*. This is Class D or (at most) Class C change. Thus, the magnitude of $\bar{w}_{ij}$ is more relevant than its angle if the latter is in Quadrants I or IV; **b)** When $\angle\bar{w}_{ij}$ is in Quadrant I or III, the effect of changing $\angle\bar{w}_{ij}$ will cause real and imaginary parts of $\bar{w}_{ij}P_{R,j}$ to change in such a way that their effects on $|P_{R,i} + \bar{w}_{ij}P_{R,j}|$ *stack* (i.e., either both real and imaginary increase in $|P_{R,i} + \bar{w}_{ij}P_{R,j}|$ or both will decrease). This is Class A or (at least) Class B change. By contrast, the effect of changing $|\bar{w}_{ij}P_{R,j}|$ will cause imaginary and real parts to *partially offset each other* (i.e., if the real part change contributes to an increase in

$P_{R,\,i} + \bar{w}_{ij} P_{R,\,j}$, the imaginary part will contribute to its decrease, and vice versa). This is Class D or (at most) Class C change. Thus, the angle of $\bar{w}_{ij}$ is more relevant than its magnitude if it is in Quadrants I or IV; **c)** When $\angle \bar{w}_{ij}$ is close to $\pm 90^{\circ}$, substantial changes in the value of $|\bar{w}_{ij} P_{R,\,j}|$ yield moderate change in $|P_{R,\,i} + \bar{w}_{ij} P_{R,\,j}|$. By contrast, only moderate changes in $\angle \bar{w}_{ij}$ are needed to get substantial changes in $|P_{R,\,i} + \bar{w}_{ij} P_{R,\,j}|$. Further, a slight change in the angle significantly influences the effect of moderate or substantial changes in the magnitude. We see this when we compare Fig. 4.6.(I) and Fig. 4.6.(III). A small decrease in $\angle \bar{w}_{ij}$ noticeably boosted the effect of $|\bar{w}_{ij} P_{R,\,j}|$ increase on $|\bar{w}_{ij} P_{R,\,j}|$; **d)** When $\angle \bar{w}_{ij}$ is close to $\pm 90^{\circ}$, substantial changes in $|\bar{w}_{ij} P_{R,\,j}|$ barely offset the effect of even small changes in $\angle \bar{w}_{ij}$ (in Fig. 4.6.(IV), the increase in $|\bar{w}_{ij} P_{R,\,j}|$ could not increase the value of $|P_{R,\,i} + \bar{w}_{ij} P_{R,\,j}|$ by an amount large enough to offset its decrease due to $\angle \bar{w}_{ij}$ change). By contrast, small to moderate changes in $\angle \bar{w}_{ij}$ offset and reverse the effect of moderate changes in $|\bar{w}_{ij} P_{R,\,j}|$ (in Fig. 4.6.(V), the change in $\angle \bar{w}_{ij}$ increased $|P_{R,\,i} + \bar{w}_{ij} P_{R,\,j}|$ which reversed the expected effect of $|\bar{w}_{ij} P_{R,\,j}|$), and **e)** From Items c and d, it is clear that when the angle of $\bar{w}_{ij}$ is close to $\pm 90^{\circ}$, then $\angle \bar{w}_{ij} P_{R,\,j}$ is more dominant than $|\bar{w}_{ij} P_{R,\,j}|$.

4.5. Numerical Verification

In this Section, we present numerical results showing the accuracy of the remarks we emphasized in Section 4.4. Using MATPOWER package in MATLAB (available online at www.pserc.cornell.edu/matpower), we simulated the IEEE 118-bus system. During the simulation, we modeled 5 RESs at different buses and with different real power injection levels. We used Eq. (C.7) to replace 3 of the RESs with their equivalent impedance (which is of pure negative real value since RESs are operating at unity power factor). The voltage-current relationship would then be given by Eqs. (4.7) and (4.8). Certain elements in Eq. (4.9) were used to calculate $\bar{w}_{ij}$. We repeated this for all of the 179 lines (with $3\,\mathrm{p.u}$ change in susceptance in each line).

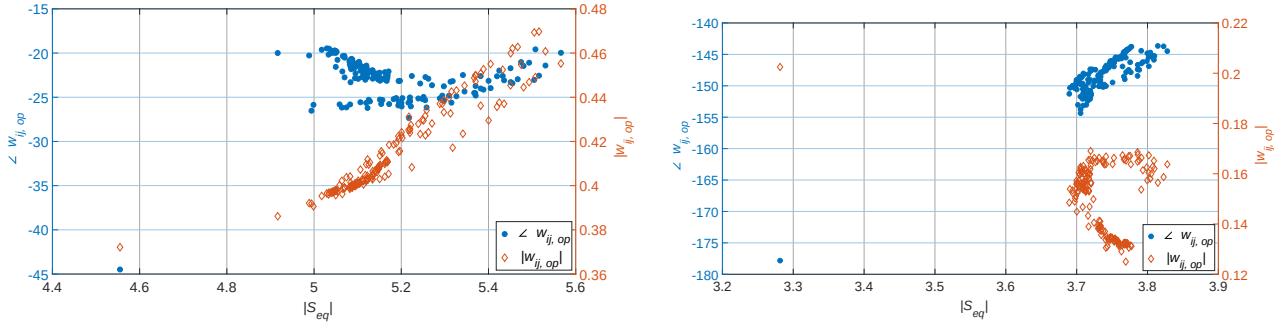

(I) All Angles are in Quadrant IV

(II) All Angles are in Quadrant III

Fig. 4.7. Scatter Plots of $|\bar{w}_{ij}|$ and $\angle\bar{w}_{ij}$ Against $|S_{eq,i}|$ for $\angle\bar{w}_{ij}$ in Quadrants III and IV

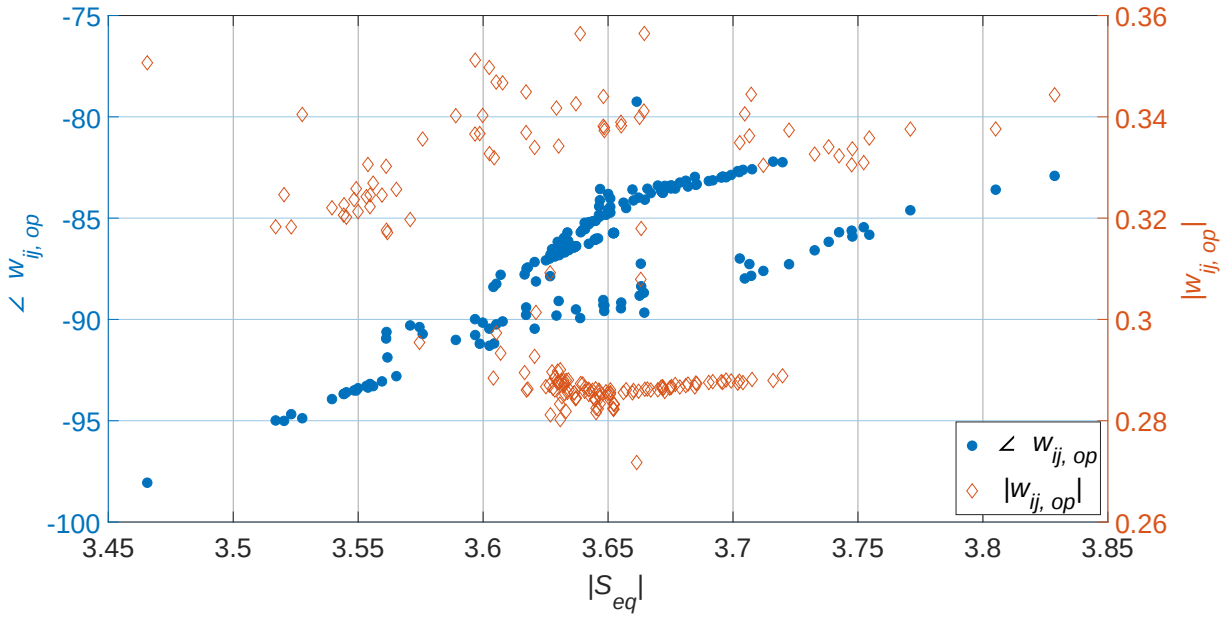

Fig. 4.8. Scatter Plots of $|\bar{w}_{ij}|$ and $\angle\bar{w}_{ij}$ Against $|S_{eq,i}|$ for $\angle\bar{w}_{ij}$ in Both of Quadrants III and IV

TABLE 4.1.
DETERMINATION OF CRITICAL LINES AMONG RESS BASED ON OPERATIONAL INTERACTION OPERATORS

Quadrant	POI i	POI j	Other POIs			Critical Line Based on $\angle\bar{w}_{ij}$ or $\lvert\bar{w}_{ij}\rvert$	Actual Critical Line (based on Eq. (4.2))	$\lvert S_{eq,i}\rvert$	$SDSCR_i$	$\frac{Max\ SDSCR_i}{Mean\ SDSCR_i}$
III	101	64	96	106	37	86-87	86-87	4.38	2.02	1.41
IV	79	96	9	81	33	9-10	9-10	3.40	5.13	1.28
III IV[a]	97	60	39	37	86	43-44	43-44	3.98	3.18	1.07

[a] angles of $\angle\bar{w}_{ij}$ exist in both quadrants

By doing what is previously mentioned, we wind up with 179 value of $\bar{w}_{ij}$. Next, we calculate the magnitudes and angles of these OIOs and plot $|S_{eq,\,i}|$ found by Eq. (4.3) (not Eq. (4.10)) against the angle and magnitude of $\bar{w}_{ij}$. Thus, we wind up with scatter plot whose x-axis is $|S_{eq,\,i}|$ and has two y-axes, one for $\angle\bar{w}_{ij}$ and the other for $|\bar{w}_{ij}|$. If the concepts in Sections 4.3. and 4.4. are correct then we will see that: **a)** Eqs. (4.10) and (4.11) can be used as simplified alternative for Eqs. (4.3) and (4.4), and **b)** there proportionality between $|\bar{w}_{ij}|$ and $|S_{eq,\,i}|$ in Quadrants I and IV and another proportionality between $\angle\bar{w}_{ij}$ and $S_{eq,\,i}$ in Quadrants II and III (but when $\angle\bar{w}_{ij}$ is close to $\pm 90^{^\circ}$, the angle of $\bar{w}_{ij}$ is more dominant than its magnitude).

Fig. 4.7.(I) shows a a scatter plot in Quadrant IV. It is clear that there is a high correlation between $|\bar{w}_{ij}|$ and $|S_{eq,\,i}|$, which is stronger than the one between $\angle\bar{w}_{ij}$ and $|S_{eq,\,i}|$. In terms of statistical numbers, we did a simple linear regression between these variables. We found that R^{mag}_{square} (R-square of the simple linear model $|S_{eq,\,i}|$ as a function $|\bar{w}_{ij}|$) is 0.9 and has a p-value of (almost) zero. High R^{mag}_{square} means that a lot of variation in $|S_{eq,\,i}|$ can be explained by $|\bar{w}_{ij}|$ while a low p-value means it was not a mere coincidence to get a well-fit model between $|S_{eq,\,i}|$ and $|\bar{w}_{ij}|$.

Fig. 4.7.(II) shows a a scatter plot in Quadrant III. It is clear that there is a high correlation between $\angle\bar{w}_{ij}$ and $|S_{eq,\,i}|$, which is stronger than the one between $|\bar{w}_{ij}|$ and $|S_{eq,\,i}|$. R^{angle}_{square} is 0.8 and has a p-value of (almost) zero. Similar to what we previously mentioned, high R^{angle}_{square} means that a lot of variation in $|S_{eq,\,i}|$ that can be explained by $|\bar{w}_{ij}|$ while a low p-value means it was not a mere coincidence to get a well-fit model between $|S_{eq,\,i}|$ and $|\bar{w}_{ij}|$.

Finally, Fig. 4.8. shows a scatter plot where angles exist in both Quadrants III and IV. For both angle and magnitude of $\bar{w}_{ij}$ the data points look more 'randomized' than in Fig. 4.7. However, Fig. 4.8. still shows that there is a modest correlation between $\angle\bar{w}_{ij}$ and $|S_{eq,\,i}|$. With R^{angle}_{square} of 0.62 and p-value of nearly zero we conclude that $|S_{eq,\,i}|$ can be (more or less but not as

much as when all angles are entirely in Quadrant II or III) explained by $\angle\bar{w}_{ij}$, which is not due to a mere coincidence.

4.6. Short Numerical Example

The mathematical approach and the concepts developed in Sections 4.3. and 4.4. are meant to advance our theoretical understanding of the interaction among RESs. In this section, we present a short example on how such understanding can be beneficial. One benefit of our analysis is that the angle and magnitude of $\bar{w}_{ij}$ are important variables/parameters that contain valuable information about system structure and its strength at the same time. However, as we explained before, each one is more dominant in specific regions. We apply such concept of 'dominance' to help us find the most influential line on a certain $|S_{eq,\,i}|$ (Eq. (4.3)). Such line is denoted as *critical* line because changing susceptance at both of its ends significantly changes $|S_{eq,\,i}|$. We study the IEEE 118-bus system with five RESs and denote one RES POI as i and the another one as j. By following similar procedure to the ones mentioned in Section 4.5. we wind up collecting some data on the influence of lines on $|S_{eq,\,i}|$.

TABLE 4.1. shows some results for different RESs combinations that result in $\bar{w}_{ij}$ angles being in different regions (Quadrant III, IV, or in both). It is clear that estimating line shunt susceptance influence on system strength based on how they affect $\angle\bar{w}_{ij}$ and $|\bar{w}_{ij}|$ leads us to an accurate identification of critical lines, implying that $\bar{w}_{ij}$ contains valuable information about system strength and interaction among RESs. Further, the last column in TABLE 4.1. shows the ratio of the maximum $SDSCR_i$ (the one we get by changing the susceptance of the critical line) to the mean $SDSCR_i$ (the average of all $SDSCR$ by changing the susceptance of each other line). It is clear from this column that the significant difference in $SDSCR_i$ means that finding the critical line and providing theoretical justification as to why that line was 'critical' is worth the effort.

It is clear that there is a high correlation between $\angle\bar{w}_{ij}$ and $|S_{eq,\,i}|$, which is stronger than the one between $|\bar{w}_{ij}|$ and $|S_{eq,\,i}|$. R^{angle}_{square} is 0.8 and has a p-value of (almost) zero. Similar to what we previously mentioned, high R^{angle}_{square} means that a lot of variation in $|S_{eq,\,i}|$ that can be explained by $|\bar{w}_{ij}|$ while a low p-value means that this is not a mere coincidence to get a well-fit model between $|S_{eq,\,i}|$ and $|\bar{w}_{ij}|$.

4.7. Conclusions

In this dissertation, we investigate and characterize interaction among RESs. We explain why $S_{eq,\,i}$ in $SDSCR$ expression can be hard to use as a means to understand the interaction. Thus, we develop the concept of operational transfer impedances and OIOs, which significantly help us establish a simplified vector-based understanding of the interaction among RESs. We show that the advantage of OIOs over interaction operators is that we identify which lines are more influential than others by merely checking either their angles or magnitudes changes. With interaction operators, however, we cannot identify which one of them is more important than others and whether magnitudes or angles are more important under certain conditions. The concepts are then verified by numerical simulation with statistical analysis.

We show how OIOs contain valuable information by using them to identify critical lines with respect to interaction amount and showing that these lines do indeed have a strong influence on system strength at RES POI i.

Other potential applications of OIOs include: **a)** placement of new RESs while taking into account the interaction with pre-existing ones; **b)** interaction-constrained load flow solution, power system operation, or wind turbine controllers design and testing, and **c)** inclusion of OIOs magnitude or angle when defining the fitness function of swarm intelligence algorithms when used to optimize power system operation.

4.8. References

[1] Grant, "Report in the Matter of Integration and Transmission Study for the Future Renewable Energy Standard," Minnesota Department of Commerce, Tech. Rep., Nov. 2014.

[2] S. Achilles, A. Isaacs, J. MacDowell, and C. Smith, "Integrating Inverter-Based Resources into Low Short Circuit Strength Systems," NERC, Tech. Rep., Dec. 2017.

[3] Y. Zhou, D. Nguyen, P. Kjaer, and S. Saylors, "Connecting wind power plant with weak grid-Challenges and solutions," in *Power and Energy Society General Meeting (PES), 2013 IEEE*, IEEE, 2013, pp. 1–7.

[4] Y. Zhang, S. F. Huang, *et al.*, "Evaluating system strength for large-scale wind plant integration," in *2014 IEEE PES General Meeting | Conference Exposition*, Jul. 2014, pp. 1–5.

[5] J. Schmall, S.-H. Huang, *et al.*, "Voltage stability of large-scale wind plants integrated in weak networks: An ERCOT case study," in *Power & Energy Society General Meeting, 2015 IEEE*, IEEE, 2015, pp. 1–5.

[6] A. Gavrilovic, "AC/DC system strength as indicated by short circuit ratios," in *AC and DC Power Transmission, 1991., International Conference on*, IET, 1991, pp. 27–32.

[7] P. Krishayya, R. Adapa, M. Holm, *et al.*, "IEEE guide for planning DC links terminating at AC locations having low short-circuit capacities, part I: AC/DC system interaction phenomena," *IEEE Std. France: CIGRE*, 1997.

[8] J. Chen-chen, W. Jun, and B. Xiao-yu, "Study of the effect of AC system strength on the HVDC startup characteristics," 2012.

[9] S. L. Lorenzen, A. B. Nielsen, and L. Bede, “Control of a grid connected converter during weak grid conditions,” in *Power Electronics for Distributed Generation Systems (PEDG), 2016 IEEE 7th International Symposium on*, IEEE, 2016, pp. 1–6.

[10] H. Urdal, R. Ierna, *et al.*, “System strength considerations in a converter dominated power system,” *IET Renewable Power Generation*, vol. 9, no. 1, pp. 10–17, 2014.

[11] C. Moné, A. Smith, B. Maples, and M. Hand, “Essential Reliability Services Task Force Measures Framework Report,” NERC, Tech. Rep., Nov. 2015.

[12] R. Fernandes, S. Achilles, and J. MacDowell, “Report to NERC ERSTF for Composite Short Circuit Ratio (CSCR) Estimation Guideline,” GE, Tech. Rep., Jan. 2015.

[13] J. Schmall, S.-H. Huang, *et al.*, “Voltage stability of large-scale wind plants integrated in weak networks: An ERCOT case study,” in *Power & Energy Society General Meeting, 2015 IEEE*, IEEE, 2015, pp. 1–5.

[14] D. Wu, G. Li, *et al.*, “Assessing Impact of Renewable Energy Integration on System Strength Using Site-Dependent Short Circuit Ratio,” *IEEE Transactions on Sustainable Energy*, 2017.

[15] Y. Zhang, S.-H. F. Huang, *et al.*, “Evaluating system strength for large-scale wind plant integration,” in *PES General Meeting| Conference & Exposition, 2014 IEEE*, IEEE, 2014, pp. 1–5.

[16] J. Z. Zhou and A. M. Gole, “VSC transmission limitations imposed by AC system strength and AC impedance characteristics,” 2012.

[17] R. Grünbaum, P. Halvarsson, and P. Jones, “Series compensation for increased power transmission capacity,” 2010.

[18] S. Grunau and F. W. Fuchs, “Effect of wind-energy power injection into weak grids,” in *Proc. EWEA*, 2012, pp. 1–7.

[19] A. S. Subburaja, N. Shamim, and S. B. Bayne, “Battery Connected DFIG Wind System Analysis for Strong/Weak Grid Scenarios,” in *Green Technologies Conference (GreenTech), 2016 IEEE*, IEEE, 2016, pp. 112–117.

[20] Y. Wang, X. Li, C. Wen, and Y. He, “Impact of AC System Strength on Commutation Failure at HVDC Inverter Station,” in *2012 Asia-Pacific Power and Energy Engineering Conference*, Mar. 2012, pp. 1–4.

CHAPTER 5. CONCLUDING REMARKS

5.1. Significance of Results

A part of significance of the outcomes of this dissertation is mentioned in Section 1.3. (Item c on page 12). The significance of results is mentioned in each paper in its independent chapter. However, I summarize some more benefits of this work as follows

5.1.1. Help Determine the Weakest Combination for Contingency Analysis and Ancillary Services Allocation

When multiple RES interact, they could weaken the strength of each others' POIs. Thus, a fast determination of the weakest combination of RESs provides system operators with more time to conduct a more detailed contingency analysis for these combinations and, if necessary, procure ancillary services that could be necessary to maintain healthy operating conditions in the system (e.g., voltage level or reactive power losses).

5.1.2. Faster Calculation of $\boldsymbol{Z}_{bus}$ is Beneficial for Other Researches

Eqs. (3.23) to (3.26) were derived specifically to rapidly modify $\boldsymbol{Z}_{bus}$ to account for series impedance changes in a line, which would then allow us to recalculate the impedances used in Eqs. (1.14) to (1.16). However, the benefits of fast calculation of $\boldsymbol{Z}_{bus}$ is not limited to grid strength calculations using SDSCR. More recent works show that $\boldsymbol{Z}_{bus}$ contains very useful structural characteristics information that we could employ in loss allocation in deregulated environments [1], voltage stability margin estimation [2], real-time overload relief of transmission lines [3], determination of fault location in transmission networks [4], [5], modeling voltage controllers in load flow [6], and harmonic sources identification [7].

Thus, the importance of such calculation speed can be summarized as follows: **a)** many researchers develop methods that employ $\boldsymbol{Z}_{bus}$ or a part of its elements in the analysis, identification, allocation, etc. Some of these achievements could be more beneficial if an online version of them is developed and deployed; **b)** clearly, in a real-life operation of a power system, its structure changes, and one of these changes could be the continuous variation of the series impedance of branches (e.g., using thyristor controlled series capacitor); **c)** as a result, the methods developed before must update $\boldsymbol{Z}_{bus}$ as they work in real-time; **d)** with the existing methods, the change of the series impedance of a line requires too much of computational effort and time to calculate the new $\boldsymbol{Z}_{bus}$, which slows down estimations, corrective actions, preparing for vulnerabilities, etc, and **e)** developing a new method to increase the speed of constructing $\boldsymbol{Z}_{bus}$ would help mitigate these computational impediments.

5.1.3. Establishing a Scientific Explanation on Interaction Helps Develop Better System Dispatch and Planning Strategies

In SubSection 4.2.2., we explained how multiple RESs could make it challenging to decide which interaction operator must be modified to help mitigate the interaction or improve system strength. In Chapter 4., we establish a simpler mathematical model by removing some of these operators from Eqs. (4.2) to (4.4) and replacing them with one operator between only two RESs of interest. Such approach helps us advance our theoretical understanding of interaction since the simplified model will contain only one interaction operator, thereby help us develop a set of concepts on how the angle and magnitude of such operator influence the overall amount of interaction. Further, such concepts can serve as a basis to further develop better system dispatch and planning strategies. This is especially true since the used vector diagrams contain only two vectors.

5.2. Conclusions

Preceding research on grid strength for RES integration focuses on control of RES power electronic interfaces, evaluating the strength of a power system, or evaluating the accuracy of RES models in weak grids. The goals of this dissertation are to: **a)** develop new methods to help reduce the computational burden relevant to power system strength evaluation, and **b)** advance our theoretical understanding of the interaction among RESs and how it relates to the structure and operating conditions of a power system. Both goals are obsolete in the literature. A summary that highlights some important contributions resulting from the work on these goals is shown in Fig. 1.4. Section 1.3. summarizes the morale behind these goals.

I anticipate that the advances made in this dissertation will lay grounds for: **a)** better and faster power system dispatch and planning strategies while taking into account interaction among RESs; **b)** more systematic analysis of the relationship between grid structure and POI strength of RESs, and **c)** facilitation of real-time deployment of solutions that rely on the bus impedance matrix in their analyses.

5.3. References

[1] A. S. Alayande, A. A. Jimoh, and A. A. Yusuff, "An alternative algorithm for solving generation to load matching and loss allocation problems," *International Transactions on Electrical Energy Systems*, vol. 27, no. 8, e2347, 2017.

[2] H.-Y. Su and C.-W. Liu, "Estimating the voltage stability margin using PMU measurements," *IEEE Transactions on Power Systems*, vol. 31, no. 4, pp. 3221–3229, 2016.

[3] B. Gou and H. Zhang, "Fast real-time corrective control strategy for overload relief in bulk power systems," *IET Generation, Transmission & Distribution*, vol. 7, no. 12, pp. 1508–1515, 2013.

[4] N. Kang and Y. Liao, “Double-circuit transmission-line fault location with the availability of limited voltage measurements,” *IEEE transactions on power delivery*, vol. 27, no. 1, pp. 325–336, 2012.

[5] Q. Jiang, X. Li, B. Wang, and H. Wang, “Pmu-based fault location using voltage measurements in large transmission networks,” *IEEE transactions on power delivery*, vol. 27, no. 3, p. 1644, 2012.

[6] I. Džafić, R. A. Jabr, E. Halilovic, and B. C. Pal, “A sensitivity approach to model local voltage controllers in distribution networks,” *IEEE Transactions on Power Systems*, vol. 29, no. 3, pp. 1419–1428, 2014.

[7] D. Saxena, S. Bhaumik, and S. Singh, “Identification of multiple harmonic sources in power system using optimally placed voltage measurement devices,” *IEEE Transactions on Industrial Electronics*, vol. 61, no. 5, pp. 2483–2492, 2014.

APPENDIX A. DERIVATION OF THE NEW $\boldsymbol{Z}_{BUS}$ WHEN MODIFYING THE SERIES IMPEDANCE OF A BRANCH

A.1. The Derivation

The work presented here is very similar to that in [1], [2] except for slight differences in the notation and the presentation method. In particular, the illustrations here are more oriented to explain how we obtained Eq. (3.1) from Fig. 3.1.

Fig. A.1. shows a network with buses k and p extracted from it and a new impedance Z_b is inserted between them. It is worth noting that the old branch between k and p and its effect on the voltage-current relationships in the network was accounted for in the original $\boldsymbol{Z}_{bus}$. Thus, we only examine the changes in voltages and currents because of the presence of the new branch Z_b, not Z_b^{old}. When Z_b is added between k and p, a current will flow in the new branch. Denote this current as I_b with its direction being shown in Fig. A.1. Since the system is linear, the voltage at a certain bus, say bus 1, is a superposition of the voltage that would have existed if the new branch had not been inserted (V_1^0) plus a voltage change due to the insertion of that branch (ΔV_1), which we write mathematically as

$$V_1 = V_1^0 + \Delta V_1 \tag{A.1}$$

$$\Delta V_1 = Z_{1k} I_b - Z_{1p} I_b \tag{A.2}$$

Here, $Z_{1k} I_b$ is the voltage added because of adding I_b to I_k and $-Z_{1p} I_b$ is the voltage added because of subtracting I_b from I_p. Rewriting Eq. (A.1) in an expanded form

$$V_1 = \underbrace{Z_{11}I_1 + \cdots + Z_{1k}I_k + \cdots + Z_{1p}I_p + \cdots + Z_{1N}I_N}_{V_1^0} + \underbrace{(Z_{1k} - Z_{1p})I_b}_{\Delta V_1} \tag{A.3}$$

Likewise, for any bus, h, Eqs. (A.1) to (A.3) are generalized as

$$V_h = V_h^0 + \Delta V_h \tag{A.4}$$

$$\Delta V_h = (Z_{hk} - Z_{hp})I_b \tag{A.5}$$

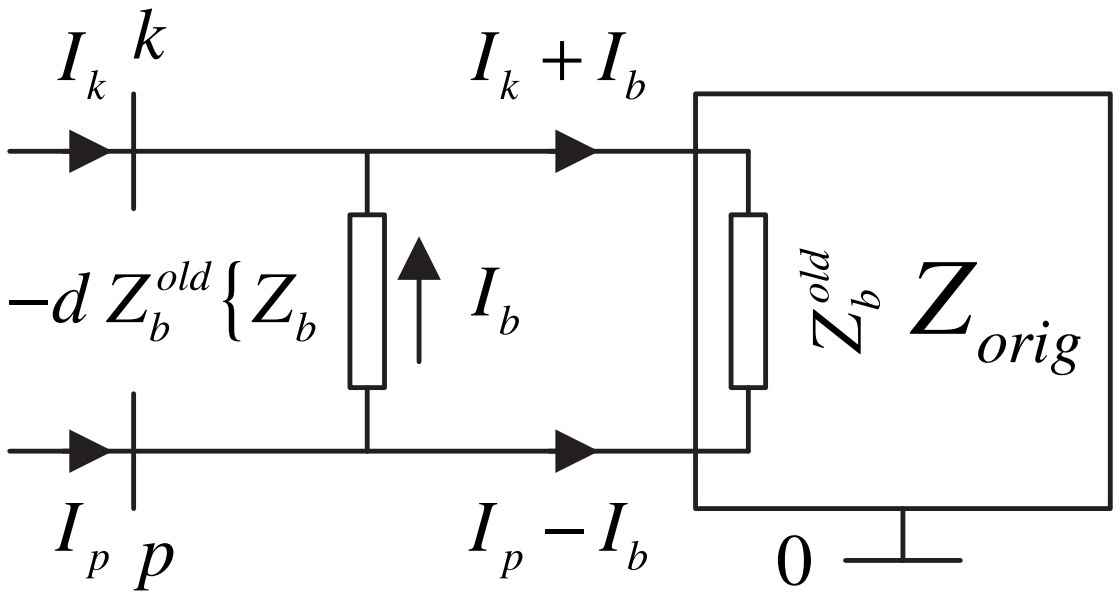

Fig. A.1. Changes in Current Injections at buses k and p When a Branch is Inserted Between Them

$$V_h = \underbrace{Z_{h1}I_1 + \cdots + Z_{hk}I_k + \cdots + Z_{hp}I_p + \cdots + Z_{hN}I_N}_{V_h^0} + \underbrace{(Z_{hk} - Z_{hp})I_b}_{\Delta V_h} \tag{A.6}$$

The value of I_b is unknown. However, we are rather interested in node voltages due to current injections into them (not due to currents in branches). Thus, we must remove it. The current I_b can be given as [see 2, pages 290-292]

$$I_b = \frac{V_p - V_k}{Z_b} = \frac{V_p^0 - V_k^0}{Z_{th,\,kp} + Z_b} \tag{A.7}$$

Where

$$Z_{th,kp} = Z_{kk} + Z_{pp} - Z_{kp} - Z_{pk} \tag{A.8}$$

Rearranging Eq. (A.7)

$$0 = V_k^0 - V_p^0 + (Z_{th,\,kp} + Z_b) I_b \tag{A.9}$$

By substituting V_k^0 and V_p^0 as defined by Eq. (A.6) in Eq. (A.9), we get

$$0 = \Big[row.\,k - row.\,p \Big] \begin{bmatrix} \\ I_1 \\ \\ \vdots \\ \\ I_k \\ \\ \vdots \\ \\ I_p \\ \\ \vdots \\ \\ I_N \\ \\ \end{bmatrix} + (Z_{th,\,kp} + Z_b) I_b \tag{A.10}$$

Eq. (A.6) shows that the new voltage at bus h due to adding the impedance Z_b is the superposition of the original voltage that would have existed if the impedance was not inserted (i.e., V_h^0) added to the voltage difference resulting from adding I_b to I_k and subtracting I_b from I_p (i.e., $\Delta\, V_h^0$). Thus, rewrite Eq. (A.6) in a matrix format by adding a column to it where each element with index h is $Z_{hk} - Z_{hp}$. However, since one more current is introduced in the derivation (i.e., I_b), we must also add a new row to maintain the matrix squareness. This row is given in Eq. (A.10). Combining Eq. (A.6) ($\forall\, h$) and Eq. (A.10) in a matrix format and substituting $-d\, Z_b^{old}$ for Z_b

$$\left[\begin{array}{c} V_1 \\ \vdots \\ V_k \\ \vdots \\ V_p \\ \vdots \\ \hline V_q = 0 \end{array}\right] = \left[\begin{array}{c|c} & \\ \boldsymbol{Z}_{orig} & col.\,k - col.\,p \\ & \\ \hline row.\,k - row.\,p & Z_{th,\,kp} - d\,Z_b^{old} \end{array}\right] \left[\begin{array}{c} I_1 \\ \vdots \\ I_k \\ \vdots \\ I_p \\ \vdots \\ \hline I_b \end{array}\right] \tag{A.11}$$

Which is the same as Eq. (3.1). Eq. (A.11) shows that we can think of the last row as that of a 'virtual' node, q, being added to the system but whose voltage is 0. Thus, we can reduce the new $\boldsymbol{Z}_{bus}$ in Eq. (A.11) to its original size using Kron reduction as we do in Section 3.3., thereby removing I_b from the mathematical representation we obtained.

A.2. References

[1] H. E. Brown, *Solution of Large Networks by Matrix Methods*. Wiley New York et al., 1985.

[2] J. J. Grainger and W. D. Stevenson, *Power System Analysis*. McGraw-Hill New York, 1994, vol. 621.

APPENDIX B. AN EXAMPLE ON EXTENDED BROWN METHOD

Fig. B.1. shows a 4-bus system with impedances given in per-unit values. The goal of what follows is to provide a simple numerical example of what I did in Chapter 3. Here we assume that the reader is already familiar with the $\boldsymbol{Z}_{bus}$ and $\boldsymbol{Y}_{bus}$ formation. Good references on this are Grainger and Stevenson [1] and Bergen [2]. The units of calculations are removed because all of them are in per-unit system.

1. Calculate the bus impedance matrix using Brown method and $\boldsymbol{Y}_{bus}$ inversion method

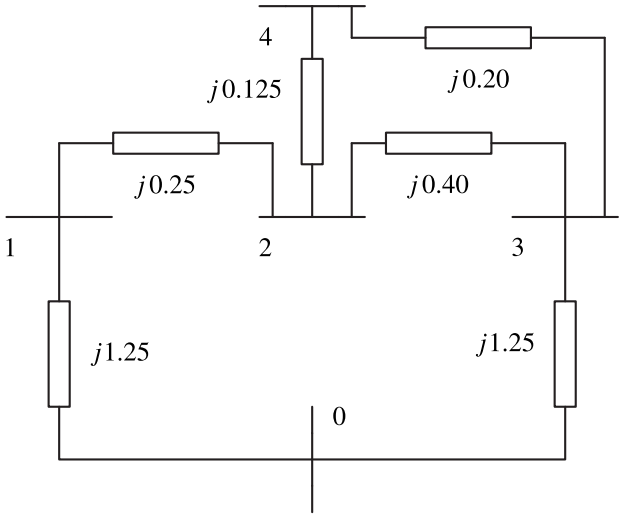

Fig. B.1. Simple 4-bus System

Connect bus 1 to ground

$$\boldsymbol{Z}_{bus,\,1} = \begin{array}{c} \\ \textcircled{1} \end{array} \begin{array}{c} \textcircled{1} \\ \begin{bmatrix} j1.2500 \end{bmatrix} \end{array} \tag{B.1}$$

Connect bus 1 to bus 2

$$\boldsymbol{Z}_{bus,\,1} = \begin{array}{c} \\ ① \\ ② \end{array} \begin{array}{c} \begin{array}{cc} ① & ② \end{array} \\ \begin{bmatrix} j1.2500 & j1.2500 \\ j1.2500 & j1.5000 \end{bmatrix} \end{array} \tag{B.2}$$

Connect bus 2 to bus 3

$$\boldsymbol{Z}_{bus,\,3} = \begin{array}{c} \\ ① \\ ② \\ ③ \end{array} \begin{array}{c} \begin{array}{ccc} ① & ② & ③ \end{array} \\ \begin{bmatrix} j1.2500 & j1.2500 & j1.2500 \\ j1.2500 & j1.5000 & j1.5000 \\ j1.2500 & j1.5000 & j1.9000 \end{bmatrix} \end{array} \tag{B.3}$$

Connect bus 3 to the reference node

$$\boldsymbol{Z}_{bus,\,4} = \begin{array}{c} \\ ① \\ ② \\ ③ \\ \hline ⓠ \end{array} \begin{array}{c} \begin{array}{cccc} ① & ② & ③ & ⓠ \end{array} \\ \left[\begin{array}{ccc|c} j1.2500 & j1.2500 & j1.2500 & j1.2500 \\ j1.2500 & j1.5000 & j1.5000 & j1.5000 \\ j1.2500 & j1.5000 & j1.9000 & j1.9000 \\ \hline j1.2500 & j1.5000 & j1.9000 & j3.1500 \end{array}\right] \end{array} \tag{B.4}$$

Using Kron reduction

$$\boldsymbol{Z}_{bus,\,5} = \begin{bmatrix} j1.3 & j1.3 & j1.3 \\ j1.3 & j1.5 & j1.5 \\ j1.3 & j1.5 & j1.9 \end{bmatrix} - \begin{bmatrix} j1.3 \\ j1.5 \\ j1.9 \end{bmatrix} [\, j3.2 \,]^{-1} \begin{bmatrix} j1.3 & j1.5 & j1.9 \end{bmatrix} \tag{B.5}$$

$$\boldsymbol{Z}_{bus,\,5} = \begin{array}{c} \\ ① \\ ② \\ ③ \end{array} \begin{array}{c} \begin{array}{ccc} ① & ② & ③ \end{array} \\ \begin{bmatrix} j0.75397 & j0.65476 & j0.49603 \\ j0.65476 & j0.78571 & j0.59524 \\ j0.49603 & j0.59524 & j0.75397 \end{bmatrix} \end{array} \tag{B.6}$$

Connect bus 3 to bus 4.

$$\boldsymbol{Z}_{bus,\,6} = \begin{array}{c} \\ ① \\ ② \\ ③ \\ ④ \end{array} \begin{array}{c} \begin{array}{cccc} ① & ② & ③ & ④ \end{array} \\ \begin{bmatrix} j0.75397 & j0.65476 & j0.49603 & j0.49603 \\ j0.65476 & j0.78571 & j0.59524 & j0.59524 \\ j0.49603 & j0.59524 & j0.75397 & j0.75397 \\ j0.49603 & j0.59524 & j0.75397 & j0.95397 \end{bmatrix} \end{array} \tag{B.7}$$

Connect bus 2 to bus 4

$$\boldsymbol{Z}_{bus,7} = \begin{array}{c} \\ \textcircled{1} \\ \textcircled{2} \\ \textcircled{3} \\ \textcircled{4} \\ \textcircled{q} \end{array} \begin{array}{c} \begin{array}{cccc} \textcircled{1} & \textcircled{2} & \textcircled{3} & \textcircled{4} \end{array} \quad \textcircled{q} \\ \left[\begin{array}{cccc|c} j0.75 & j0.65 & j0.50 & j0.50 & j0.65 - j0.50 \\ j0.65 & j0.79 & j0.60 & j0.60 & j0.79 - j0.60 \\ j0.50 & j0.60 & j0.75 & j0.75 & j0.60 - j0.75 \\ j0.50 & j0.60 & j0.75 & j0.95 & j0.60 - j0.95 \\ \hline j0.65 - j0.50 & j0.79 - j0.60 & j0.60 - j0.75 & j0.60 - j0.95 & j0.55 + j0.13 \end{array}\right] \end{array} \tag{B.8}$$

$$\boldsymbol{Z}_{bus,7} = \begin{array}{c} \\ \textcircled{1} \\ \textcircled{2} \\ \textcircled{3} \\ \textcircled{4} \\ \textcircled{q} \end{array} \begin{array}{c} \begin{array}{ccccc} \textcircled{1} & \textcircled{2} & \textcircled{3} & \textcircled{4} & \textcircled{q} \end{array} \\ \left[\begin{array}{cccc|c} j0.75397 & j0.65476 & j0.49603 & j0.49603 & j0.15873 \\ j0.65476 & j0.78571 & j0.59524 & j0.59524 & j0.19047 \\ j0.49603 & j0.59524 & j0.75397 & j0.75397 & -j0.15730 \\ j0.49603 & j0.59524 & j0.75397 & j0.95397 & -j0.35873 \\ \hline j0.15873 & j0.19047 & -j0.15730 & -j0.35873 & j0.67421 \end{array}\right] \end{array} \tag{B.9}$$

Using Kron reduction

$$\boldsymbol{Z}_{bus,\,old} = \begin{array}{c} \\ ① \\ ② \\ ③ \\ ④ \end{array} \begin{array}{c} \begin{array}{cccc} ① & ② & ③ & ④ \end{array} \\ \begin{bmatrix} j0.71660 & j0.60992 & j0.53340 & j0.58049 \\ j0.60992 & j0.73190 & j0.64008 & j0.69659 \\ j0.53340 & j0.64008 & j0.71660 & j0.66951 \\ j0.58049 & j0.69659 & j0.66951 & j0.76310 \end{bmatrix} \end{array} \tag{B.10}$$

Also, the same matrix $\boldsymbol{Z}_{bus,\,old}$ can be obtained by inverting $\boldsymbol{Y}_{bus}$. Construct $\boldsymbol{Y}_{bus}$

$$\boldsymbol{Y}_{bus,\,old} = \begin{array}{c} \\ ① \\ ② \\ ③ \\ ④ \end{array} \begin{array}{c} \begin{array}{cccc} ① & ② & ③ & ④ \end{array} \\ \begin{bmatrix} -j4.8000 & j4 & 0 & 0 \\ j4 & -j14.500 & j2.5000 & j8 \\ j0 & j2.5000 & -j8.3000 & j5 \\ j0 & j8 & j5 & -j13 \end{bmatrix} \end{array} \tag{B.11}$$

Invert it

$$
\boldsymbol{Z}_{bus,\,old} = \begin{array}{c} \\ ① \\ ② \\ ③ \\ ④ \end{array} \begin{array}{c} \begin{array}{cccc} ① & ② & ③ & ④ \end{array} \\ \begin{bmatrix} j0.71660 & j0.60992 & j0.53340 & j0.58049 \\ j0.60992 & j0.73190 & j0.64008 & j0.69659 \\ j0.53340 & j0.64008 & j0.71660 & j0.66951 \\ j0.58049 & j0.69659 & j0.66951 & j0.76310 \end{bmatrix} \end{array} \tag{B.12}
$$

2. Assume that we want to change impedance of the line connecting buses 1 and 2 (i.e., $k-p=1-2$) from $j0.25$ to $j0.15$. Calculate the new $\boldsymbol{Z}_{bus}$ using extended Brown method, Brown method, and $\boldsymbol{Y}_{bus}$ inversion method

With the proposed method, we account for such modification as follows. We take the imaginary parts of the elements and apply the following

$$
\boldsymbol{X}_{bus}^{new} = \boldsymbol{X}_{bus}^{old} + \varepsilon_X \left[\boldsymbol{X}_{bus}^{old} (\boldsymbol{e}_k - \boldsymbol{e}_p)(\boldsymbol{e}_k - \boldsymbol{e}_p)^T \boldsymbol{X}_{bus}^{old} \right] \tag{B.13}
$$

$$
\varepsilon_X = \frac{(X_b^{new} - X_b)}{X_{th,kp}\,(X_b - X_b^{new}) + X_b^{new}\,X_b} \tag{B.14}
$$

To calculate ε_X, we plug numbers in Eq. (B.14)

$$
\varepsilon_X = \frac{(0.15000 - 0.25000)}{[0.71660 + 0.73190 - 2 \cdot 0.60992]\ (0.25000 - 0.15000) + 0.15000 \times 0.25000} \tag{B.15}
$$

$$
= -1.6566 \tag{B.16}
$$

The elements $\boldsymbol{e}_k$ and $\boldsymbol{e}_p$ are

$$\boldsymbol{e}_k = \begin{bmatrix} 1 \\ 0 \\ 0 \\ 0 \end{bmatrix}, \quad \boldsymbol{e}_p = \begin{bmatrix} 0 \\ 1 \\ 0 \\ 0 \end{bmatrix} \tag{B.17}$$

Thus, we write

$$\varepsilon_X \, (\boldsymbol{e}_k - \boldsymbol{e}_p)(\boldsymbol{e}_k - \boldsymbol{e}_p)^T = \begin{bmatrix} -1.6566 & 1.6566 & 0 & 0 \\ 1.6566 & -1.6566 & 0 & 0 \\ 0 & 0 & 0 & 0 \\ 0 & 0 & 0 & 0 \end{bmatrix} \tag{B.18}$$

Now apply Eq. (B.13)

$$\boldsymbol{X}_{bus,\,new} = \begin{array}{c} \\ ① \\ ② \\ ③ \\ ④ \end{array} \begin{array}{c} \begin{array}{cccc} ① & ② & ③ & ④ \end{array} \\ \begin{bmatrix} 0.69450 & 0.63050 & 0.55140 & 0.60000 \\ 0.63050 & 0.70730 & 0.61850 & 0.67310 \\ 0.55140 & 0.61850 & 0.69770 & 0.64900 \\ 0.60000 & 0.67310 & 0.64900 & 0.74080 \end{bmatrix} \end{array} \tag{B.19}$$

Putting back the operator j and writing for $\boldsymbol{Z}_{bus,\,new}$

$$\boldsymbol{Z}_{bus,\,new} = \begin{array}{c} \\ \textcircled{1} \\ \textcircled{2} \\ \textcircled{3} \\ \textcircled{4} \end{array} \begin{array}{c} \begin{array}{cccc} \textcircled{1} & \textcircled{2} & \textcircled{3} & \textcircled{4} \end{array} \\ \begin{bmatrix} j0.69450 & j0.63050 & j0.55140 & j0.60000 \\ j0.63050 & j0.70730 & j0.61850 & j0.67310 \\ j0.55140 & j0.61850 & j0.69770 & j0.64900 \\ j0.60000 & j0.67310 & j0.64900 & j0.74080 \end{bmatrix} \end{array} \tag{B.20}$$

To check the validity of this result, repeat the same calculations by reconstructing $\boldsymbol{Z}_{bus,\,new}$ all over again.

Connect bus 1 to ground

$$\boldsymbol{Z}_{bus,\,1} = \begin{array}{c} \\ \textcircled{1} \end{array} \begin{array}{c} \begin{array}{c} \textcircled{1} \end{array} \\ \begin{bmatrix} j1.2500 \end{bmatrix} \end{array} \tag{B.21}$$

Connect bus 1 to bus 2

$$\boldsymbol{Z}_{bus,\,1} = \begin{array}{c} \\ \textcircled{1} \\ \textcircled{2} \end{array} \begin{array}{c} \begin{array}{cc} \textcircled{1} & \textcircled{2} \end{array} \\ \begin{bmatrix} j1.2500 & j1.2500 \\ j1.2500 & j1.4000 \end{bmatrix} \end{array} \tag{B.22}$$

Connect bus 2 to bus 3

$$\boldsymbol{Z}_{bus,\,3} = \begin{array}{c} \\ ① \\ ② \\ ③ \end{array} \begin{array}{c} \begin{array}{ccc} ① & ② & ③ \end{array} \\ \begin{bmatrix} j1.2500 & j1.2500 & j1.2500 \\ j1.2500 & j1.4000 & j1.4000 \\ j1.2500 & j1.4000 & j1.8000 \end{bmatrix} \end{array} \tag{B.23}$$

Connect bus 3 to the reference node

$$\boldsymbol{Z}_{bus,\,4} = \begin{array}{c} \\ ① \\ ② \\ ③ \\ \\ q \end{array} \begin{array}{c} \begin{array}{cccc} ① & ② & ③ & q \end{array} \\ \left[\begin{array}{ccc|c} j1.2500 & j1.2500 & j1.2500 & j1.2500 \\ j1.2500 & j1.4000 & j1.4000 & j1.4000 \\ j1.2500 & j1.4000 & j1.8000 & j1.8000 \\ \hline j1.2500 & j1.4000 & j1.8000 & j3.0500 \end{array}\right] \end{array} \tag{B.24}$$

Using Kron reduction

$$\boldsymbol{Z}_{bus,\,5} = \begin{array}{c} \\ ① \\ ② \\ ③ \end{array} \begin{array}{c} \begin{array}{ccc} ① & ② & ③ \end{array} \\ \begin{bmatrix} j0.73770 & j0.67620 & j0.51230 \\ j0.67620 & j0.75740 & j0.57380 \\ j0.51230 & j0.57380 & j0.73770 \end{bmatrix} \end{array} \tag{B.25}$$

$$\boldsymbol{Z}_{bus,\,6} = \begin{array}{c} \\ \textcircled{1} \\ \textcircled{2} \\ \textcircled{3} \\ \textcircled{4} \end{array} \begin{array}{c} \begin{array}{cccc} \textcircled{1} & \textcircled{2} & \textcircled{3} & \textcircled{4} \end{array} \\ \begin{bmatrix} j0.73770 & j0.67620 & j0.51230 & j0.51230 \\ j0.67620 & j0.75740 & j0.57380 & j0.57380 \\ j0.51250 & j0.57380 & j0.73770 & j0.73770 \\ j0.51230 & j0.57380 & j0.73770 & j0.93770 \end{bmatrix} \end{array} \tag{B.26}$$

$$\boldsymbol{Z}_{bus,\,7} = \begin{array}{c} \\ \textcircled{1} \\ \textcircled{2} \\ \textcircled{3} \\ \textcircled{4} \\ \textcircled{q} \end{array} \begin{array}{c} \begin{array}{ccccc} \textcircled{1} & \textcircled{2} & \textcircled{3} & \textcircled{4} & \textcircled{q} \end{array} \\ \left[\begin{array}{cccc|c} j0.73770 & j0.67620 & j0.51230 & j0.51230 & j0.16390 \\ j0.67620 & j0.75740 & j0.57380 & j0.57380 & j0.18360 \\ j0.51250 & j0.57380 & j0.73770 & j0.73770 & -j0.16390 \\ j0.51250 & j0.57380 & j0.73770 & j0.93770 & -j0.36390 \\ \hline j0.16390 & j0.18360 & -j0.16390 & -j0.36390 & j0.67250 \end{array}\right] \end{array} \tag{B.27}$$

With Kron reduction

$$\boldsymbol{Z}_{bus,\,new} = \begin{array}{c} \\ ① \\ ② \\ ③ \\ ④ \end{array} \begin{array}{c} \begin{array}{cccc} ① & ② & ③ & ④ \end{array} \\ \begin{bmatrix} j0.69780 & j0.63150 & j0.55220 & j0.60100 \\ j0.63150 & j0.70730 & j0.61850 & j0.67310 \\ j0.55220 & j0.61850 & j0.69780 & j0.64900 \\ j0.60100 & j0.67310 & j0.64900 & j0.74080 \end{bmatrix} \end{array} \tag{B.28}$$

We may obtain the same matrix by inverting $\boldsymbol{Y}_{bus}$. Construct $\boldsymbol{Y}_{bus}$

$$\boldsymbol{Y}_{bus,\,new} = \begin{array}{c} \\ ① \\ ② \\ ③ \\ ④ \end{array} \begin{array}{c} \begin{array}{cccc} ① & ② & ③ & ④ \end{array} \\ \begin{bmatrix} -j7.4670 & j6.6667 & 0 & 0 \\ j6.6667 & -j17.170 & j2.5000 & j8 \\ j0 & j2.5000 & -j8.3000 & j5 \\ j0 & j8 & j5 & -j13 \end{bmatrix} \end{array} \tag{B.29}$$

Invert it

$$
\boldsymbol{Z}_{bus,\,new} = \begin{array}{c} \\ ① \\ ② \\ ③ \\ ④ \end{array} \begin{array}{c} \begin{array}{cccc} ① & ② & ③ & ④ \end{array} \\ \begin{bmatrix} j0.69626 & j0.62984 & j0.55083 & j0.59945 \\ j0.62984 & j0.70546 & j0.61695 & j0.67142 \\ j0.55083 & j0.61695 & j0.69637 & j0.64750 \\ j0.59945 & j0.67142 & j0.64750 & j0.73914 \end{bmatrix} \end{array} \tag{B.30}
$$

3. In terms of elements of $\boldsymbol{Z}_{bus}^{old}$, calculate the change in $\boldsymbol{Y}_{bus}$ due to changing the impedance of line $1-2$

The equations that depict the change in the bus admittance matrix are given as

$$
\boldsymbol{Y}_{bus}^{new} = \boldsymbol{Y}_{bus}^{old} + \boldsymbol{Y}_{bus}^{mod} \tag{B.31}
$$

$$
\boldsymbol{Y}_{bus}^{mod} = \frac{\boldsymbol{u}_{k-p}\boldsymbol{u}_{k-p}^{T}}{\gamma} \tag{B.32}
$$

$$
\gamma = -\left(1 + \boldsymbol{u}_{k-p}^{T}\boldsymbol{Y}_{bus}^{old\,-1}\boldsymbol{u}_{k-p}\right) \tag{B.33}
$$

$$
\boldsymbol{u}_{k-p} = \sqrt{\varepsilon_{k-p}}\,(\boldsymbol{e}_k - \boldsymbol{e}_p) \tag{B.34}
$$

Note that the equations above do not assume that only the imaginary part exists. Thus, we must also use the generalized form to calculate $\boldsymbol{Z}_{bus}^{new}$. Since the new impedance is specified explicitly (rather than in terms of compensation rate for the imaginary part), we use

$$
\boldsymbol{Z}_{bus}^{new} = \boldsymbol{Z}_{bus}^{old} + \varepsilon_Z \left[\boldsymbol{Z}_{bus}^{old}(\boldsymbol{e}_k - \boldsymbol{e}_p)(\boldsymbol{e}_k - \boldsymbol{e}_p)^T\boldsymbol{Z}_{bus}^{old}\right] \tag{B.35}
$$

Where

$$
\varepsilon_Z = \frac{(Z_b^{new} - Z_b^{old})}{Z_{th,kp}\,(Z_b^{old} - Z_b^{new}) + Z_b^{new}\,Z_b^{old}} \tag{B.36}
$$

Since $\sqrt{\varepsilon_{k-p}} = \sqrt{\varepsilon_Z} = \sqrt{j1.6566} = 0.91020 + j0.91020$, we write $\boldsymbol{u}_{k-p}$ as follows

$$\boldsymbol{u}_{k-p} = 0.91020 + j0.91020 \left[\begin{bmatrix} 1 \\ 0 \\ 0 \\ 0 \end{bmatrix} - \begin{bmatrix} 0 \\ 1 \\ 0 \\ 0 \end{bmatrix} \right] = \begin{bmatrix} 0.91020 + j0.91020 \\ -0.91020 - j0.91020 \\ 0 \\ 0 \end{bmatrix} \tag{B.37}$$

The value of γ can be calculated using $\boldsymbol{u}_{k-p}$ and $\boldsymbol{Y}_{bus}^{old\,-1}$ (i.e., $\boldsymbol{Z}_{bus}^{old}$) and is -0.62110. Thus, when calculating $\boldsymbol{Y}_{bus}^{mod} = \frac{\boldsymbol{u}_{k-p}\boldsymbol{u}_{k-p}^T}{\gamma}$, we get

$$\boxed{\boldsymbol{Y}_{bus}^{mod} = \begin{bmatrix} -j2.6678 & j2.6678 & 0 & 0 \\ j2.6678 & -j2.6678 & 0 & 0 \\ 0 & 0 & 0 & 0 \\ 0 & 0 & 0 & 0 \end{bmatrix}} \tag{B.38}$$

Which is the same as the result of subtracting the old $\boldsymbol{Y}_{bus}$ from the new one. To test, write

$$\boldsymbol{Y}_{bus,\,new} - \boldsymbol{Y}_{bus,\,old} =$$

$$\begin{bmatrix} -j7.4670 & j6.6667 & 0 & 0 \\ j6.6667 & -j17.170 & j2.5000 & j8 \\ j0 & j2.5000 & -j8.3000 & j5 \\ j0 & j8 & j5 & -j13 \end{bmatrix} - \begin{bmatrix} -j4.8000 & j4 & 0 & 0 \\ j4 & -j14.500 & j2.5000 & j8 \\ j0 & j2.5000 & -j8.3000 & j5 \\ j0 & j8 & j5 & -j13 \end{bmatrix}$$

$$\boldsymbol{Y}_{bus,\,new} - \boldsymbol{Y}_{bus,\,old} = \begin{bmatrix} -j2.6670 & j2.6667 & 0 & 0 \\ j2.6667 & -j2.6800 & 0 & 0 \\ 0 & 0 & 0 & 0 \\ 0 & 0 & 0 & 0 \end{bmatrix} \tag{B.39}$$

B.1. References

[1] J. J. Grainger and W. D. Stevenson, *Power System Analysis*. McGraw-Hill New York, 1994, vol. 621.

[2] A. R. Bergen, *Power Systems Analysis*. Pearson Education India, 2009.

APPENDIX C. MODIFYING Z_{BUS} TO ACCOUNT FOR OPERATING CONDITIONS OF RENEWABLE ENERGY SOURCES

C.1. The Necessary Constraints

If we want to modify $\boldsymbol{Z}_{bus}$ by removing some current injections in the network, we should do so under the following constraints: **a)** complex power injection at each bus must stay the same as before the reduction, and **b)** voltage level at each bus must stay the same in both angle and magnitude. The next derivation in this appendix shows how to calculate the equivalent impedance of RESs while satisfying both of the previously mentioned conditions.

C.2. The Derivation

Assume that we have a load whose complex power is $S_{L,n}$. Using fundamental concepts of power system analysis, we write

$$S_{L,n} = V_n \, I_{L,n}^{*} \tag{C.1}$$

Replacing the current in Eq. (C.1)

$$S_{L,n} = V_n \left(\frac{V_n}{Z_{L,n}} \right)^{*} \tag{C.2}$$

Where $Z_{L,n}$ is the load impedance at bus n. Since $|V_n|^2 = V_n V_n^{*}$

$$S_{L,n}^{*} = \frac{|V_n|^2}{Z_{L,n}} \tag{C.3}$$

$$S_{L,n} = P_{L,n} + jQ_{L,n} \tag{C.4}$$

By isolating Eq. (C.3) for $Z_{L,\,n}$

$$Z_{L,\,n} = \frac{|V_n|^2}{S^*_{L,\,n}} \tag{C.5}$$

Thus, Eq. (C.5) is the amount of impedance that if we place at bus n, we will get the same amount of bus voltage and complex power as the one we get before replacing that impedance (consequently, the current withdrawn at bus n will necessarily stay the same as well). When bus n is a generator or RES bus, the amount of its generation can be thought of as *negative* load. Thus, for generators or RESs, Eq. (C.5) becomes

$$Z_{G,\,n} = -\frac{|V_n|^2}{S^*_{G,\,n}} \tag{C.6}$$

$$Z_{RES,\,n} = -\frac{|V_n|^2}{S^*_{RES,\,n}} \tag{C.7}$$

Eq. (C.7) is the one we use to calculate the impedance that we place at RES bus n as a replacement of the RES current injection.